QATAR UNIVERSITY

COLLEGE OF MEDICINE

STRUCTURAL AND FUNCTIONAL APPROACHES TOWARD ACTIVITY RESTORATION OF NOVEL CYSTATHIONINE BETA-SYNTHASE MUTATIONS

BY

DUAA WALID AL-SADEQ

A Dissertation Submitted to

the College of Medicine

in Partial Fulfillment of the Requirements for the Degree of

Doctorate of Medical Sciences

June 2024

COMMITTEE PAGE

The members of the Committee approve the Dissertation of
Duaa Al-Sadeq defended on 13/05/2024.

Dr. Michail Nomikos
Thesis/Dissertation Supervisor

Dr. Gheyath Khaled Nasrallah
Thesis/Dissertation Co-Supervisor

Dr. Prasanna Kolatkar
Committee Member

Dr. Nader Aldewik
Committee Member

Approved:

Marwan Abu Hijleh, Acting Dean of the College of Medicine

ABSTRACT

ALSADEQ, DUAA, W., Doctorate : June : 2024, Doctorate of Medical Sciences

Title: Structural and Functional Approaches Toward Activity Restoration of Novel Cystathionine Beta-Synthase Mutations

Supervisor of Dissertation: Michail Nomikos.

Homocystinuria, a rare disorder stemming from mutations in the CBS gene, results in cystathionine β-synthase (CBS) deficiency. CBS is a pivotal enzyme whose activity is enhanced by the allosteric regulator S-adenosylmethionine (SAM) and mediates the conversion of serine and homocysteine to cystathionine in the transsulfuration pathway. ,. Beyond its enzymatic role, CBS contributes to hydrogen sulfide (H_2S) production, a gaseous signaling molecule with diverse regulatory functions within the vascular, nervous, and immune systems. This study investigates the impact of five pathogenic CBS missense mutations [c.1006C>T (p.R336C), c.689T>A (p.L230Q), 215A>T (p.K72I), c.707C>A (p.T236N), and c.457G>A (p.G153R)] identified in homocystinuria patients and appeared to be resistant to pyridoxine treatment on the biochemical and biophysical properties of CBS protein. Our hypothesis posits that novel pathogenic missense mutations within critical functional domains of CBS protein will exert varying effects on protein structure, stability and eventually function. We anticipate that mutations affecting conserved residues or cofactor binding sites will lead to pronounced disruptions in enzymatic activity and protein stability and allow us to elucidate the underlying molecular mechanisms of disease pathogenesis for each CBS-associated missense mutation. Utilizing a multidisciplinary approach, including site-directed mutagenesis and DNA cloning, recombinant protein expression, affinity chromatography purification, circular dichroism spectroscopy, enzymatic assays, and *in silico* modeling, we assessed the

impact of these mutations on CBS stability and function. Only one mutation (p.K72I) showed no discernible impact on the spectroscopic and catalytic properties of the full-length CBS enzyme. In contrast, all the other CBS mutation studies did not fully retain heme and, when compared to the wild-type enzyme, exhibited more significant impairments in both the canonical cystathionine synthesis and the alternative H_2S-producing reactions. This reduced activity is consistent with both *in vitro* and *in silico* evidence, which indicates that the studied CBS mutations, except p.K72I, significantly decrease the overall protein's stability, which may represent the underlying cause of their pathogenicity. In addition to molecular and biochemical characterization, crystallographic studies are underway to provide further insight into the structural alterations induced by the identified CBS missense mutations. Furthermore, screening for potential chemical and molecular chaperones is being initiated to explore therapeutic avenues for mitigating the deleterious effects of these mutations on CBS protein stability and function.

DEDICATION

To my dearest family..

To my beloved husband..

ACKNOWLEDGMENTS

Initially, I extend profound gratitude to the God, the ultimate source of enlightenment, wisdom, and inspiration, whose grace, mercy, and guidance have been instrumental in reaching this significant achievement. I am incredibly thankful foremost to my supervisor, Dr. Michail Nomikos, for his invaluable guidance, support, and mentorship throughout this journey. Your unwavering belief in my potential, coupled with your constructive feedback, has significantly contributed to my professional and personal growth. Your mentorship has been a cornerstone in my academic life, and for that, I am eternally grateful.

I am also immensely grateful to my co-supervisor, Dr. Gheyath Nasrallah. Your continuous support, insightful suggestions, and encouragement have been vital in shaping my research. Your dedication and commitment to my project have provided me with the confidence to overcome numerous challenges.

I sincerely appreciate the esteemed members of my committee, Dr. Prasanna Kolatkar from Qatar Biomedical Research Institute and Dr. Nader Aldewik from Hamad Medical Corporation, for their valuable insights and constructive feedback. A special thanks to my external examiner, Dr. Omar Albagha. Your thorough review, critical feedback, and valuable suggestions have significantly improved my dissertation. Your time and effort in examining my work are greatly appreciated.

I would also like to thank our PhD coordinator, Dr. Asad Zeidan, for his dedicated efforts in ensuring the smooth progress of our PhD program. Your guidance and support have been invaluable in navigating the administrative aspects of this journey.

I am thankful to Dr. Luis Alfonso Martinez from CIC Biogune Research Center Bilbao Spain, as well as Dr. Alessandra Astegno and Dr. Carolina Conter from the University of Verona for their collaboration and contributions to this research. I am

very grateful for giving me the opportunity to join their lab, learn new techniques, and conduct some experiments.

My heartfelt thanks go to my dearest parent whose endless love, patience, and encouragement have been my driving force. Your sacrifices and unwavering belief in me have been my greatest motivation. To my siblings, Khalid, Ibrahim, and Raghad, thank you for your constant support, understanding, and for being my biggest cheerleaders.

I would like to express my deepest gratitude to my beloved husband Sami. Your unwavering support, patience, and belief in me have been my anchor throughout this journey. Thank you for your love, understanding, and for standing by me through the highs and lows. Your presence has made this journey possible.

To my best friend, Samar Shurbaji, your unwavering support and assistance have been a constant source of strength. Thank you for always being there, for your encouragement, and for your belief in my abilities. Your friendship has been a pillar of support throughout this journey.

Lastly, I extend my heartfelt thanks to my friends and colleagues at the Biomedical Research Center (BRC) and College of Medicine at Qatar University (QU). Your camaraderie, collaboration, and support have made this journey memorable and enjoyable. The shared experiences and collective efforts have greatly enriched my academic life.

Thank you all for your invaluable contributions to my academic and personal development. Your support, guidance, and encouragement have made this achievement possible, and I am deeply grateful to each and every one of you.

TABLE OF CONTENTS

LIST OF TABLES

LIST OF FIGURES

LIST OF ABBREVIATIONS

ANOVA One-way Analysis of Variance

APS Ammonium Persulfate

Arg Argenine

BCA Bicinchoninic acid

CBL cystathionine β-lyase

CBS Cystathionine β-synthase

CD Circular Dichroism

CSE cystathionine gamma-lyase

Cth cystathionine

Cys cysteine

DBS Dried Blood Spot

E. coli Escherichia coli

FBS Fetal Bovine Serum

GuHCl Guanidinium Chloride

HCl Hydrochloric acid

Hcy Homocysteine

HEK293T Human embryonic kidney cells

HPLC High-Performance Liquid Chromatography

IBC Institutional Biosafety Committee

IPTG Iisopropyl β-D-thiogalactopyranoside

kDa kilodalton

LDH Lactate-dehydrogenase

MAT Methionine Adenosyltransferase

MCS Multiple Cloning Site

MD molecular dynamics

Met Methionine

MSUD maple syrup urine disease

MTHFR methylenetetrahydrofolate reductase

MTs methyltransferases

MWCO Molecular weight cut-off

NaCl Sodium chloride

PCR polymerase chain reaction

PKU phenylketonuria

PMSF Phenylmethylsulfonyl Fluoride

PVDF Polyvinylidene Difluoride membrane

RBS Ribosome Binding Sequence

RPM Round Per Minute

SAM S-adenosylmethionine

SAH S-adenosylhomocysteine

SAHH SAH hydrolase

SDS-PAGE Sodium Dodecyl Sulfate-polyacrylamide gel electrophoresis

Ser Serine

TBST Tris-Buffered Saline with tween

TEMED Tetramethylethylenediamine

Tm Transition Midpoint

UPR Unfolded Protein Response

WT Wild-type

Chapter 1: Introduction

Inborn metabolic errors are a significant class of inherited genetic disorders affecting cellular metabolism. The majority of these disorders are caused by mutations in single genes that code for enzymes catalyzing vital biological reactions. One out of every 2,500 births is estimated to have a genetically caused inborn metabolic error (Applegarth & Toone, 2000). The majority of these metabolic disorders are inherited in autosomal recessive patterns, where two defective gene copies are required for the clinical manifestation of the disease. Mutations in the gene encoding an enzyme can alter protein structure, diminish activity and/or alter regulation, reducing product formation or accumulating a toxic intermediate. Homocystinuria due to cystathionine beta-synthase (CBS) deficiency is a prototypical example of an inherited metabolic (S. Mudd, Levy, & Kraus, 2001).

Classical homocystinuria (OMIM 236200) is an autosomal recessive inborn error disorder due to a deficiency in the CBS enzyme. It is the most common form of homocystinuria worldwide and is characterized by abnormally high levels of homocysteine in the blood and urine. CBS catalyzes the condensation of serine and homocysteine to form cystathionine. Consequently, due to the CBS enzyme deficiency, homocysteine accumulates in both the blood and the urine. Subsequently, this accumulation may cause intellectual disability, psychiatric and behavioral disorders, nearsightedness, dislocated eye lenses, skeletal disabilities, vaso-occlusive disease, and vascular system complications (W. Kruger, Wang, Jhee, Singh, & Elsas, 2003; Lai & Kan, 2015).

The global prevalence of homocystinuria is estimated to be 1:200,000 births. As a result, it is generally regarded as a rare genetic disease. However, it is extremely common in the Gulf region, particularly in Qatar, which has the world's highest prevalence (1:1,800 newborns affected) (Ismail et al., 2019). As a result,

homocystinuria is regarded as the most common inherited monogenic disease in Qatar. This high incidence rate has been attributed to a founder mutation in the Qatari population, c.1006 C>T in the CBS gene (p.Arg366Cys or p.R336C). This founder mutation is a missense mutation in which arginine is substituted (R) by cysteine (C) residue. Approximately 6% of the Qatari population have a heterozygous p.R336C mutation with an allele frequency of 1% (Zschocke et al., 2009). Most of the *CBS* gene mutations are missense mutations in which a single codon is altered, resulting in amino acid substitution in the protein sequence.

Clinically, homocystinuria patients exhibit numerous manifestations due to the disruption of many organ systems' development. CBS patients have adverse effects that usually affect four main target systems. These include mental retardation (brain), lens dislocation (eyes), osteoporosis (bones), and arterial and venous thromboembolism (blood clotting system). Other clinical manifestations include myopia, psychiatric disturbances, Marfanoid habitus, and other mental and skeletal deformities (Gupta et al., 2019). Homocystinuria was first identified in mentally disabled patients in 1962 (N. A. Carson & Neill, 1962). Shortly after, CBS enzyme deficiency was identified as the cause of this abnormality (S. H. Mudd, Finkelstein, Irreverre, & Laster, 1964).

Patients with classical homocystinuria are treated with a combination of high-dose homocysteine metabolism cofactors, such as pyridoxine, and a methionine-restricted diet. However, more than half of those affected do not respond to treatment, and no significant reduction in plasma homocysteine levels has been reported (Schiff & Blom, 2012). Treating homocystinuria patients with traditional therapies is difficult because a restricted diet is difficult to maintain and some CBS mutations, such as p.R336C, are pyridoxine insensitive. Untreated homocystinuria patients may experience severe complications such as physical deformity, developmental issues, mental retardation, and death. As a result, this disease imposes a significant financial

and clinical burden on society, necessitating the development of more effective therapeutic strategies.

Moreover, the treatment of inborn error metabolic disorders, such as homocystinuria, is complicated by the need to consider an individual's specific allele(s) when developing a treatment regime. For instance, pyridoxine (vitamin B6) supplement was reported to be effective in approximately 50% of reported disease-associated alleles. Unfortunately, Qatari p.R366C homozygous patients do not respond to high doses of pyridoxine. Therefore, untreated Qatari patients usually have severe complications, including mental retardation, physical deformation, and potentially fatal thromboembolic events. We recently demonstrated that the CBS^{R336C} enzyme and other novel reported mutations are nonfunctional due to decreased protein stability, leading to accelerated protein degradation (Ismail et al., 2019).

Hypothesis:

We postulate that the novel missense mutations identified in the CBS gene of homocystinuria patients, including c.1006C>T (p.R336C), c.689T>A (L230Q), 215A>T (K72I), c.707C>A (T236N), and c.457G>A (G153R), will exhibit varying degrees of impact on CBS protein structure and function. Specifically, we anticipate that mutations affecting highly conserved residues within critical functional domains of CBS will lead to pronounced disruptions in enzymatic activity and protein stability. Furthermore, we propose that mutations interfering with essential cofactor binding sites or allosteric regulation mechanisms will result in severe impairments in cystathionine synthesis. Our hypothesis extends to suggest that the observed pathogenicity of these mutations will be attributable not only to the destabilization of the CBS protein but also to alterations in its dynamic conformational landscape, as elucidated through a comprehensive array of biochemical, biophysical, and computational analyses. It might be possible to rescue the CBS structural stability and, thus, the functional defect of the

CBS mutations by combining various chemical chaperone treatments, since chemical chaperone treatment approached, can potentially represent promising alternative therapies for Qatari patients.

A thorough understanding of the structure-function relationship underlying the CBS homocystinuria-associated mutations can provide a further insight into the molecular mechanisms leading to the design of powerful treatments. **To address this hypothesis, the specific aims of this dissertation include:**

1- Perform molecular cloning, bacterial expression and large-scale purification of recombinant CBS wild-type and pathogenic mutant proteins.

2- Perform molecular characterization of the most prevalent, founder mutation in Qatari population, R336C mutant CBS protein, in order to assess the effect of this point mutation on the biochemical and biophysical properties of CBS protein.

3- Carry out crystallization and X-ray structure determination of the CBS^{R336C} enzyme.

4- Perform molecular characterization of the novel mutated CBS proteins, K72I and L230Q, that were reported in compound heterozygous homocystinuria patient, and CBS T236N and G153R which were reported in homozygous homocystinuria patients. The effect of these point mutations on protein structural, biochemical, biophysical, and functional characteristics will be assessed.

5- Restore the activity and functionality of the mutant CBS proteins using potential therapeutic chemical chaperone and proteasome inhibitors *in vitro* using CRISPR/Cas9 p.R336C knock-in HEK293T cell line.

The novelty of this project lies primarily in the multidisciplinary approach that

we employed with the ultimate goal of identifying alternative treatment approaches related to homocystinuria due to CBS mutations. The proposed work tackles a highly significant health issue in Qatar that interests diverse stakeholders. The success of this project and the development of a novel therapeutic intervention could alleviate the burden of homocystinuria on Qatari society. On a larger scale, the results generated from this project will be used as a platform to formulate new hypotheses and experimental goals. As a continuation of this project, our future goal is to establish a vast network of investigators from the academic, health, and pharmaceutical fields interested in drug discovery and clinical trials of new therapeutic drug targets that implicate the health and management of homocystinuria patients.

Chapter 2: literature review

Amino acid metabolic disorders: a brief perspective

In mammals and humans, dietary proteins are an important source of essential amino acids, whereas non-essential amino acids can be synthesized endogenously. Humans utilize twenty amino acids, nine of which cannot be synthesized and must be obtained through food. Although amino acids are the building blocks of proteins, some function as neurotransmitters or are synthesized into essential molecules in the body, such as hormones and oxygen-carrying molecules (Brittanica, 2022).

Amino acid metabolic disorders are a group of inherited disorders characterized by disturbances in the metabolism of essential amino acids. These disorders result from defects in enzymes, transporters, or cofactors involved in amino acid metabolic pathways. Understanding the molecular basis of these disorders is critical for accurate diagnosis and the development of effective treatment strategies. Numerous studies have shed light on the genetic mutations underlying amino acid metabolism disorders, revealing the intricate interplay of metabolic pathways and the consequences of these defects (Lee & Kim, 2022). For instance, phenylketonuria (PKU) is caused by mutations in the phenylalanine hydroxylase gene, resulting in impaired conversion of phenylalanine to tyrosine and subsequent accumulation of phenylalanine in the blood (Blau, Van Spronsen, & Levy, 2010). Similarly, maple syrup urine disease (MSUD) is caused by mutations in genes encoding the branched-chain alpha-keto acid dehydrogenase complex, resulting in the accumulation of branched-chain amino acids (DT, 2001). Treatment includes dietary changes or drug therapy, such as methionine restriction for homocystinuria.

Amino acid metabolism and transport disorders are rare, but collectively, they affect perhaps 1 in 1000 newborns (Longo, 2014). Most of these metabolic disorders are inherited autosomal recessive conditions, requiring two defective gene copies for clinical symptoms to manifest. These genetic defects in amino acid metabolic disorders

result in a broad spectrum of clinical presentations. Neurological symptoms such as developmental delay, mental retardation, seizures, and movement disorders are common in many amino acid metabolism disorders (Huemer et al., 2017). For instance, homocystinuria, caused by mutations in genes involved in homocysteine metabolism, can be associated with neurological symptoms, including cognitive impairment and psychiatric disorders (Selley, Close, & Stern, 2002). In addition, amino acid metabolic disorders can affect other organ systems and lead to manifestations such as hepatomegaly, cardiomyopathy, and oculocutaneous abnormalities (Ficicioglu, 2017).

Classical homocystinuria

Classical homocystinuria, also known as cystathionine beta-synthase deficiency, is a rare hereditary metabolic disorder characterized by impaired methionine metabolism. Mutations in *CBS* gene result in reduced enzyme activity in this autosomal recessive disorder (Weber Hoss, Sperb-Ludwig, Schwartz, & Blom, 2020). Consequently, impaired CBS activity leads to an accumulation of homocysteine and its metabolites, which contribute to various clinical manifestations. Numerous studies reported that classical homocystinuria is associated with multiple systemic complications, including skeletal, ocular, cardiovascular, and central nervous system abnormalities. Cardiovascular complications such as thromboembolism, premature atherosclerosis, and stroke are major causes of patient morbidity and mortality (Huemer et al., 2017). Common ocular findings in classical homocystinuria include ectopia lentis, myopia, and glaucoma (D. W. Al-Sadeq & Nasrallah, 2020).

Classical homocystinuria is a relatively rare disorder with an incidence rate ranging from one in every 200,000 to 335,000 births worldwide (D. W. Al-Sadeq & Nasrallah, 2020). However, its prevalence in the Gulf region, notably Qatar, is exceptionally high and reached 1:1800 (Ismail et al., 2019). One of the causes is the high consanguinity rate in the MENA region, which is considered a significant factor

in increasing the prevalence of various metabolic diseases. The diagnosis of classical homocystinuria involves biochemical analysis and genetic testing. Elevated plasma homocysteine and methionine levels are characteristic laboratory findings (Yap et al., 2001). In addition, implementing newborn screening techniques for homocystinuria has facilitated the early detection and accurate estimation of the homocystinuria incidence. Yet, it could have a poor sensitivity as it detects methionine rather than homocysteine. Since methionine can only be obtained through diet, babies who were screened may not have been exposed to enough methionine to identify abnormal levels. Furthermore, the cut-off values for increased methionine are considered insufficiently strict. It is commonly accepted that newborn screening for homocystinuria in the United States results in a high number of false negatives (Walter, Jahnke, & Remmington, 2011). Many patients are not diagnosed until they exhibit clinical symptoms later in life; some may never be diagnosed.

Management of classical homocystinuria primarily involves dietary interventions, including restriction of methionine and supplementation of cofactors such as pyridoxine (vitamin B6), folic acid, and betaine (Morris et al., 2017b). A low-methionine diet aims to prevent the accumulation of toxic metabolites, while the supplementation of cofactors supports alternative metabolic pathways and helps normalize homocysteine levels (Yap et al., 2001). Long-term monitoring, including regular plasma amino acid and homocysteine level assessment, is essential for adjusting dietary interventions and optimizing patient outcomes (Morris et al., 2017a).

Sulfur-Containing Amino Acids

Sulfur-containing amino acids are vital for human physiology and are essential for protein synthesis, enzymatic reactions, and the maintenance of overall cellular function. They play a significant role in maintaining the cellular system integrity and capacity to detoxify toxic compounds, reactive oxygen species, and free radicals (Townsend, Tew, & Tapiero, 2004).

The primary sulfur-containing amino acids in mammas are methionine and cysteine.

Methionine is an essential amino acid that initiates protein synthesis and is critical in various metabolic processes (Stipanuk, 2004). Methionine is metabolized through the reverse transsulfuration pathway, which involves the conversion of methionine to cysteine. Several enzymes are required for this pathway, including CBS and cystathionine gamma-lyase (CSE). These enzyme deficiencies or dysfunctions can result in disorders such as classical homocystinuria and cystathioninuria, characterized by homocysteine or cystathionine accumulation, respectively (W. Kruger et al., 2003).

Cysteine, conversely, is a non-essential amino acid involved in forming disulfide bonds, which contribute to the stability and structure of proteins (Bhopatkar, Uversky, & Rangachari, 2020). Cysteine is primarily derived from methionine via transsulfuration but can also be obtained through dietary sources. It is a precursor for glutathione, a key antioxidant molecule involved in cellular defense against oxidative stress (Lu, 2013). Cysteine is also involved in synthesizing bioactive compounds like coenzyme A and hydrogen sulfide (Mustafa, Gadalla, & Snyder, 2009). Furthermore, the thiol group in cysteine's unique reactivity allows for the formation of disulfide bonds, which contributes to protein structure and stability.

Both amino acids contribute significantly to the cellular pool of organic sulfur and sulfur homeostasis. Therefore, genetic defects in the enzymes that regulate the sulfur pool could lead to various diseases, including homocysteinemia, homocystinuria, and neural tube defects (Townsend et al., 2004). In addition, an imbalance in the thiol

balance has been linked to numerous diseases, including vascular disease and Alzheimer's disease.

The Reverse Transsulfuration Pathway

The reverse transsulfuration pathway is an essential metabolic pathway in cysteine biosynthesis. This pathway is critical for maintaining the body's sulfur amino acid balance. Methionine (Met), obtained from dietary proteins, is condensed with ATP by methionine adenosyltransferase (MAT) to form S-adenosylmethionine (SAM; also known as AdoMet, an allosteric activator) (**Figure 1**). SAMs serve as universal methyl donors for multiple methylation reactions catalyzed by different methyltransferases (MTs) to generate methylated products and S-adenosylhomocysteine (SAH). SAH is hydrolyzed to adenosine and homocysteine (Hcy) by SAH hydrolase (SAHH). Hcy undergoes an irreversible diversion from the methionine cycle to the transsulfuration pathway via condensation with serine (Ser), catalyzed by CBS, resulting in cystathionine (Cth) formation. Cystathionine gamma-lyase (CSE) subsequently hydrolyzes cystathionine to produce cysteine (Cys). The flux of Hcy through competing pathways is regulated by SAM, which allosterically activates CBS while inhibiting methylenetetrahydrofolate reductase (MTHFR). Intriguingly, enzymes involved in both the transsulfuration pathway and the remethylation cycle rely on various B vitamins, including riboflavin (B2) in MTHFR, pyridoxine (B6) in CBS, and folate (B9) as a one-carbon carrier in the remethylation cycle. The pathway's activity is tightly regulated, as imbalances can disrupt sulfur amino acid metabolism and potentially contribute to various health problems. Deficits or dysfunctions in CBS or CSE enzymes, for instance, can result in metabolic disorders such as classical homocystinuria or cystathioninuria, which are characterized by the accumulation of homocysteine or cystathionine.

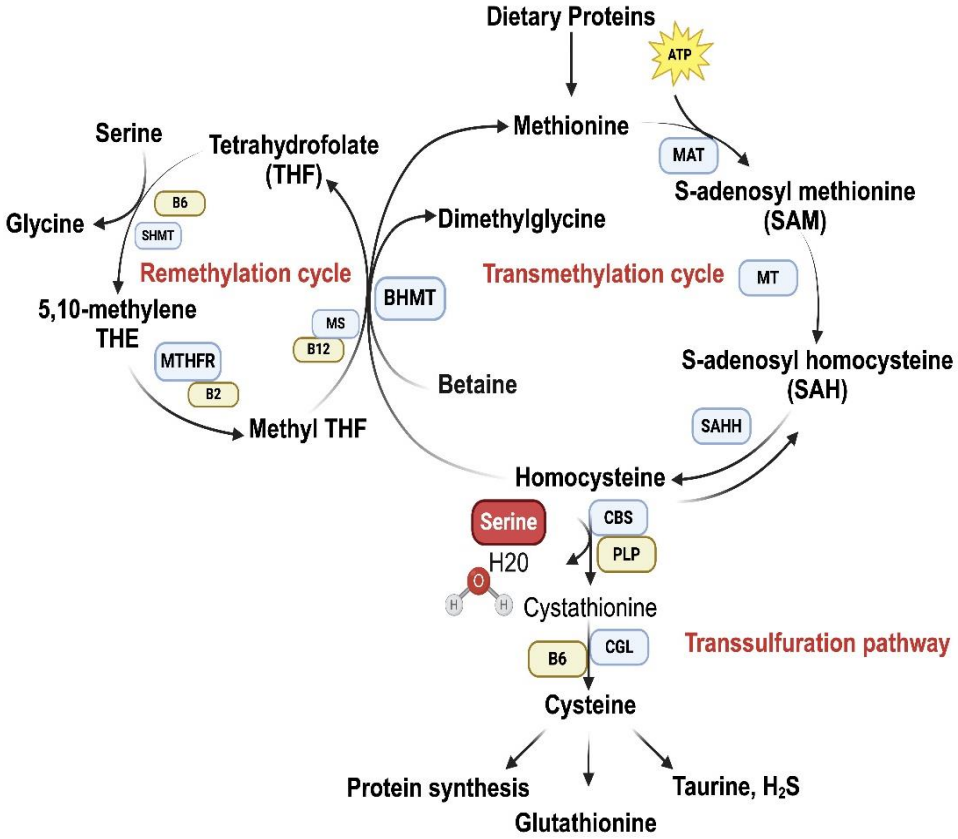

Figure 1. Homocysteine metabolism pathway. Methionine adenosyltransferase (MAT); methyltransferase (MT); S-adenosylhomocysteinase hydrolase (SAHH); betaine-homocysteine methyltransferase (BHMT); pyridoxal-phosphate (PLP); cystathionine gamma-lyase (CGL); methionine synthase (MS); serine-hydroxymethyltransferase (SHMT); methyl-tetrahydrofolate-reductase (MTHFR), hydrogen sulfide (H_2S). Adopted from (D. W. Al-Sadeq & Nasrallah, 2020).

Cystathionine β-Synthase

5.1 The molecular structure of CBS

The architecture of the CBS protein and catalytic process has been extensively studied. Human CBS, a PLP-dependent enzyme, is a tetramer of 63-kDa subunit, spanning 551 amino acid residues (**Figure 2**). Each subunit comprises three distinct domains: an N-terminal, heme-binding domain whose function has been intensively debated for decades and spans ~70 residues, a central catalytic core of ~340 residues, which binds one pyridoxal-5′-phosphate (PLP, the active form of vitamin B6) molecule in Schiff base linkage with active-site lysine (K119), and a C-terminal regulatory domain of ~140 residue that binds to SAM (Karim Zuhra, Fiona Augsburger, Tomas Majtan, & Csaba Szabo, 2020). The N-terminal domain consists of two distinct regions. The first 40 residues represent an intrinsically disordered region involved in transient heme binding and protein aggregation. Residues 40–70 form a folded region that binds to the heme cofactor (Karim Zuhra et al., 2020).

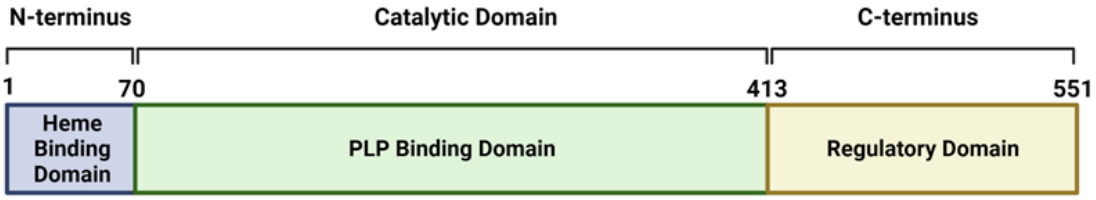

Figure 2. The structural arrangement of human CBS comprises three distinct regions. The N-terminal domain, encompassing residues 1-70, is responsible for binding the heme cofactor. Within the conserved catalytic core, spanning residues 70-386, lies the PLP cofactor, facilitating catalytic reactions. Finally, the C-terminal regulatory domain, spanning residues 386-551, consists of a flexible linker and a tandem of CBS domains (CBS1 and CBS2), which serve as binding sites for SAM.

Each domain is presumed to perform a specific function. Although their precise function has not yet been elucidated, the physiological importance of the CBS domain is highlighted by the observation that point mutations that occur in the CBS domain can significantly impair certain protein functions. For instance, heme influences folding and acts as a redox sensor. Thus, removing the heme domain could cause a loss of redox sensitivity (Yamanishi, Kabil, Sen, & Banerjee, 2006). However, the deletion of the heme-binding domain from hCBS yields a hemeless variant that retains approximately 40% activity compared to the wild-type enzyme, demonstrating that heme is not essential for activity (Evande, Ojha, & Banerjee, 2004). Furthermore, lower eukaryotic CBS enzymes, such as yeast CBS, lack a heme-binding domain yet catalyze the same overall reaction suggesting that heme is not required for catalysis in hCBS (Jhee, McPhie, & Miles, 2000).

The catalytic core, where the catalysis occurs, contains the PLP cofactor and spans residues 70–386. The PLP generates an internal aldimine intermediate in its resting state via the Schiff base bonding with the ε-amino group of Lys119 (Karim Zuhra et al., 2020). Nevertheless, the CBS active site undergoes a conformational change upon binding with the serine substrate. The CBS binding site is not well defined and some associated mutations, such as G307S, were proposed to disrupt homocysteine binding (Meier, Oliveriusova, Kraus, & Burkhard, 2003).

The C-terminal regulatory domain contains CBS motifs, CBS1 and CBS2, which form the binding site for the allosteric regulator SAM and span residues 386–551. The CBS activity is limited to a "basal" state by the autoinhibitory action of the C-terminal domain in the absence of SAM (Scott et al., 2004). Although the activation mechanism has not been elucidated yet, SAM activates the enzyme by binding with the C-terminal regulatory domain and increases the hCBS activity ~2-4-fold (Evande, Blom, Boers, & Banerjee, 2002). The human CBS C-terminal domain exhibits an autoinhibitory effect on the CBS activity by blocking the active site while binding SAM would relieve the autoinhibitory effect. The proposed mechanism states that SAM binding to the CBS motifs would rotate them away from the catalytic core, thus exposing the binding site for further SAM binding (Ereño-Orbea, Majtan, Oyenarte, Kraus, & Martínez-Cruz, 2013; Pey, Majtan, Sanchez-Ruiz, & Kraus, 2013). It causes a domain rearrangement and results in the release of intrasteric block from the catalytic site. Therefore, a mutation in CBS domains could significantly reduce activation by SAM and thus cause homocystinuria.

The C-terminal regulatory domain is also involved in the oligomeric status of the protein and the formation of the hCBS homotetramer (Kery, Poneleit, & Kraus, 1998). For instance, the C-terminal regulatory domain deletion will form dimers. Therefore, since the full-length CBS enzyme has a high tendency to aggregate, ten

amino acid residue (516-525) segment of the hCBS C-terminal domain has been removed. It was proposed that this segment participates in higher-order oligomerization of the enzyme, and their removal enabled the successful crystallization of full-length human CBS (Ereño-Orbea, Majtan, et al., 2013).

5.2 Reaction pathway

The reverse transsulfuration pathway has been extensively studied in higher organisms and plays an essential role in synthesizing cysteine from methionine, producing intermediates such as homocysteine and cystathionine (Carolina Conter et al., 2020). Two major pyridoxal-5'-phosphate (PLP)-dependent enzymes, CBS and cystathionine gamma-lyase (CGL), regulate this pathway. In the first step of the pathway, CBS catalyzes a β-replacement reaction in which the - OH group of serine is replaced by the thiol of homocysteine to form cystathionine (reaction 1, **Figure 3**) (Carolina Conter et al., 2020). Subsequently, CGL cleaves cystathionine into cysteine, α-ketobutyrate, and ammonia. In addition to its vital role in the metabolism of sulfur-containing amino acids, CBS is also a remarkable source of hydrogen sulfide (H_2S), an important signaling molecule involved in the modulation of physiological responses in various diseases and the regulation of oxidative stress (Szabo, 2007). CBS can generate H_2S by several pathways, including the β-elimination of cysteine (reaction 3, **Figure 3**), β-replacement of two molecules of cysteine (reaction 4, **Figure 3**), or the condensation of cysteine with homocysteine (reactions 5, **Figure 3**), with the latter considered the primary mechanism for H_2S production by the enzyme (S. Singh, Padovani, Leslie, Chiku, & Banerjee, 2009).

These CBS reaction mechanisms, both in the canonical reaction and the H_2S production pathways, highlight the enzyme's versatility and ability to contribute to sulfur amino acid metabolism and H2S signaling. Understanding the intricate

mechanisms of CBS catalysis provides insights into the regulation and importance of these pathways in maintaining cellular homeostasis and overall physiological function.

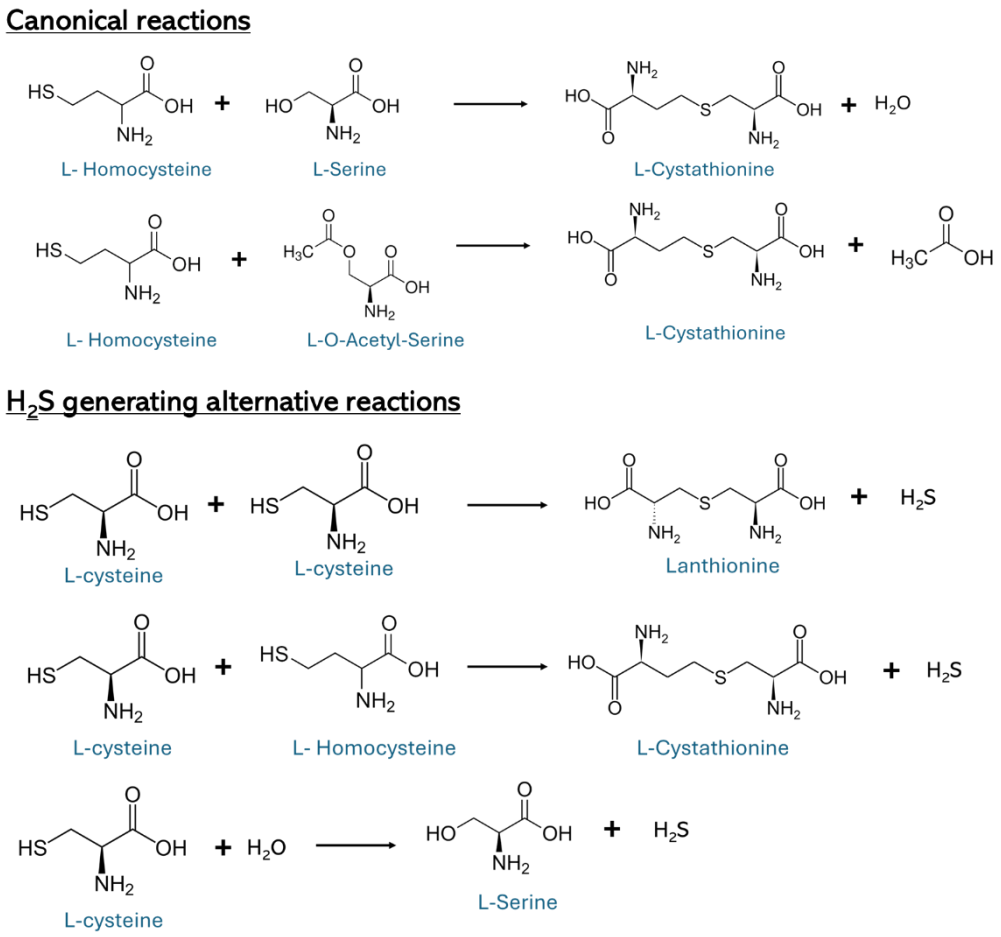

Figure 3. Reactions catalyzed by CBS. Adopted from (Carolina Conter et al., 2020).

5.3 SAM Regulation in CBS

Enzyme regulatory mechanisms are crucial processes that regulate enzyme activity to maintain cellular homeostasis and ensure that metabolic pathways function efficiently. Among the mechanisms involved in enzyme control include allosteric modulation, post-translational modifications, and feedback inhibition. These regulatory mechanisms enable cells to respond to changes in their environment, metabolic demands, and communication pathways, allowing them to precisely control the speeds of biochemical reactions. Understanding enzyme regulation mechanisms is essential for understanding cellular function, disease pathophysiology, and developing therapeutic approaches that target specific enzymatic processes.

One of the primary regulatory mechanisms involves the allosteric inhibition of CBS by SAM, which acts as a negative feedback regulator for high levels of CBS. Hence, increased levels of SAM suggest an ample presence of metabolites downstream in the transsulfuration pathway, serving as a signal to decrease the synthesis of cystathionine. The interaction between SAM and CBS leads to structural modifications that diminish CBS's affinity for its substrates, effectively restraining the enzyme's catalytic function (Gupta & Kruger, 2011). In addition, the availability of SAM can influence the level of CBS expression. Studies have shown that alterations in SAM levels affect CBS mRNA stability and protein expression. When SAM levels are decreased, CBS expression rises as a compensatory mechanism to restore cysteine biosynthesis (Mudd et al., 2007). Conversely, increased SAM levels suppress CBS expression and provide tight regulation of cystathionine production (Mudd et al., 2007).

Overall, SAM acts as a key regulator of CBS activity and cystathionine production and maintains sulfur amino acid homeostasis. Its allosteric inhibition, post-translational modifications, and its influence on CBS expression provide multiple aspects of regulation of CBS activity in response to cellular metabolic conditions and signaling pathways.

5.4 CBS distribution in various cells

CBS is a cell-specific constitutively expressed enzyme; post-transcriptional modifications primarily regulate its expression under normal physiological conditions. In mammalian cells, CBS mRNA and protein are found mainly in the liver, kidney, brain, and pancreas (Damba et al., 2019; Dicker-Brown, Fonseca, Fink, & Kern, 2001). Although the CBS expression is highly abundant in hepatocytes, it can be detected at lower levels in other liver cells, such as hepatic stellate and Kupffer cells (Damba et al., 2019). Similarly, the CBS expression was detected in the glomeruli, collecting duct, and interlobular arterial endothelium of the kidney and in both the islet and acinar cells of the pancreas (Tamizhselvi, Moore, & Bhatia, 2007; Yuan et al., 2017). In addition, all brain regions express CBS at various levels, yet the highest expression was reported in the cerebral cortex, cerebellum, and hippocampus (Abe & Kimura, 1996).

According to the biochemical and clinical data, the primary physiological role of CBS is to produce cysteine from methionine amino acid by degrading homocysteine. CBS can also catalyze the condensation of cysteine and homocysteine to produce cystathionine and H_2S (S. Singh et al., 2009). H_2S is a gasotransmitter molecule involved in various physiological responses and is suggested to affect the energy metabolism, cardiovascular, and central nervous systems. For instance, a study aimed to evaluate the retinal vascular integrity in CBS-deficient mice reported that H_2S is a gaseous signaling molecule with neuroprotective properties (Tawfik et al., 2014). It also has a role in stimulating angiogenesis and reendothelialization (Majumder et al., 2018). In addition, H_2S is a vital regulator of numerous central nervous system functions. Under normal physiological conditions, it acts as a neuromodulator, neurotransmitter, and neuroprotective factor. Yet, the overproduction of H_2S was reported as a potential causative factor in the pathogenesis of neurological dysfunction in Down syndrome and disrupted brain wave patterns (Panagaki et al., 2022). Other tissues express CBS at

lower levels, including the lungs, muscle tissues, the gastrointestinal tract, endocrine tissues, the bladder, adipose tissue, and lymphoid tissue (Uhlén et al., 2015).

Homocystinuria-associated Mutations of CBS

Homocystinuria is an autosomal recessive disorder where the marriage of two carrier parents with defective gene copies can result in having a child with homocystinuria. The CBS gene is located on human chromosome 21 in the subtelomeric short arm 22.3 region (21q22.3) (The Human Gene Database, 2022). It contains 23 exons, 16 of which code for a polypeptide of 551 amino acids. For decades, extensive research has focused on CBS-inactivating mutations, particularly in relation to their role in homocystinuria (Tomas Majtan et al., 2017). Over 1,000 public variants have been documented, with the majority identified in individuals of Caucasian European descent, while relatively few have been reported in Asian or African-American populations (Ignoul & Eggermont, 2005). Around 87% of these mutations are missense mutations that do not directly affect the catalytic site of CBS; instead, they produce unstable, misfolded proteins devoid of normal biological function, rendering them prone to degradation (Kraus et al., 1999). Furthermore, a considerable proportion of CBS mutants exhibit impaired responsiveness to SAM binding, which serves as an allosteric modulator of enzyme activity and protein stability.

The most reported pathogenic mutations worldwide are p.G307S (31%), and p.I278T (24%) (Database, 2019). The p.G307S mutation is Ireland and Australia's most prevalent CBS deficiency mutation (Gallagher et al., 1995; Scriver, 2001). It is located on exon 8 of the *CBS* gene and homozygous patients are severely affected and are non-responsive to pyridoxine treatment (R. de Franchis, E. Kraus, V. Kozich, G. Sebastio, & J. P. Kraus, 1999; Kelly et al., 2003). In addition, the molecular dynamic simulations showed that p.G307S mutation is structurally stable but functionally inactive and hence

does not respond to pyridoxine treatment or chaperone-based therapy (Gupta et al., 2018).

Similarly, the p.I278T mutation is considered the most prevalent mutation worldwide and affects the CBS catalytic domain (Tomas Majtan et al., 2017). Yet, it confers responsiveness to pyridoxine treatment (Scriver, 2001). Pathogenicity of the p.I278T CBS mutation was demonstrated to be due to a lack of catalytic activity in yeast and bacterial expression systems. For instance, p.I278T was shown to have only 2.4% of the human wild-type CBS enzymatic activity in the yeast *S. cerevisiae* model and failed to complement the growth phenotype (W. D. Kruger & Cox, 1995). Therefore, patients with p.I278T usually had connective tissue and vascular defects.

Pathogenic missense CBS mutations inflicting homocystinuria were reported to reduce the enzyme's affinity for the PLP cofactor, resulting in less CBS enzyme-PLP saturation and thus impaired catalytic activity (Karim Zuhra et al., 2020). Yet, if the mutation is causing a moderate PLP affinity reduction, it can be rescued by pyridoxine supplementation. In contrast, mutations with significantly reduced affinity for PLP will not respond to pyridoxine supplement treatment. However, since the molecular mechanisms that confer pyridoxine responsiveness remain unclear, the lack of correlation between patients and data suggests potential benefits of pyridoxine supplementation that need to be confirmed.

One of the pyridoxine non-responsive CBS mutations is p.R336C (c.1006C>T), located in exon 11 of the *CBS* gene. Indeed, Arginine (Arg; R) residues account for almost 15% of missense mutations in genetic disorders, and interestingly, more than half of these missense mutations lead to Arg to Cysteine (Cys; C) substitutions (Gallego-Villar et al., 2017). The human CBS contains 28 Arg residues, of which five present pathogenic R>C substitutions. Remarkably, the p.R336C variant is the highest prevalent pathogenic R>C substitutions in CBS-deficient patients in Qatar (El Bashir,

Dekair, Mahmoud, & Ben-Omran, 2014). This demonstrated a founder effect of p.R336C mutation, in combination with the high consanguineous marriage incidence. The p.R336C mutation was first reported in a patient of English descent (Raffaella de Franchis, Eva Kraus, Viktor Kozich, Gianfranco Sebastio, & Jan P Kraus, 1999). Later, it was reported in patients from Australia (Gaustadnes et al., 2002), the Iberian Peninsula (R. Urreizti et al., 2003) and Korea (S. J. Lee et al., 2005). Although p.R336C mutation has recurred independently in different populations, no apparent link could establish a clear relationship between this mutation in the Qatari population and other countries. Therefore, it demonstrates the strong founder effect of the p.R336C mutation and makes the Qatari population an excellent study model for this mutation.

Clinical diagnosis and disease detection

The clinical manifestation of untreated homocystinuria patients depends on mutation type and severity (Keller et al., 2019). The delayed diagnosis would decrease the likelihood of optimal development and increase the risk of multisystem consequences. Thus, disease management and treatment could cost more than the early detection of CBS patients. Clinically, homocystinuria patients exhibit numerous manifestations due to the disruption of many organ systems development. CBS patients have adverse effects that usually affect four main target systems. These include mental retardation (brain), lens dislocation (eyes), osteoporosis (bones), and arterial and venous thromboembolism (blood clotting system). Other clinical manifestations include myopia, psychiatric disturbances, Marfanoid habitus, and other mental and skeletal deformities (Al-Dewik et al., 2019). The initial observation of homocystinuria occurred in Northern Ireland in 1962, where affected patients exhibited symptoms of mental retardation (N. A. Carson & Neill, 1962). Subsequent investigations identified CBS enzyme deficiency as the underlying cause of this condition (S. H. Mudd et al.,

1964). Since its discovery, significant advancements have been made in the diagnosis of homocystinuria.

7.1 Newborn Screening programs

Although there are variabilities in homocystinuria diagnosis and management among countries worldwide, it is mainly diagnosed based on the patient's clinical manifestations and routine metabolic testing. The analysis of amino acids in both the plasma and urine will show a frequent elevation of homocysteine (>100 µmol/L) and methionine (>50 µmol/L). Since early diagnosis and prompt treatment are essential for improved prognosis, many countries have implemented newborn screening (NBS) programs for numerous metabolic disorders, including homocystinuria. NBS was first implemented in the 1960s for phenylketonuria (PKU), a single inborn error of metabolism resulting in the accumulation of phenylalanine. Subsequently, it led to irreversible brain damage (Matern, Tortorelli, Oglesbee, Gavrilov, & Rinaldo, 2007). Since the NBS improved the prognosis of PKU patients, additional inborn error of metabolism disorders were included in the NBS program. The screening was initially based on the bacterial inhibition assay to identify specific metabolite accumulation. Eventually, other laboratory techniques, such as tandem mass spectrometry (MS/MS), were adopted and implemented.

Numerous studies have proposed to adopt two-tier screening approaches (Gramer et al., 2017; Huemer et al., 2015; Matern et al., 2007; Okun et al., 2016; Tortorelli et al., 2010; Turgeon et al., 2010). These consist of assessing the primary markers in the first step, which include elevated methionine and/or methionine-to-phenylalanine ratio from dried blood spots (DBS). Subsequently, the second step is assessing the total homocysteine level, which many countries have adopted within the screening program. For instance, Qatar is considered an international pioneer for NBS

for homocystinuria (Wiley, Webster, & Loeber, 2019). In the early 2000s, Qatar declared that the NBS program is a priority, accepting the need for enabling legislation, funding, and recruiting adequate personnel. In 2006, NBS for homocystinuria was performed by measuring total homocysteine. Consequently, introducing this newly established screening program has extensively helped in the early detection of newborn cases. The prenatal genetic service was then established in 2013 as part of Clinical and Metabolic Genetic services to meet further the needs of the Qatari population (Elsaid et al., 2007; Gan-Schreier et al., 2010; Zschocke et al., 2009).

Nowadays, the national NBS program consists of both molecular and biochemical screening approaches. These include combining tandem mass spectrometry with HPLC to quantify the total homocysteine in DBS. Besides, they developed an improved strategy for the NBS panel in Qatar, where the total homocysteine is assessed as a primary marker and other metabolites from tandem-mass spectrometry screening as secondary markers (Gramer et al., 2017). The two-tier strategy showed 100% specificity and sensitivity in homocystinuria NBS (Okun et al., 2016). In addition, rapid high-throughput genetic screening has also been introduced to detect CBS gene mutations identified in the Qatari population (El-Said et al., 2006). Implementing screening programs has greatly facilitated the timely identification of newborns with homocystinuria. The prevalence of the condition in Qatar can be attributed to all identified cases being homozygous for the founder p.R336C mutation, coupled with the high rate of consanguinity within families. (El-Said et al., 2006; Gan-Schreier et al., 2010; Lindner et al., 2007).

Current and potential treatment approaches

The clinical aim of treating an enzyme deficiency metabolic disorder is to limit the intake and prevent substrate formation, eliminate any toxic intermediate metabolites, provide more of the product, and try to increase the enzymatic activity (B.

Wilcken, 2017). The initial attempts to treat classical homocystinuria were to lower the plasma methionine and homocysteine levels and keep them close to the normal level as possible. Therefore, a methionine-restricted diet and administration of pyridoxine and folic acid supplements are considered effective therapy. In fact, these supplements enhanced the residual activity of the CBS enzyme in more than half of the patients (Longhi, Fleisher, Tallan, & Gaull, 1977). However, their therapeutic effect was not observed in homocystinuria patients with pyridoxine non-responsive mutations such as the p.R336C (El-Said et al., 2006). To date, there is no curative treatment for homocystinuria. Yet, the therapeutic approaches below could be promising alternative treatments for homocystinuria patients.

8.1 Pyridoxine supplements

Pyridoxine (vitamin B6) is one of the eight water-soluble B vitamins essential to the highly optimized brain and essential for all life forms. Vitamin B6 is involved in the folate cycle and synthesizes the neurotransmitters serotonin, norepinephrine, and dopamine. In addition, vitamin B6 protects the blood-brain barrier (BBB) by regulating the homocysteine levels. Excess homocysteine can damage blood vessels lining and neurons, resulting in cognitive decline. Pyridoxal-5'-phosphate (PLP) is the intracellular active form of vitamin B6 and contributes to controlling the inflammation in the brain. Therefore, severe inflammation in the brain that could result in neurodegenerative diseases such as Alzheimer's and Parkinson's is associated with low levels of PLP. Under normal conditions, vitamin B6 is a cofactor and critical component for synthesizing all neurotransmitters. Besides, it acts as a coenzyme for various apoenzymes involved in the biosynthesis, interconversion, and degradation of amino acids (N. Carson & Carre, 1969).

There are three forms of PLP, pyridoxine, pyridoxal, and pyridoxamine, which could be obtained from the diet (**Figure 4**). Once absorbed, they will be transported to

the hepatic cells (Medscape, 2016). The pyridoxal kinase phosphorylates the hydroxyl group on the molecule using the phosphate from the ATP to generate pyridoxine-5'-phosphate. With the help of pyridoxine oxidase, the latter will be oxidized and converted into pyridoxal-5'-phosphate (PLP). Pyridoxal obtained from the diet will be converted to PLP with the one-step reaction of phosphorylation with the help of pyridoxal kinase. Once PLP is obtained, it will be fully activated through the ligation with PLP-dependent enzymes. These enzymes use the lysine residue on their structure to form a shift base linkage in the PLP structure and make it active and ready to be involved in PLP-dependent reaction mechanisms. PLP could remain in the hepatocyte and bind to an apoenzyme or will be released into the serum and bound tightly to albumin. Excess PLP could be converted back to pyridoxal through phosphate removal by pyridoxal phosphate phosphatase.

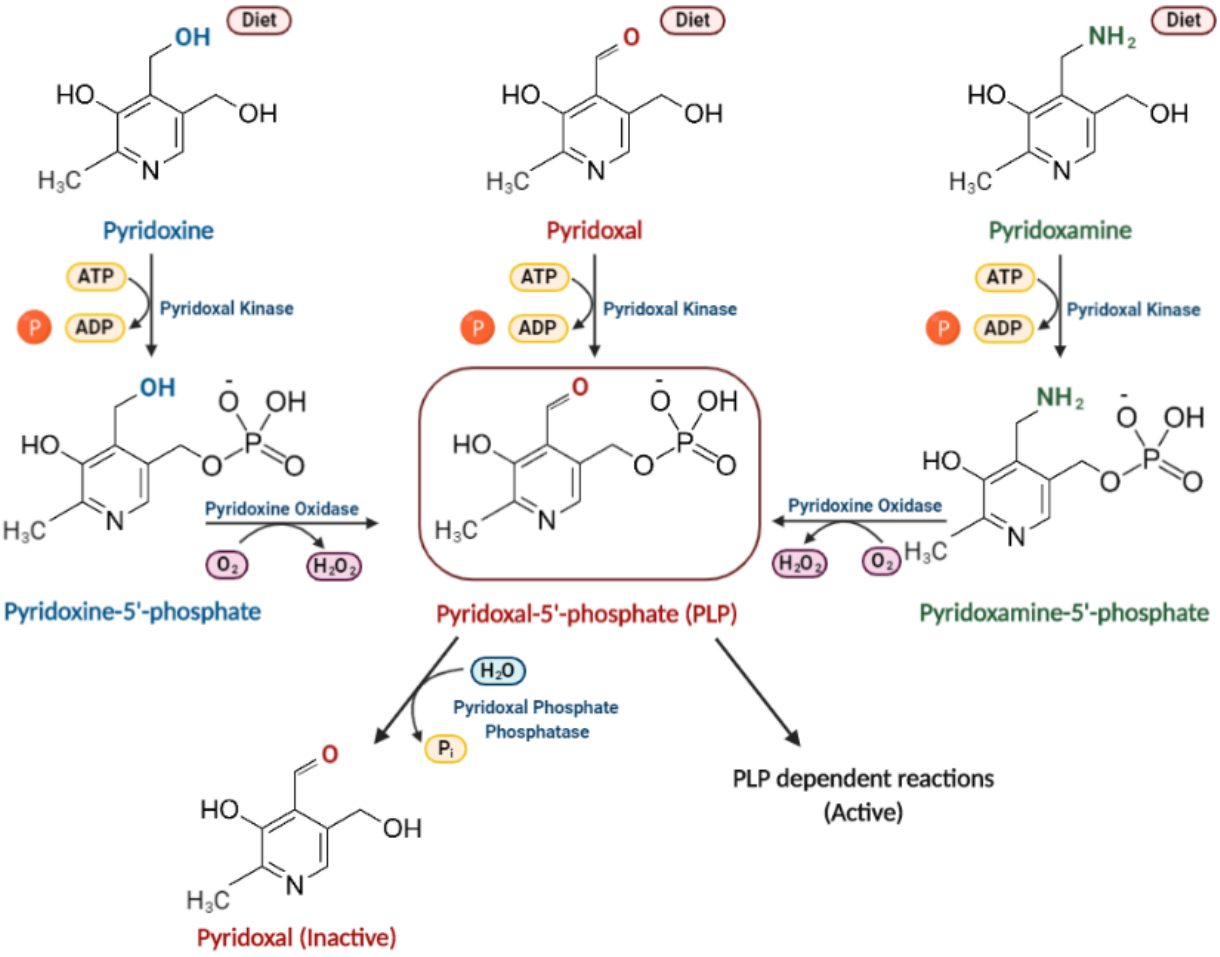

Figure 4. Pyridoxal-5’-phosphate (PLP) metabolism and pathway in mammalian cells.

Homocysteine metabolism depends on pyridoxine as a cofactor; consequently, high levels of homocysteine could result from pyridoxine deficiency (Medscape, 2016). Therefore, administering high doses of pyridoxine significantly decreased the plasma homocysteine level in approximately 50% of the patients with homocystinuria (S. H. Mudd, Edwards, Loeb, Brown, & Laster, 1970). In fact, a study showed that oral administration of pyridoxine significantly lowered the plasma homocysteine level in half of the patients (B. Wilcken, 2017). The pyridoxine dosage ranges from 100 to 500 mg daily and could be administered with folic acid (1-5 mg per day) to avoid folate depletion (Schiff & Blom, 2012). Pyridoxine has been reported to be a successful treatment for homocystinuria since 1967 (Barber & Spaeth, 1967). Three homocysteine patients were administered pyridoxine hydrochloride daily. Results showed reduced plasma methionine, and homocysteine was eliminated from both plasma and urine. Later, a study conducted in 1969 showed that 54% of the recruited patients responded to pyridoxine treatment, and their plasma amino acid pattern returned to almost normal (N. Carson & Carre, 1969).

Similarly, a study reported the responsiveness of 54% of homocysteine patients to pyridoxine with a reduced serum methionine level and the complete disappearance of homocysteine from the serum (Cusworth & Dent, 1969). However, two patients showed an intermediate response to treatment with lowering serum methionine and homocysteine levels, and three were non-responsive. Another study reported pyridoxine responsiveness in only 14% of homocystinuria patients (Poloni et al., 2018).

This suggested that other homocysteine-lowering strategies are required for pyridoxine-nonresponsive patients, such as a low-methionine diet, vitamin B12, folic acid, and betaine (S. Mudd et al., 2001). In fact, a study conducted on 158 homocystinuria patients aimed to explore the effectiveness of long-term homocysteine-lowering treatments on cardiovascular risk. CBS-deficient patients treated with

different combinations of low-methionine diet, pyridoxine, betaine, folic acid, and vitamin B12 showed a substantial improvement in vascular outcome (Yap et al., 2001). Yet, the level of circulating homocysteine remained moderately elevated in most patients. Besides, the level was three to five times above the normal limit in pyridoxine-nonresponsive patients. Indeed, some studies showed that high doses of pyridoxine treatment could have deleterious adverse effects, such as peripheral neuropathy (Clayton, 2006).

Additionally, CBS mutations result in different responses to pyridoxine and associated doses. For instance, 10-40 mg of pyridoxine can achieve the desired biochemical targets in some homocystinuria patients with the p.I278T and p.P49L mutations (Stabler et al., 2013). Though, higher doses are required for partially pyridoxine-responsive homocystinuria patients. It is worth mentioning that the in vivo response to pyridoxine treatment does not correlate with the in vitro response in many cases (Yap, 2012). The extent of responsiveness to pyridoxine is difficult to assess; hence, calculating the precise dose of pyridoxine for each patient might be challenging. Therefore, this disease requires the development of more efficient therapeutic approaches, especially since pyridoxine-nonresponsive patients could present more severe clinical phenotypes and complications.

8.2 Molecular and Chemical Chaperones

Protein homeostasis is a delicate balance of the protein cycle, including synthesis, proper folding, trafficking and degradation. Protein folding is a fundamental process in the routine operations of cells and involves a range of molecular chaperones and enzymes. Yet, under stress conditions, such as heat, toxins, oxidative stress, or chemicals, proteins may lose their proper folding and confirmation (Ciechanover & Kwon, 2017). Therefore, the protein quality control system ensures that proteins are folded appropriately and any cytotoxic agent is eliminated promptly. The process

occurs mainly in the endoplasmic reticulum, where misfolded proteins are either corrected or enter the ubiquitin-proteasome pathway for degradation (Nature, 2020). Misfolded protein accumulation is toxic for the cell and will cause endoplasmic reticulum stress (Adams, Kopp, Larburu, Nowak, & Ali, 2019). Consequently, the unfolded protein response (UPR) cell signalling is activated.

The UPR principle targets restoring the normal endoplasmic reticulum function through different strategies (Bravo et al., 2013). For instance, the expression of endoplasmic reticulum chaperone will increase to correct the protein folding and prevent aggregation. In addition, the protein translation mechanism will be temporarily inhibited. Moreover, the endoplasmic reticulum-associated protein degradation (ERAD) process will be activated to degrade the misfolded proteins. Besides, three different endoplasmic reticulum stress pathways, IRE1α, PERK, and activating transcription factor (ATF6) will be initiated, leading to the upregulation of chaperone proteins expression.

Both molecular and pharmacological chaperons are considered the core of revolutionary therapeutic approaches for protein misfolding disorders (Gámez et al., 2018). Molecular chaperones play a vital role in protein quality control systems. One of the conserved families of molecular chaperones are the heat shock proteins (Hsps) and they are classified according to the molecular weight (Hsp100, Hsp90, Hsp70, Hsp60, Hsp40, and the small Hsp) (Gámez et al., 2018; Gorenberg & Chandra, 2017). The key roles of Hsps are assessing the proper folding of the newly synthesized protein, preventing protein aggregation, and facilitating the degradation of damaged proteins. Yet, the imbalance in protein homeostasis and excessive formation of aggregated proteins are crucial to disease onset and progression in many metabolic disorders. Therefore, molecular chaperones were proposed to effectively treat misfolded protein disorders such as homocystinuria. For instance, a study showed that the elevation of

Hsp70 aid in the correct folding of I278T CBS protein (L. R. Singh & Kruger, 2009). Similarly, another study aimed to restore the function of I278T mutated CBS using different treatments that could affect the intracellular chaperone environment (L. R. Singh, Gupta, Honig, Kraus, & Kruger, 2010). The study concluded that the induction of Hsp70 is necessary for treating missense mutations leading to disorders, but it is not sufficient. It also requires the help of chemical chaperones and proteasome inhibitors.

Recently, studies showed that chemical chaperones could have a therapeutic potential in minimizing the accumulation of misfolded proteins. Consequently, this will reduce the downstream pathological complications (D. W. Al-Sadeq & Nasrallah, 2020). For instance, pharmacological chaperones, (3-amino-2-benzyl-7-nitro-4-(2-quinolyl)-1,2-dihydroisoquinolin-1-one) and (5,6-dimethyl-3-(4-methyl-2-pyridinyl)-2-thioxo-2,3-dihydrothieno[2,3- d]pyrimidin-4(1H)-one), stabilized the functional tetrameric conformation of recombinant wild type and mutant PAH enzyme (Pey et al., 2008). Additionally, they substantially increased the activity of wild-type and mutant PAH protein *in vitro* cell culture and *in vivo* mouse models.

Regarding CBS, a study aimed to conduct a library screening for different drugs to rescue the growth defect of a yeast strain with human I278T CBS mutations (L. R. Singh, Chen, Kožich, & Kruger, 2007). Results showed dimethylsulfoxide (DMSO) folded the I278T mutant enzyme into a more active conformation. Consequently, it enhanced the enzyme activity and rescued the yeast growth on cysteine-free media. A similar effect was observed in glycerol, proline, trimethylamine N-oxide (TMAO), and sorbitol. Yet, the study concluded that increasing the dose of the abovementioned chemical chaperones could have an adverse effect and induce growth inhibition. Similarly, another study aimed to test three different compounds, heme arginate, aminooxyacetic acid (AOAA), and 4-phenylbutyric acid (4-PBA), to evaluate their ability to restore proper folding of mutant CBS in mammalian cells (Melenovská et al.,

2015). PBA is an FDA-approved chemical chaperone for urea cycle disorders (Uppala, Gani, & Ramaiah, 2017). It attenuates the endoplasmic reticulum stress and acts as an ammonia scavenger in urea cycle disorders (Vang, Longley, Steer, & Low, 2014). Yet results showed that 4-PBA and AOAA exhibited only a weak effect, while heme arginate significantly increased the formation of mutant CBS protein tetramers and the catalytic activity of p.R369C, p.R125Q, p.K102N, p.R266K, and p.A114V CBS mutations.

Shifting to *in vivo* models, a mouse model with CBS deficiency phenotype was generated and exhibited significantly elevated tissue and plasma levels of homocysteine, methionine, SAM, and SAH (Maclean et al., 2010). The study showed that betaine treatment significantly lowered the average total homocysteine levels in the mice. Betaine is an amino acid that was first discovered in sugar beets juice and could be found in many foods, including whole grains and spinach (Craig, 2004). The physiological roles of betaine are as a methyl donor in various biochemical pathways and act as an organic osmolyte in stress conditions to protect the cells ("Betaine. Monogragh," 2003). It was proposed that betaine deficiency could elevate the homocysteine level in the plasma. For instance, betaine supplements are used as a treatment option for homocystinuria patients (MedlinePlus, 2020). In a recent study where 125 homocystinuria patients were enrolled, results showed that betaine treatment caused a reduction of 29% in plasma homocysteine levels (Valayannopoulos et al., 2019). It was shown that betaine uses an alternative pathway to convert homocysteine into methionine and is considered to be effective in pyridoxine non-responsive homocystinuria patients (D. E. Wilcken, Dudman, & Tyrrell, 1985). Yet, a study was conducted using knock-in p.R336C mutation in the HEK293T cell line, attempting to rescue the defective activity of the CBS enzyme (Ismail et al., 2019).

Different chaperones (betaine, proline, sorbitol, and glycerol) were used to treat the cells with different concentrations. Interestingly, betaine restored the structural defect of the p.R336C protein in vivo, yet not the activity of the p.R336C mutation. Similarly, in a study where δ-aminolevulinic acid (δ-ALA) was used on 27 different CBS mutants, four mutants showed an increased formation of CBS tetramers, and 14 mutants showed an increase in the enzymatic activity (Kopecka, Krijt, Rakova, & Kozich, 2011). It is worth mentioning that aminothiols, such as cysteamine, were also proven to hold a potential clinical promise to target different genetic disorders with arginine to cysteine mutations (Gallego-Villar et al., 2017).

8.3 Proteasome inhibitor

Additional treatment approaches include the administration of protein stabilizing and proteasome inhibitors to prevent the early degradation of mutated CBS protein (D. W. Al-Sadeq & Nasrallah, 2020). For instance, bortezomib is the first therapeutic proteasome inhibitor to be tested in humans (Bank, 2020). It is currently approved for treating leukemia and myeloma (Field-Smith, Morgan, & Davies, 2006). Besides, bortezomib was tested on a transgenic mouse lacking expressing p.R266K human CBS mutation (Tg-R266K Cbs−/−) aiming to rescue the protein folding and activity (Gupta, Wang, & Kruger, 2017). Results showed a 97% reduction in plasma homocysteine after treatment with bortezomib and a 2381% increase in liver CBS activity. They performed a similar experiment on another transgenic mouse model with p.R336C CBS mutation (Tg-R336C Cbs-/-). Mice that were treated with bortezomib showed increased amounts of liver CBS protein. Lysates from these livers indicate that the bortezomib stabilized enzyme has activity levels similar to the hCBS but, surprisingly, only had a modest effect on lowering total homocysteine.

To understand why total homocysteine was still elevated in bortezomib-treated animals, they examined the response of the enzyme to serine and homocysteine concentrations (Km) and the enzyme's requirement for PLP. Results showed that the Km for serine was significantly higher in CBS^{R336C} compared to hCBS, but the Km for homocysteine was unaffected. Additionally, the CBS^{R336C} was entirely dependent on adding exogenous PLP to the in vitro enzyme reaction, while the wild-type hCBS was fully active in the absence of PLP. Based on these findings, they hypothesized that the p.R336C alteration expressed in the liver causes a misfolding of the enzyme, which makes it less stable and subject to increased protein turnover. In addition, they hypothesized that the misfolded protein holds on to the PLP-serine complex (the first step in the reaction mechanism) less tightly than the wild-type enzyme. From these findings, we speculated that combining serine, pyridoxine, and proteasome inhibitors might effectively lower total homocysteine in Tg-R336C Cbs-/- mice.

Chapter 3: Materials and Methods

3.1 Ethical Compliance

This work was done under Qatar University/ Institutional Biosafety Committee (IBC) approval QU-IBC-2022/049. No human or animal samples were used during this study.

3.2 Construction of CBS^{WT} and site-directed variants

Human CBS (NCBI Reference Sequence NM_000071.2) in pLW2:hCBS was used to amplify the full length *CBS* gene using a standard polymerase chain reaction (PCR) protocol. A pair of primers was utilized, with the forward primer containing the NdeI restriction site and the reverse primer containing the XhoI site. Following amplification, the PCR product was purified via agarose gel electrophoresis and subsequently digested with NdeI and XhoI restriction enzymes. The resulting digested PCR fragment was then ligated into a pET-28a vector, previously digested with the same restriction enzymes. Verification of gene integration within the vector was confirmed through DNA/Sanger sequencing. Additionally, several mutants were generated using site-directed mutagenesis techniques by using an overlap extension PCR method with suitable primers. (**Table 1**). The amplified mutants were cloned into pET-28a vector, similarly to the cloning of WT. The vector encodes an N-terminal 6-His tag.

Table 1. Oligonucleotides used for the site-directed mutagenesis reaction

CBS variant	DNA change	Primer	Sequence (5'-3')
p.Arg336Cys	c.1006C>T	R>C336 F	5'-CAGTCATATGCCTTCTGAGACCCCCCA-3'
		R>C336 R	5'-GATACTCGAGTCACTTCTGGTCCCGCTC-3'
p.Thr236Asn	c.707C>A	T>N236 F	5'-AATCCATTGGCTCATTACGATACTAACGC AGACGAAATTTTGCAACAGTGC-3'
		T>N236 R	5'-GCACTGTTGCAAAATTTCGTCTGCGTTAG TATCGTAATGAGCCAATGGATT-3'
p.Gly153Arg	c.457G>A	G>R153 F	5'-AACCAACTTCCGGTAATACCGGTATTAGA TTAGCATTAGCAGCAGCAGTTAGAGG-3'
		G>R153 R	5'-CCTCTAACTGCTGCTGCTAATGCTAATCTA ATACCGGTATTACCGGAAGTTGGTT-3'
p.Lys72Ile	c.215A>T	K>I72 F	5'-CCACATCATCATACAGCTCCAGCTATATC CCCAAAGATTTTGCCAGACATC-3'
		K>I72 Rs	5'-GATGTCTGGCAAAATCTTTGGGGATATAG CTGGAGCTGTATGATGATGTGG-3'
p.Leu230Gln	c.689T>A	L>Q230 F	5'-ATTTTGTTTAACTTTAAGAAGGAGATATA CCATGGGCAGCAGCCATCATCATCATC-3'
		L>Q230 R	5'-TGTTAGCAGCCGGATCTCAGTGGTGGTGG TGGTGGTGCTCGAGTTCACTTCTGGTCCCGCTC CTGG-3'

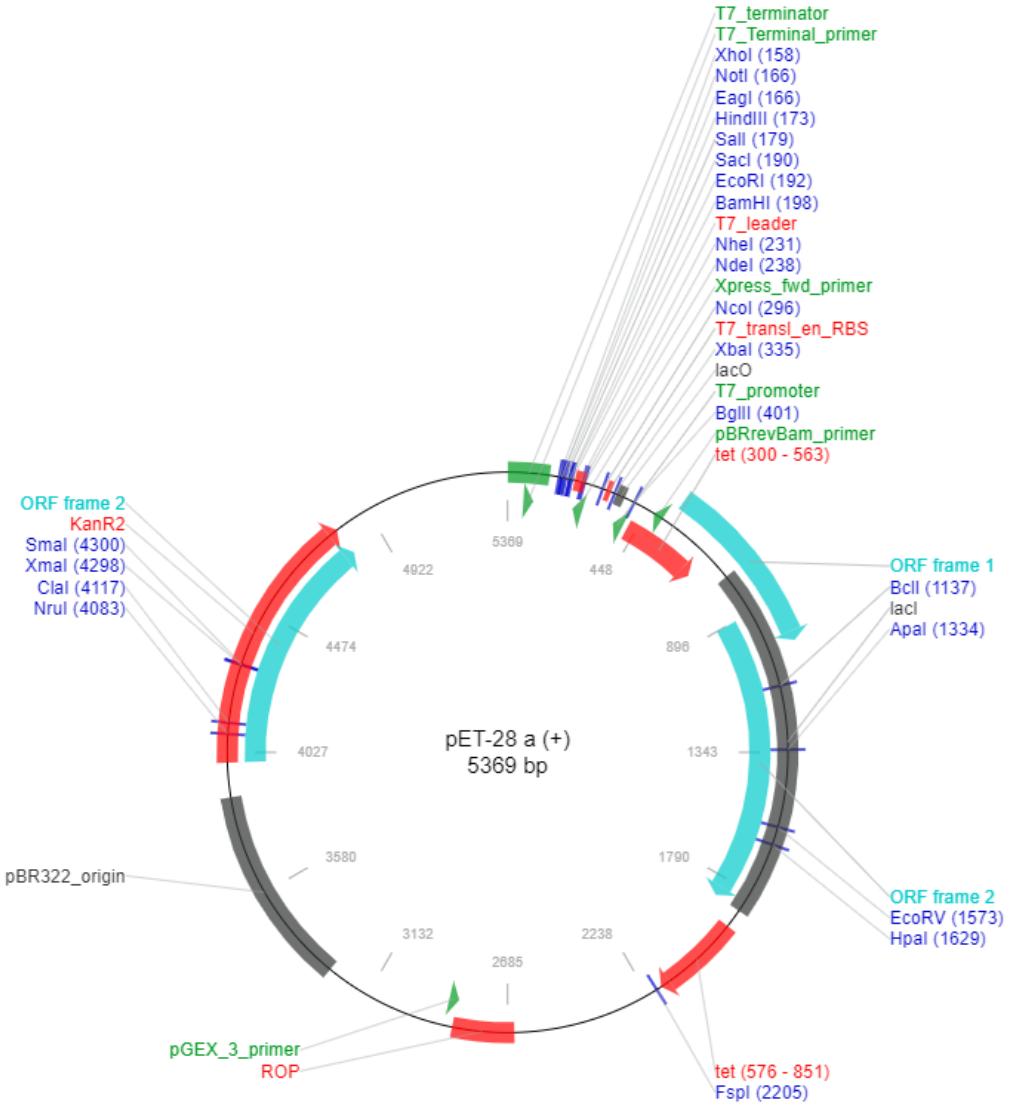

Figure 5. Schematic representation of the pET28b vector. The figure shows the: Multiple Cloning Site (MCS), T7 promoter, six CAT codon sequence, thrombin cleavage site, Ribosome Binding Sequence (RBS) and the start ATG codon [adapted from (Addgene, 2024)].

The mutagenesis reaction was conducted using the buffer provided by the manufacturer, with a final volume of 50 µl comprising 125 ng of each primer, dNTP mix, 50 ng of template DNA, and 2.5 U of PfuUltra HF DNA polymerase. DNA amplification was carried out using a PCR Express Thermocycler (Hybaid) with the template program outlined in Table 3. Adjustments to the hybridization temperature (62ºC) and elongation temperature (72ºC) were made in step 2 as needed, based on the Tm of the primers. Subsequently, DpnI was utilized to degrade the parental methylated DNA (wild type), and the amplified product was introduced into competent *E. coli* cells.

Table 2. Amplification program utilized for site-directed mutagenesis

Step	Number of cycles	Temperature (ºC)	Time (min)
1	1	95	2
2	12	95	1
		68	1
		72	1.5/kb DNA template
3	1	68	15

Later, the plasmid was transformed into TOP10 bacterial competent cells. The transformed cells were grown on LB agar supplemented with kanamycin (50mg/ml). After incubation overnight at 37ºC, three isolated colonies (one in each tube) were chosen to inoculate 10mL of LB/Kan, which was further incubated overnight at 37ºC, under constant stirring of 200 RPM. The bacterial culture was used to obtain a cellular pellet from which the plasmid DNA was purified using Miniprep. Successful mutagenesis was confirmed by Sanger sequencing (Applied Biosystem 3500xL DX Genetic Analyzer), and additional mutational events were excluded.

3.3 Expression of CBS^{WT} and variants in *Escherichia coli*

The pET28a vector presents upstream the multiple cloning site (MCS): (1) the T7 promoter recognized by the RNA polymerase of *E. coli* phage 7; (2) a sequence of six CAT codons encoding a small peptide chain of six histidine residues (6xHis Tag); (3) a thrombin cleavage site positioned after the 6xHis Tag and before the start codon of the recombinant protein, facilitating the removal of the 6xHis Tag; (4) a ribosome binding site (RBS) sequence; and (5) the start ATG codon. Additionally, the vector includes the T7 terminator downstream of the cloned CBS cDNA, the LacI gene sequence for efficient promoter repression by the lac repressor, and the kanamycin resistance gene for selection of the vector using the appropriate culture medium.

CBS^{WT} and variants constructs were transformed in competent *E. coli* [BL21-CodonPlus (DE3)-RILP; Stratagene] cells by heat shock method. To produce the recombinant CBS proteins, 100mL of LB/Kan was inoculated with an isolated colony. After overnight growth, at 37ºC, under constant stirring of 200 RPM, the culture was used to inoculate 5L of LB/Kan. The culture was incubated at 37ºC, under a constant stirring of 200 RPM, until the OD600 reached 0.5-0.6. Protein expression was induced for 18 hours at 16°C with 0.1mM IPTG (isopropyl β-D-thiogalactopyranoside).

Bacterial cell pellets were harvested by centrifugation at 6,000 g for 15 minutes at 4°C. Recombinant CBS proteins were then purified as described below or stored at -80ºC for further assays and analysis.

3.4 Purification of Recombinant CBS Proteins

Affinity chromatography is a technique used for the selective isolation and purification of enzymes, capitalizing on their inherent ability to bind ligands specifically and reversibly. The method involves passing the protein of interest through a column containing a solid polymer or gel linked to a specific competitive inhibitor or ligand. Proteins with weak binding to the ligand will flow through the column, while those binding to the inhibitor will be retained based on their affinity constant under the given conditions. In this study, recombinant proteins are tagged with a 6xHis tag at the N-terminus, which has a strong affinity for Ni2+ ions, facilitating protein purification through immobilized metal affinity chromatography using a Ni2+-chelating resin. To isolate the expressed proteins, a pellet of *E. coli* BL21 (DE3) cells was suspended in 200 mL of lysis buffer (25 mM Tris HCl pH 8.5, 500 mM NaCl, 20 mM Imidazole, 2 mM β-Mercaptoethanol, 2% glycerol) and then the addition of 1 mM phenylmethylsulfonyl fluoride (PMSF), 1 ml of DNAse, and 500 µl protease inhibitors. This is followed by ultra-sonication for 10 minutes. The cell lysate was centrifuged at 19,000 RPM, for one hour, at 4ºC, obtaining an insoluble (pellet) and a soluble (supernatant) fraction.

A total of 10µl of the supernatant was kept apart for a Sodium Dodecyl Sulphate-Polyacrylamide Gel Electrophoresis (SDS-PAGE) gel run. A total of 25 ml of equilibrium buffer (25 mM Tris HCl pH 8.5, 500 mM NaCl, 20 mM Imidazole, 2% glycerol) was passed through the Ni-NTA column to make sure the pH of the beads was the same as the lysis buffer. The supernatant was then loaded into a Ni-NTA

column and 10µl of the flow-through was collected for the SDS-gel. This was followed by loading 25ml of wash buffer 1 (25 mM Tris HCl pH 8.5, 500 mM NaCl, 20 mM Imidazole, 2 mM β-Mercaptoethanol, 2% glycerol) and 25 ml of wash buffer 2 (25 mM Tris HCl pH 8.5, 500 mM NaCl, 30 mM Imidazole, 2 mM β-Mercaptoethanol, 2% glycerol). Finally, 20 ml of elution buffer (25 mM Tris HCl pH 8.5, 150 mM NaCl, 300 mM Imidazole, 2 mM β-Mercaptoethanol, 2% glycerol) was loaded, and flow-through containing the recombinant proteins was collected. Overnight dialysis using 1xPBS was performed at 4˚C to remove imidazole and exchange buffer to physiologic buffer. Then, the BCA assay was used to estimate protein concentration. When necessary samples were concentrated by ultrafiltration using an Amicon Ultra 15 centrifugal filter device (MWCO 30 kDa). The samples were centrifuged at 4000 rmp, for 30 minutes, at 4ºC until a final volume of approximately 1 mL. The solution was softly resuspended between each centrifugation to desorb protein that might accumulate at the filter membrane. The obtained protein was stored at -80ºC.

3.5 SDS and Native polyacrylamide gel electrophoresis

SDS-PAGE is a method for separating proteins according to their molecular weights. It works by placing polyacrylamide gels on a horizontal slab and running an electric current through the gel, with applied voltage determining the mobility of the proteins and hence their final separation at different locations on the gel. When proteins are mixed with an equal amount of SDS, its negative charge disperses the proteins and helps them mix evenly. SDS binds to hydrophobic regions leading to their unfolding and dissociation from other molecules. The larger proteins get separated from smaller ones during electrophoresis because both are negatively charged.

SDS-PAGE typically comprises a stacking gel and a resolving/separating gel, with the percentages of the resolving gel adjusted according to the size of the protein

being analyzed. In our investigation, a resolving gel of 12% and a stacking gel of 4% were formulated. Ammonium persulfate (APS) and tetramethylethylenediamine (TEMED) were used to catalyze the gel polymerization. Approximately 20 µg of each cell lysate was denatured using Laemmli SDS Sample Buffer supplemented with β-mercaptoethanol, and then heated at 95°C for five minutes before loading. Electrophoresis was performed for 15 minutes and then increased to 140 V for approximately one hour in electrophoresis running buffer 25 mM Tris, 192 mM glycine, 0.1% SDS, pH 8.3 (Bio-Rad #1610732). Thermo Scientific™ PageRuler™ Prestained Protein Ladder (Ref. #26616) served as a marker for estimating the molecular mass of the recombinant proteins. After electrophoresis, the proteins were visualized by staining with Brilliant Blue Coomassie stain.

Native polyacrylamide gel electrophoresis is used under non-denaturing conditions, followed by Western blotting to assess the oligomeric structure of the protein. Samples were subjected to electrophoresis under non-denaturing conditions using Laemmli buffer system without SDS.

3.6 Biochemical and Biophysical Characterization of CBS Recombinant Proteins

3.6.1 Molecular Dynamics Simulations

To investigate the impact of the mutations on the CBS structure, molecular dynamics simulations were performed using the GROMACS 2019.2 software (Abraham et al., 2015; Berendsen, van der Spoel, & van Drunen, 1995) along with the GROMOS96 43a1 force field (van Gunsteren et al., 1996). The structural templates used for the molecular dynamics (MD) simulations were based on the Alphafold predicted structure for the human CBS protein (Entry P35520) (Jumper et al., 2021). The CBS variants were prepared using the mutation tool in Swiss PDB Viewer 4.1 software (Guex & Peitsch, 1997), followed by energy minimization. All proteins were

solvated in a cubic box of 10 nm size using the SPC water model and NaCl was added to neutralize the total charge of each system. The resulting models were adjusted using a conjugate gradient algorithm followed by steepest descent minimization with a default tolerance value of 100 kJ/mol for a maximum of 10000 steps. All systems were equilibrated at 300 K for 1000 ps with a two-step ensemble process (NVT and NPT). As a first step, the Berendsen thermostat (Berendsen, Postma, Van Gunsteren, DiNola, & Haak, 1984) with no pressure coupling was used for the NVT (constant number of particles, volume, and temperature) equilibration phase, followed by the Parrinello–Rahman method (Bussi, Donadio, & Parrinello, 2007) with a constant pressure of 1 bar (P) for the NPT ensemble (constant number of particles, pressure, and temperature). Finally, the equilibrated system was subjected to 50 ns MD simulation with a time step of 5 fs, using a leap-frog integrator for the time evolution of trajectories.

3.6.2 CBS Enzyme Activity

3.6.2.1 CBS Assay Kit

The enzyme activity of purified recombinant WT CBS and mutant proteins was determined in a reaction volume of 200 µl, as described (Abcam, 2021), with some minor modifications. Briefly, 0.27µg of the CBS^{WT} or mutant proteins were incubated in a master mix mixture containing CBS assay buffer, CBS substrate, probe, and cofactors provided by the kit. The assay was carried out in a black 96-well plate with a clear flat bottom. The reaction was started by the addition of 30 µl of different protein concentrations (0.1µg, 0.5µg, 1µg, 2.5µg, 5µg) in the well with 170 µl of master mix. The fluorescence was measured immediately at excitation/emission 368/460 nm in kinetic mode for 40-60 minutes at 37°C. Specific enzyme activities were expressed as U/ml (the amount of enzyme that generates 1nmol of 7-amino-4-methylcoumarin per minute in pH 8.0 at 37°C).

3.6.2.2 High-Performance Liquid Chromatography (HPLC)

HPLC analysis was performed using a Jasco LC-4000 HPLC system with a FP-4020 fluorescence detector as reported in (Conter et al., 2022; Fernández-Rodríguez et al., 2023). The production of L-Cth was analyzed by incubating CBS variants (10 μM) with 1 mM L-Ser (or L-Cys) and 1 mM L-Hcys for 2 h at 37°C. After removal of the enzyme by centrifugation (Vivaspin Turbo centrifugal concentrator, Sartorius), dansyl chloride was added 2:1 to the sample solutions. After a 30-min derivatization reaction at 25°C, 20 μL of the mixture was injected onto a C-18 RP column (Agilent Poroshell 120 HPH RP-C18, 4 μm, 4.6 × 250 mm). The derivatized products were eluted at a flow rate of 1 mL/min at 40°C with a mobile phase of 33.25/66.75 (v/v) methanol/water containing 0.008% (v/v) triethylamine and 0.6% (v/v) glacial acetic acid. The excitation of the fluorescence detector was set at 335 nm and emission at 522 nm.

3.6.2.3 Lactate-dehydrogenase (LDH) coupled-coupled assay

The canonical activity of CBS variants was assessed using the continuous cystathionine β-lyase (CBL) and lactate-dehydrogenase (LDH) coupled-coupled assay as described in (Aitken & Kirsch, 2003; Conter, Favretto, Dominici, Martinez-Cruz, & Astegno, 2023) using a Jasco V750 spectrophotometer in a final volume of 200 μL at 37 °C and pH 8.6. The reaction mixture contained 20 μM PLP, 0.2 mM NADH, 1.8 μM LDH, 1.5 μM CBL, 0.1–7 μM CBS variants and 2 mM L-Hcys. The reaction was initiate by the addition of 1–30 mM L-Ser and, subsequently, the oxidation of NADH was monitored at 340 nm (**Figure 6**). Where indicated, the assay was performed in the presence of 0.5 mM SAM.

Figure 6. The assay for detection of the CBS-catalyzed condensation of L-Ser and L-Hcys. It involves the utilization of the CBL coupling enzyme, which converts cystathionine to

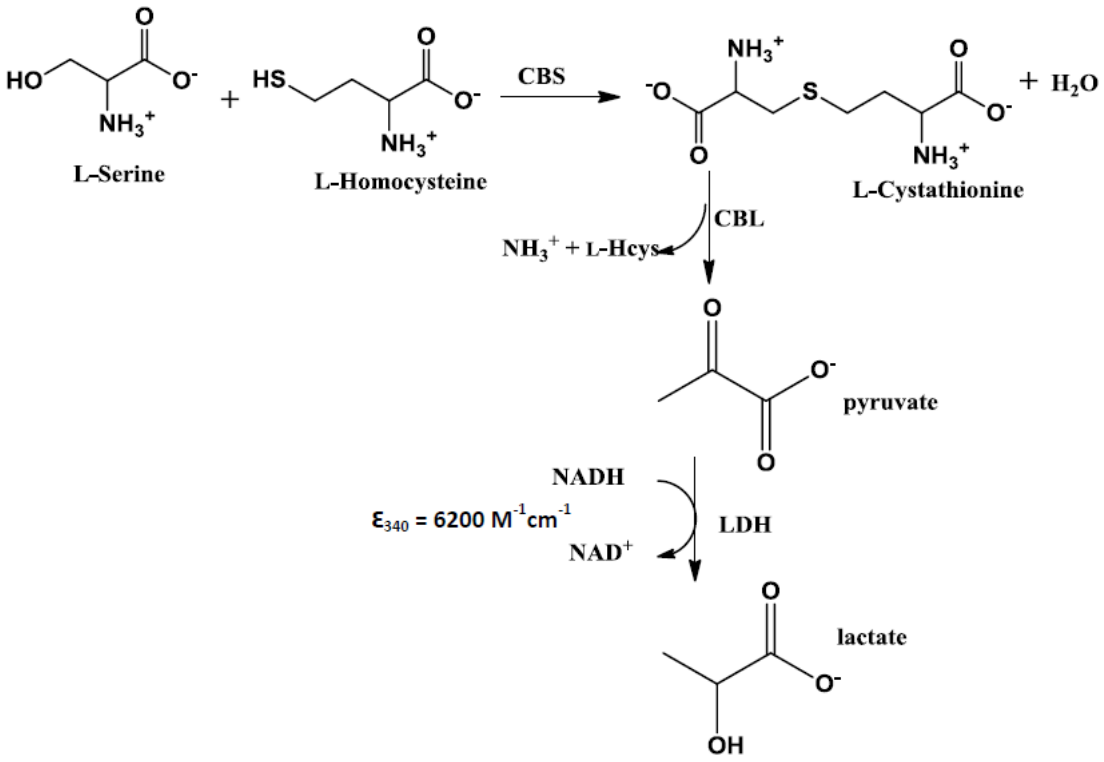

homocysteine, NH3+, and pyruvate. The pyruvate is then reduced to lactate by LDH, accompanied by the oxidation of NADH to NAD+, which is monitored at 340 nm ($\Delta\varepsilon_{340}$ = 6,200 $M^{-1}cm^{-1}$) (Aitken & Kirsch, 2003).

3.6.2.4 Lead acetate assay

The production of H_2S was determined following the formation of lead sulfide at λ = 390 nm (ε_{390} = 5500 M^{-1} cm^{-1}) as described in (C. Conter et al., 2020) at 37°C in

presence of 1-30 mM L-Cys and 2 mM L-Hcys. The composition of the reaction mixture consisted of a 50 mM Hepes buffer solution with a pH of 7.4. Additionally, it contained 20 μM pyridoxal-5'-phosphate (PLP), and 0.4 mM lead (II) acetate. Where indicated, the assay was performed in the presence of 0.5 mM SAM.

$$Pb(CH_3COO)_2 + H_2S \rightarrow PbS\ (precipitate) + 2CH_3COOH$$

3.6.3 Spectroscopic measurements

Absorption spectra were made using a Jasco V-750 UV-visible spectrophotometer in 20 mM sodium phosphate pH 7.5. CD measurements were conducted using a JASCO-1100 spectropolarimeter with a Peltier type cell holder, allowing temperature control. Wavelength scans in the far (195 to 260 nm) UV region were performed using Quartz SUPRASIL (HELLMA) precision cells of 0.1 cm path length. For each measurement, 250 μL of a 5 μM solution of protein sample in PBS buffer were loaded onto the cuvette. Each spectrum was obtained by averaging eight successive accumulations with a wavelength step of 0.2nm at a rate of 20 nm min^{-1}, response time 1s and bandwidth 1 nm. Buffer spectra were accumulated and subtracted from the sample scans. The results in all experiments have been expressed as molar ellipticity [θ] (deg cm^2 $dmol^{-1}$). The collected data were normalized as fraction of protein population in the unfolded state (fraction unfolded) according to the following equation:

$$f(T) = \frac{CD\ signal\ (T) - CD^{folded}}{CD^{unfolded} - CD^{folded}}$$

where f(T) and CD signal (T) are the fraction of the unfolded protein population and the measured CD signal at temperature T, respectively, while CD^{folded} and $CD^{unfolded}$ are the CD signals of the fully folded and fully unfolded protein populations, respectively. For a two-state transition, T_m is the temperature at which $f(T_m) = 0.5$.

For thermal denaturation experiments, the CD signal at 222nm was followed as

the sample chamber temperature was increased from 20 to 95°C using a step size of 0.5°C and at a rate of 1.5°C/min. For each measurement, 250 µL of a 5µM solution of protein sample in PBS buffer were loaded onto the cuvette. Buffer blank spectra, obtained in identical conditions, were subtracted from the raw data. The results in all experiments have been expressed as molar ellipticity change $\Delta[\theta]^{222\ nm}$ (deg cm^2 $dmol^{-1}$). The final spectra were analyzed using the CDNN program (Böhm, Muhr, & Jaenicke, 1992; Dalmas, Hunter, & Bannister, 1994).

3.6.4 Chemical denaturation

All steady state fluorescence intensity measurements were performed on a Horiba Fluoromax 4 spectrofluorometer (HORIBA Advanced Techno - Kyoto, Japan), equipped with a xenon short arc lamp (Ushio). The fluorescence emission spectra of all CBS variants were collected after injecting small aliquots of a dense 8 M guanidinium chloride (GuHCl) solution in a 1-cm path length quartz cuvette (Roth, Germany), containing 0.1 mg/mL of protein sample in PBS. Immediately after each addition of GuHCl, the protein concentration was kept constant by adding the appropriate amount of a dense protein solution to the cuvette. The sample was then stirred and incubated at 25°C until a new equilibrium was reached. The spectra were collected between 300 to 450 nm by using an excitation wavelength of 280 nm. Contributions from the buffer were measured in a separate blank experiment under identical conditions and subtracted from the final data. The titration was carried out until a final GuHCl concentration of 4.5M was reached. The denaturation profiles are plotted as the weighted average wavelength (λ_{WA}) of the emission spectra at different GuHCl concentrations, based on the equation:

$$\lambda_{WA} = \frac{\sum \lambda_i \cdot I_i}{\sum I_i}$$

where I_i is the intensity of the emission spectrum at λ_i wavelength (300 nm $\leq\lambda_i\leq$ 450 nm). Chemical denaturation data were then fitted to a two-state model, describing the

induced unfolding as a single transition between the native (N) and denatured (D) state:

$$\lambda_{WA} = \frac{(a_N + b_N[D]) + (a_D + b_D[D]) \cdot \exp \frac{(m_{DN} \cdot ([D] - [D]_{50\%}))}{RT}}{1 + \exp \frac{(m_{DN} \cdot ([D] - [D]_{50\%}))}{RT}}$$

where α_N is the signal of the native state at 0M denaturant, b_N is the signal slope ($d\alpha_N/d[GuHCl]$) at the native state, α_D and b_D are the corresponding quantities for the denatured state, m_{DN} is a constant of proportionality ($-\partial(\Delta G_{DN}) / \partial[GuHCl]$), and $[D]_{50\%}$ is the denaturant concentration at which the protein is 50% unfolded. Nonlinear least-squares fitting of this equation to the experimental data will provide an estimate for the $[D]_{50\%}$ and m_{DN} parameters and their standard deviations. The free energy change between the native and the denatured state (ΔG_{DN}) can then be calculated from the equation:

$$\Delta G_{DN} = m_{DN} \cdot [D]_{50\%}$$

3.5 Characterization of Novel CBS Mutations Using Cell Culture

3.5.1 CRISPR/Cas9 p.R336C knock-in HEK293T cells

The Human embryonic kidney cells (HEK293T) with p.R336C knock-in mutation were stored in liquid nitrogen from a previous project lead by Dr Gheyath Nasrallah (Ismail et al., 2019). HEK-293T cells vial was thawed quickly in a 37°C water bath, and the pre-warmed medium was immediately added and centrifuged for five minutes at 1000 RPM. Cells were then plated in a 75cm^2 flask. All culture media were supplemented with 10% heat-inactivated Fetal Bovine Serum (FBS) (Thermo Scientific, USA) and 1% of antibiotic suspension (Penicillin and streptomycin, Gibco, USA). The medium was pre-warmed before usage, and all cells were maintained in a humidified incubator and adjusted to 5% CO_2 at 37°C until confluency. After 24 hours of growth, the media was changed, followed by every 48 hours afterward.

3.5.2 CBS Variants Transfection in CRISPR/Cas9 p.R336C knock-in HEK293T cells

Transfection is a standard laboratory cell culture procedure involving introducing foreign nucleic acids into cells. It is a robust analytical tool that allows for the investigation of gene activities and gene products in cells. The main transfection purposes are to produce recombinant proteins or to enhance or inhibit gene expression in transfected cells. Therefore, transfection is a powerful analytical tool for the study of the function and regulation of genes or gene products and as a method for gene therapy.

In this study, the cells were transiently transfected with pcDNA3.1-EGFP plasmid using Lipofectamine® reagent (ThermoFisher Scientific, USA), according to their detailed protocol. Lipofectamine reagent comprises positively charged lipids forming circular lipid bilayers, called liposomes, which enclose the DNA plasmid. The positively charged liposomes fuse with the plasma membrane and introduce the DNA

into the cell's cytoplasm via an endocytic pathway (Maurisse et al., 2010). On the first day, cells with confluency of ~80% were cultured in a 12-well plate in DMEM medium at a density of 60% confluency overnight. On the next day, cells were washed with sterile PBS and then transfected with Lipofectamine® mixture according to the manufacturer's protocol as follows; Solution A consisted of Opti-MEM media, DNA sample, and P3000 reagent while solution B has Opti-MEM media and lipofectamine. Solution A and B were mixed together gently and incubated for 20 minutes at room temperature. Then the DNA-lipid complexes was added to the cells and incubated at 37ºC. Cells were imaged using Cytation Imaging Multi-Mode Readers fluorescent microscope 24 hours after transfection and then used for chaperone treatments.

3.5.3 Chemical Chaperone Treatment

3.5.3.1 Bacteria Chemical Chaperone Screening

A series of *in vitro* experiments were performed using *E. coli* (DE3) cells (Novagen) expression system to investigate the potential effect of chemical chaperone treatments on bacterial cells. The bacterial strain was cultured in an LB growth medium supplemented with 50 μg/ml kanamycin. For each 1L of bacterial culture, 1ml of 0.1M FeCl, 1ml of 1% thiamine, 1ml of 0.3M aminolevulinic acid, and 200ul of 12.5% pyridoxine were added in addition to one of the chemical chaperones. The optimal chaperone concentrations (0.5 mM δ-ALA, 100 mM betaine, and 50 mM taurine) were selected based on a previous study (Kopecká, Krijt, Raková, & Kožich, 2011). The bacteria were cultured under controlled conditions (37°C, 200 rpm), and the protein expression was induced by adding 1mM of IPTG when optical density (OD600) reached 0.5–0.6. The stability (tetramers) state and total amount of CBS protein were inspected by native gel Western blots and SDS-PAGE, respectively.

3.5.3.2 Cell Culture Treatment

HEK293T cells were treated with four chemical chaperones (δ-Aminolevulinic

acid, betaine, Taurine, and ethanol). Briefly, cells were cultured in 96-well plates in complete DMEM incubated overnight at 37°C and 5% CO2. Cells were then treated with different concentrations of the chemical chaperones, and viability was assessed by Alamar blue assay. Twenty-four hours after treatment, cells were lysed using RIPA buffer (Thermo Fisher). Cell lysates were collected and centrifuged at 15,000 RPM for 15 minutes for protein analysis. Protein concentration was determined using BCA assay (Pierce) using bovine serum albumin as a standard.

3.5.3.3 Alamar blue assay

AlamarBlue HS reagent (Invitrogen, ThermoFisher A50100) was used as an indicator for cell viability and proliferation. The principle depends on converting resazurin, a non-fluorescent indicator dye, to a highly red fluorescent resorufin. This is achieved through reduction reactions of metabolically active cells. Thus, the intensity of fluorescence produced is directly proportional to the number of living cells. HEK293T cells were plated onto a 96-well plate with a flat bottom (Corning). Subsequently, alamarBlue reagent was added at a concentration of 10% in complete DMEM. A blank sample was prepared in a separate well containing complete DMEM along with 10% alamarBlue reagent. Fluorescence intensity was measured using a Biotek Synergy H1 Hybrid Reader equipped with a monochromator, positioned at the bottom optics, with the gain adjusted to accommodate high well signals. The excitation wavelength was set at 560 nm and emission wavelength at 590 nm. Fluorescence readings were corrected by subtracting the fluorescence value of the blank well from all measurements. Control fluorescence was standardized to 100%, and each viability experiment was conducted in triplicate.

3.5.4 Immunoblot Assays

3.5.4.1 Protein Extraction

HEK293T cells were washed in ice-cold PBS three times prior to harvesting them in RIPA Extraction Buffer (89901, Thermo Scientific, USA), supplemented with 1x Halt protease inhibitor cocktail (78437, Pierce, USA). The cells were detached mechanically by a sterile plastic cell scraper, transferred to 1.5 ml microfuge tubes, and centrifuged at 15,000x RPM for 20 minutes at 4°C. The supernatant was stored at -80°C until use.

3.5.4.2 Protein Quantification

Extracted Protein was quantified using Pierce™ BCA Protein Assay Kit (Thermo Scientific™, USA) according to their protocol. Pierce Bicinchoninic acid (BCA) protein assay is a commonly used method to quantify total protein concentration by measuring the amount of reduced cuprous ions (Cu+) generated by chelating copper to proteins in an alkaline medium. The cuprous ions then react with BCA forming a purple water-soluble complex. The amount of protein present is directly proportional to the amount of reduction and, thus, the colourimetric change. The Bovine Serum Albumin (BSA) standards (Thermo Scientific™, USA), with concentration 2,000 µg/ml was diluted in RIPA buffer/Protease inhibitor, according to the manufacturer's recommendations. It is preferred to use the same diluent as the sample lysate during the extraction procedure. BCA working reagent was prepared by combining reagents A and B at a 50:1 ratio. A total of 25µl of each standard and each protein sample were added to 96-well plate in triplicates with 200µl of working reagents. Gently mix the plate for 30 seconds and then incubate at 37°C for 30 minutes, avoiding light. The absorbance was then measured at 562nm using the BioTek Cytation 5 multimode reader. The blank, which has only the dilution buffer, was subtracted from all standards and samples' measurements, and all triplicates values were averaged. A standard curve was prepared by plotting the average versus their relative concentrations in µg/ml. This

curve was used to determine the protein concentration of all unknown samples.

3.5.4.3 Western Blotting

After separating proteins using SDS-PAGE electrophoresis, proteins were then transferred and immobilized onto a polyvinylidene difluoride membrane (PVDF) membrane using a semi-dry transfer system (Trans-Blot SD; Bio-Rad). The blotting sandwich was prepared: two blotting pads, then the PVDF membrane, gel (protein side towards membrane), followed by 2-3 blotting pads. The transfer procedure was performed at 20 V for one hour. The success of the transfer was confirmed by Ponceau S stain (Sigma TrisbuAldrich, UK). The membrane was then blocked with 5% (w/v) of skimmed milk in tris-buffered saline with tween (TBST) buffer for one hour at room temperature. The membrane was then washed with TBST and probed with anti-CBS mouse polyclonal antibody (1:1,500 dilution; Abnova) overnight at 4°C using a shaker.

On the next day, the membrane was washed with TBST three times, each 10 minutes, and incubated with IgG goat anti-mouse (dilution-1:2,000) secondary antibody conjugated with horseradish peroxidase (HRP) for one hour at room temperature. Following three times of 10 minutes of washing, immunoblot was developed using the ECL Western Blotting Substrate Kit (Abcam, ab65623) for visualization. A luminescence signal was detected using the iBright CL100 system (Invetrogen). The densitometry quantification analysis of the western blotting protein bands was performed using ImageJ analysis software.

3.8 Protein Crystallization Setup

The crystallization process was initiated in the high-throughput crystallization facility at the X-Ray platform of CIC bioGUNE (Bilbao, Spain), assisted by liquid handling robots and automatic nanodispensers, which allowed us to examine around 475 crystallization conditions. The technique used in this initial screens was the sitting drop vapour diffusion in 96 well MRC plates . Precipitant solutions were placed in the reservoirs using TECAN Freedom EVO robot (TECAN Group Ltd.) and the protein/precipitant drop was prepared with the automatic nanodispenser MOSQUITO liquid handling robot (TTP Labtech Ltd.) mixing 200 nL of protein solution with 200 nL of reservoir. For the CBS^{R336C}, the suitable concentration is 20 mg mL^{-1} to carry out the subsequent experiments. Once the initial screens were tested, promising conditions were identified around a crystallization condition of the screens (Index), which yielded small microcrystals. Subsequently, a more specific screening, aimed to optimize the crystallization conditions, was performed. First, the droplet size was significantly increased, and the hanging drop technique was employed in 24-well VDX plates. The drops contained 1 μL of protein and 1 μL of reservoir. The volume in the reservoir was 500 μL. The plates were incubated at a constant temperature of 291K on the CIC bioGUNE platform. Crystals appeared (or not) after 48 hours.

3.9 Statistical Analysis

All results were presented as means of at least three experiments. Multiple comparisons were analyzed by one-way analysis of variance (ANOVA) using GraphPad Prism (version 8.0). The level of significant difference between groups was expressed using p values: *$p < .05$, **$p < .01$, ***$p < .001$, ****$p < .0001$.

Chapter 4: Results

The ensuing chapter, dedicated to the presentation of study findings and provides a detailed description of the mutagenesis processes, cloning tactics, expression regimens, and purification approaches utilized to create different CBS mutations. Subsequently, the chapter proceeds to delve extensively into the distinctive features of the Qatari p.R336C mutation. Following this, the present study focuses on the examination of two recently discovered CBS mutations, p.T236N and p.G153R, which have been previously reported in homozygous patients afflicted with homocystinuria. The final segment of this chapter is dedicated to the molecular characterization of another set of CBS variants, p.K72I and p.L230Q. These mutations have been identified in a compound heterozygous homocystinuria patient. This comprehensive elucidation of mutational properties and molecular insights contributes significantly to the understanding of CBS-related disorders and their potential therapeutic implications, thus enriching the field of biomedical research.

5.1 The Construction of the CBS Site-Directed Variants

The hCBS variants were sub-cloned into the pET28a vector and subjected to site-directed mutagenesis using the template program described in the Material and Methods section (**Figure 7-9**) (**Table 2**). The amplicons introduced between the *XhoI* and *NdeI* sites of the pET28a(+) expressions vector and the resulting constructs, p.R336C, p.T236N, p.G153R, p.K72I, and p.L230Q were used to transform *E. coli* strain TOP10. Following plasmid extraction and DNA purification, sequencing analysis showed the correct introduction of the desired CBS mutations. The complete sequencing data of the mutated cDNAs were further verified and aligned with WT CBS gene to confirm that no additional mutations were introduced **(Figure 10**).

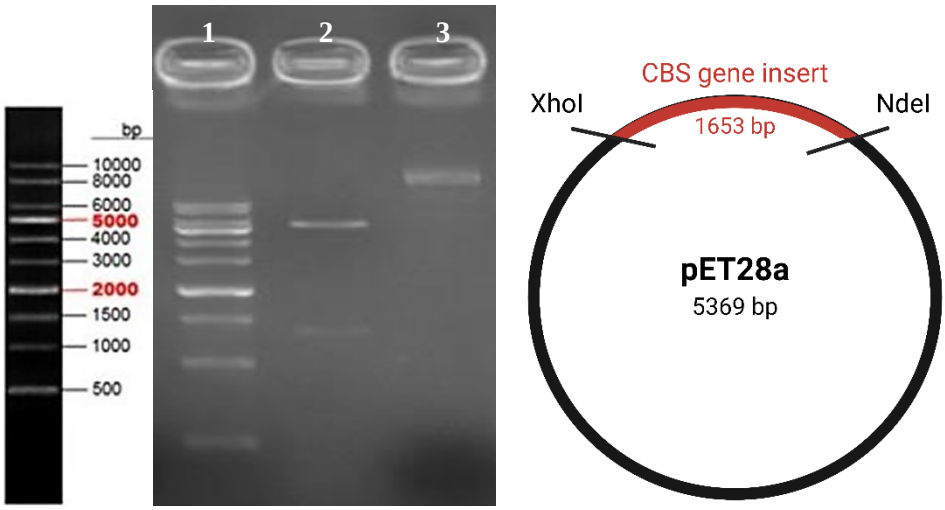

Figure 7. Gel electrophoresis analysis of CBS p.R336C clone constructs. The gel electrophoresis image displays DNA fragments of clone constructs along with a molecular weight marker (ladder). Each lane represents a different clone construct, and the positions of the DNA fragments in the gel are indicative of their sizes. Lane 1 contains the molecular weight marker, with known DNA fragment sizes, serving as a reference for estimating the sizes of the clone constructs. Lane 2 is the plasmid digested by *NdeI* and *XhoI* and Lane 3 is the uncut plasmid. The presence and migration of specific DNA fragments in the clone lanes confirm the successful generation of p.R336C construct, while the ladder provides a visual reference for the approximate size.

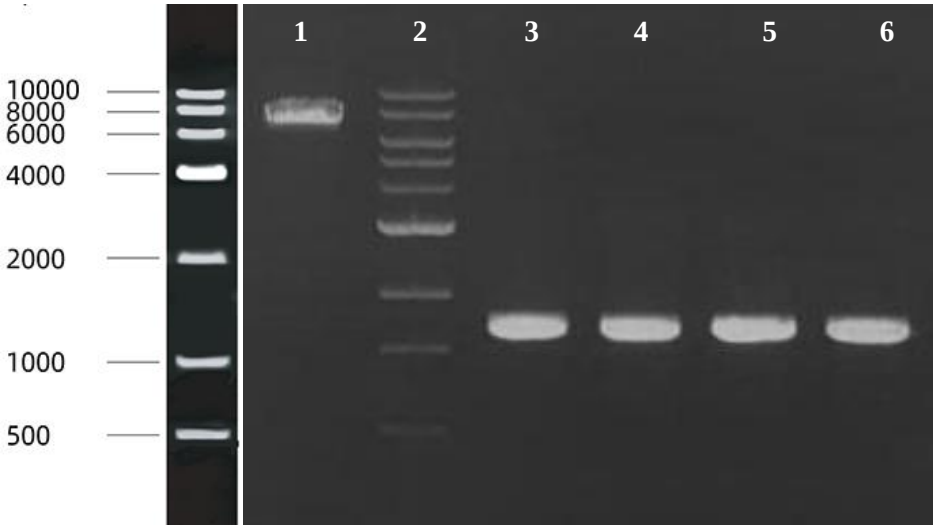

Figure 8. Gel electrophoresis analysis of CBS p.T236N, p.G153R, p.K72I, and p.L230Q clone constructs prior to ligation. The gel electrophoresis image displays DNA fragments of clone constructs along with a molecular weight marker (ladder). Each lane corresponds to a distinct clone construct, and the positions of the DNA fragments in the gel are indicative of their sizes. Lane 1 is the uncut plasmid, and Lane 2 contains the molecular weight marker with known DNA fragment sizes, serving as a reference for estimating the sizes of the clone constructs. Lanes 3-6 are the plasmid digested by *NdeI* and *XhoI*. Lane 3 corresponds to p.T236N mutation, Lane 4 is p.G153R, Lane 5 is p.K72I, and Lane 6 is p.L230Q. The presence and migration of specific DNA fragments in the clone lanes confirm the successful generation of CBS constructs, while the ladder provides a visual reference for their approximate sizes.

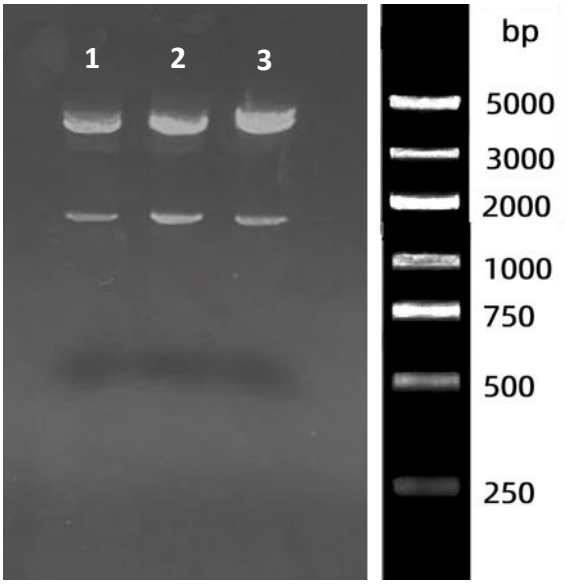

Figure 9. Gel electrophoresis analysis of CBS p.T236N, p.G153R, p.K72I, and p.L230Q clone constructs. The gel electrophoresis image displays DNA fragments of clone constructs along with a molecular weight marker (ladder). Each lane represents a different clone construct, and the positions of the DNA fragments in the gel are indicative of their sizes. Lane 1 is the plasmid with p.T236N digested by *NdeI* and *XhoI*, Lane 2 is the plasmid with p.153R digested by *NdeI* and *XhoI* and Lane 3 is the plasmid with p.K72I digested by *NdeI* and *XhoI* . The presence and migration of specific DNA fragments in the clone lanes confirm the successful generation of p.T236N, p.G153R, p.K72I, and p.L230Q constructs, while the ladder provides a visual reference for the approximate size.

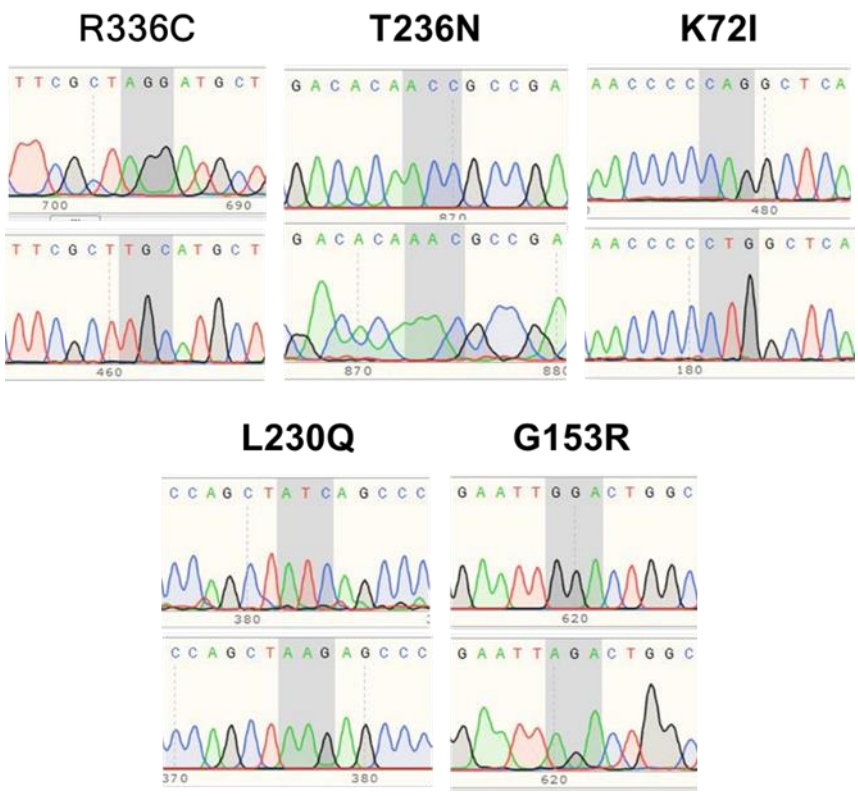

Figure 10. Sangar sequencing results for all constrcuts after site-directed mutagenesis.

5.2 Expression and Purification of Recombinant hCBS Proteins

The relevance of post-translational modifications (PMTs) in CBS function cannot be overstated. For instance, heme and PLP binding is necessary for CBS to have catalytic activity. Interestingly, decreased stability and activity of the enzyme may result from PTM disruption. It was reported that the most common PMTs for CBS are phosphorylation and SUMOylation (Kabil, Zhou, & Banerjee, 2006; K. Zuhra, F. Augsburger, T. Majtan, & C. Szabo, 2020). Another study showed that CBS enzyme is strongly activated by s-glutathionylation PTM (Niu, Yadav, Adamec, & Banerjee, 2015). When it comes to studying CBS with all its modifications, the use of a eukaryotic expression system may be appropriate. However, since our research did not specifically demand PTMs, the bacterial system was chosen as a practical solution due to its cost-effectiveness, simplicity, and rapid growth rate. This would enable us to efficiently generate vast quantities of the recombinant human protein. Previous studies have demonstrated the successful expression of active enzymes using bacterial systems, highlighting their effectiveness not only in structural investigations but also in various research applications (T. Majtan, Liu, Carpenter, & Kraus, 2010; Oyenarte et al., 2012).

The recombinant CBS variant proteins were successfully produced in the soluble fraction of *E. coli* lysates using the expression conditions described in the Material and Methods section. The WT and CBS variants were purified by Ni-NTA affinity chromatography, and their purity was assessed by SDS-PAGE. A total of 10 µl of total proteins prior to column affinity, flow-through, wash buffer, and the eluted sample were collected. The samples were applied in a final volume of 15 µL, being previously prepared in loading buffer (Tris-HCl 0.24 M pH 6.8, glycerol 40%, SDS 8%, bromophenol blue 0.02%, β-mercaptoethanol 25%) and denatured at 95ºC for 5 minutes and run on the SDS-PAGE gel.

Figure 11-15 show an SDS-PAGE image depicting the elution profile of a CBS variants protein. The CBS proteins were primarily eluted using 500 mM imidazole. The

main band of all expressed CBS proteins displayed a molecular mass of approximately 63 kDa, which corresponds to the estimated molecular mass of the recombinant CBS proteins. Notably, after gel filtration chromatography, a decrease in contaminating proteins was observed for all recombinant CBS proteins (WT and variants), resulting in a high purity grade. Protein samples were subjected to dialysis in PBS overnight. On the next day, the protein concentrations were determined by the BCA assay. The yields were between 11-45 mg per 2L culture for the hCBS variants and the samples were stored at -80°C until further analysis.

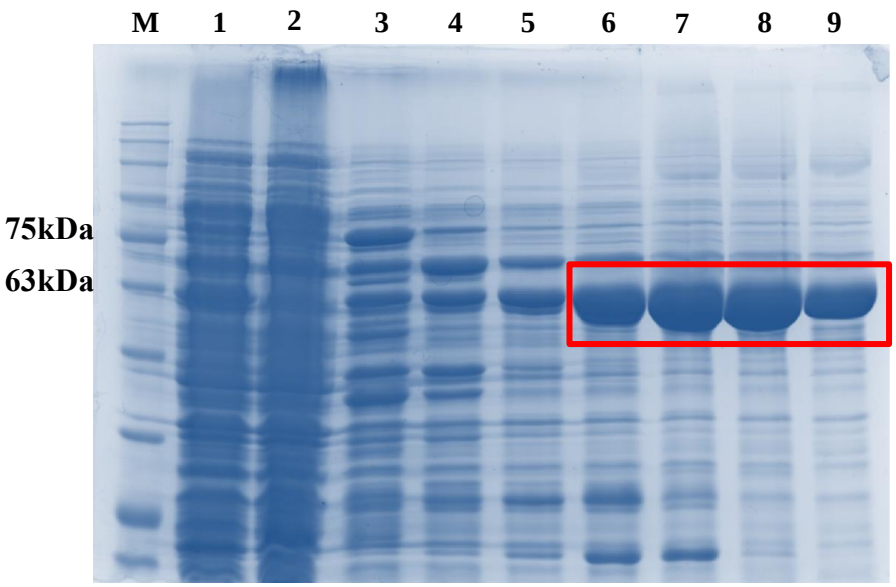

Figure 11. SDS-PAGE Analysis of CBS p.R336C Expression and Purification. Lane M represents the molecular ladder. Lane 1: A total of 10 µl of total protein sample prior to column affinity purification, representing the crude protein extract. Lane 2: The flow-through fraction after loading the crude protein extract onto the affinity column, showcasing unbound proteins. Lanes 3-5: Proteins that remained attached to the column after the application of the initial sample. Lanes 6-9: The eluted sample following affinity chromatography purification, demonstrating the isolated and purified CBS mutation protein. This gel provides a visual representation of the purification process, showing the removal of impurities and the successful isolation of the target CBS protein in Lanes 6-9.

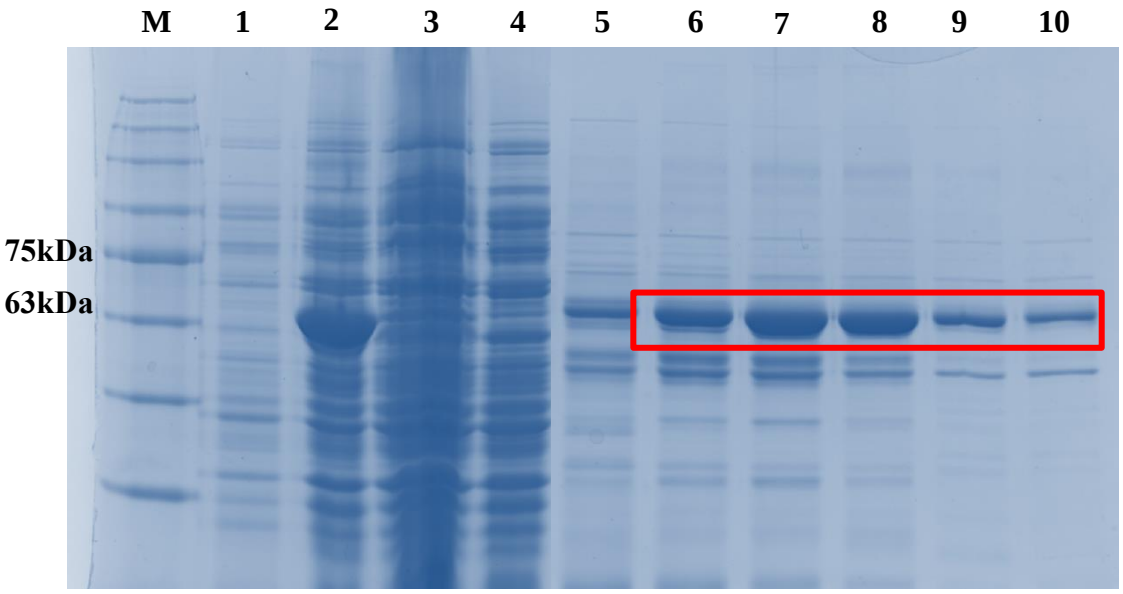

Figure 12. SDS-PAGE Analysis of p.K72I Expression and Purification. Lane M represents the molecular ladder. Lane 1: A total of 10 µl of total protein sample before inducing the protein expression and the addition of IPTG. Lane 2: A total of 10 µl of total protein sample after inducing the protein expression and the addition of IPTG. Lane 3: A total of 10 µl of total protein sample prior to column affinity purification, representing the crude protein extract. Lane 4: The flow-through fraction after loading the crude protein extract onto the affinity column, showcasing unbound proteins. Lane 5: Proteins that remained attached to the column after the application of the initial sample. Lanes 6-10: The eluted sample following affinity chromatography purification, demonstrating the isolated and purified CBS mutation protein. This gel provides a visual representation of the purification process, showing the removal of impurities and the successful isolation of the target CBS protein in Lanes 6-9.

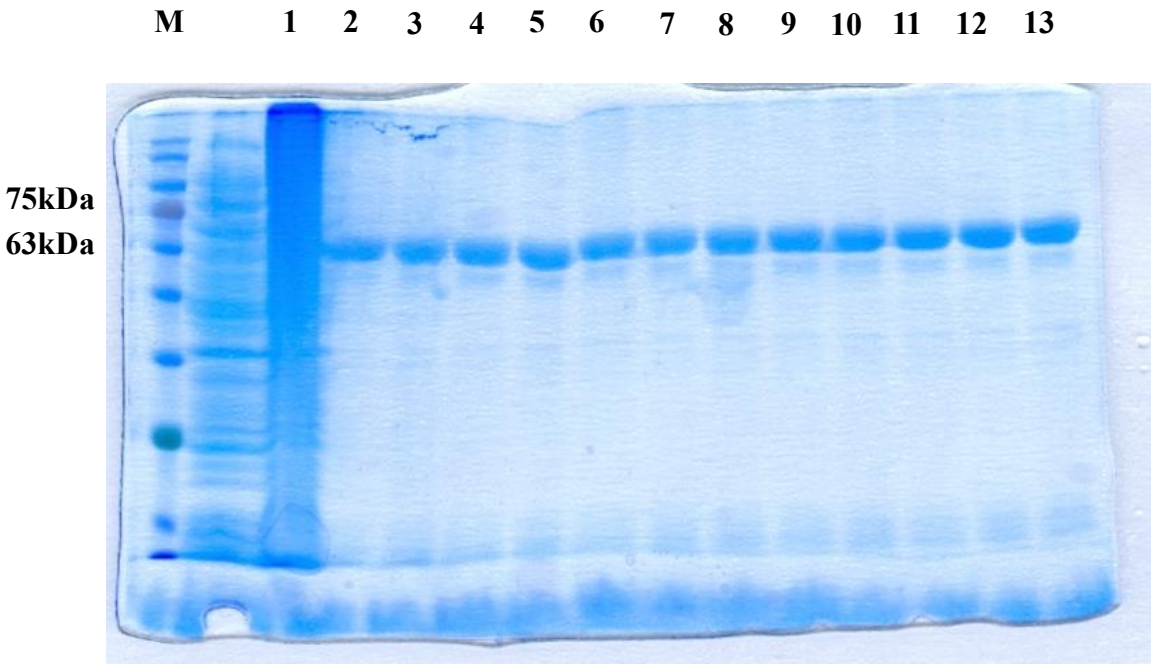

Figure 13. SDS-PAGE Analysis of CBS p.T236N Expression and Purification. Lane M represents the molecular ladder. Lane 1: A total of 10 µl of total protein sample prior to column affinity purification, representing the crude protein extract. Lanes 2-13: The eluted sample following affinity chromatography purification, demonstrating the isolated and purified CBS mutation protein.

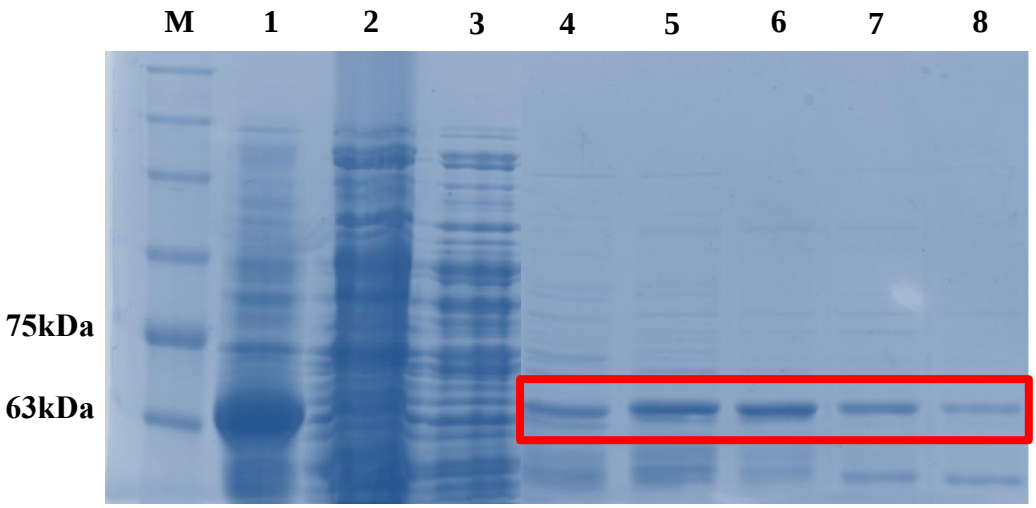

Figure 14. SDS-PAGE Analysis of CBS p.L230Q Expression and Purification. Lane M represents the molecular ladder. Lane 1: A total of 10 µl of total protein sample after inducing the protein expression and the addition of IPTG. Lane 2: A total of 10 µl of total protein sample prior to column affinity purification, representing the crude protein extract. Lane 3: The flow-through fraction after loading the crude protein extract onto the affinity column, showcasing unbound proteins. Lanes 4-8: The eluted sample following affinity chromatography purification, demonstrating the isolated and purified CBS mutation protein. This gel provides a visual representation of the purification process, showing the removal of impurities and the successful isolation of the target CBS protein in Lanes 4-8.

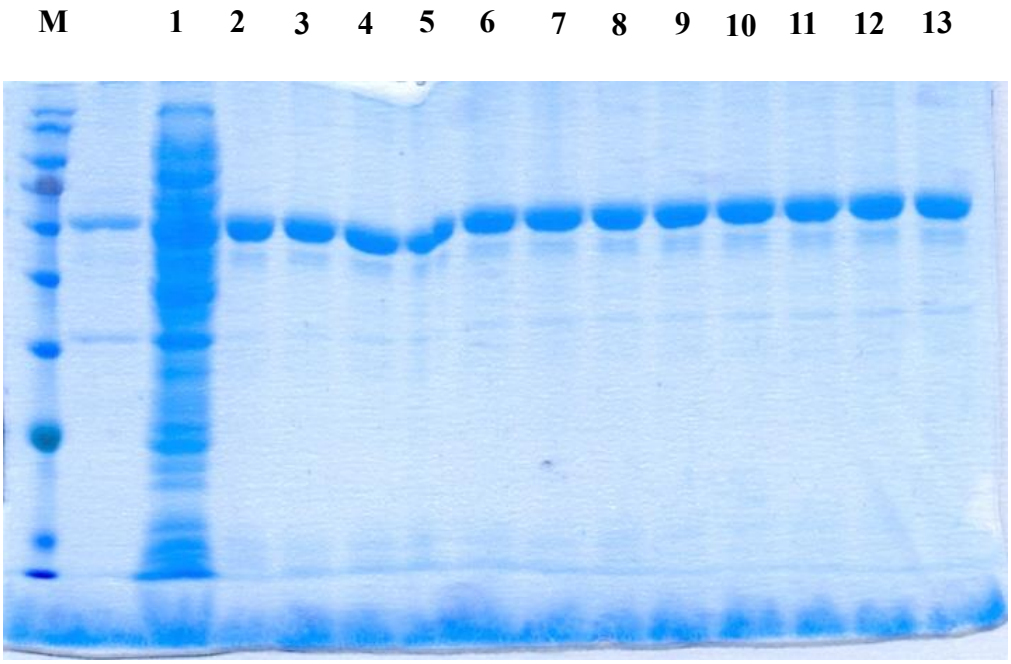

Figure 15. SDS-PAGE Analysis of CBS p.G153R Expression and Purification. Lane M represents the molecular ladder. Lane 1: A total of 10 µl of total protein sample prior to column affinity purification, representing the crude protein extract. Lanes 2-13: The eluted sample following affinity chromatography purification, demonstrating the isolated and purified CBS mutation protein.

In the UV-visible spectra analysis, we examined the absorbance profiles of the five CBS mutations, p.R336C, p.T236N, p.G153R, p.K72I, and p.L230Q, in comparison to the WT enzyme. Our findings revealed that each mutant exhibits unique spectrum patterns, suggesting the presence of structural differences within the CBS enzyme. Remarkably, the p.R336C and p.K72I mutations displayed spectra that closely resembled the WT, suggesting that these variants maintain structural conservation. In contrast, CBS^{T236N}, CBS^{G153R}, and CBS^{L230Q} mutants were particularly pronounced in the heme binding, which is critical for the interactions and catalytic activity of the CBS enzyme (**Figure 16**). The aforementioned differences emphasize the significance of these mutations in influencing the structural conformation of the protein, hence emphasizing their possible implications on its functionality.

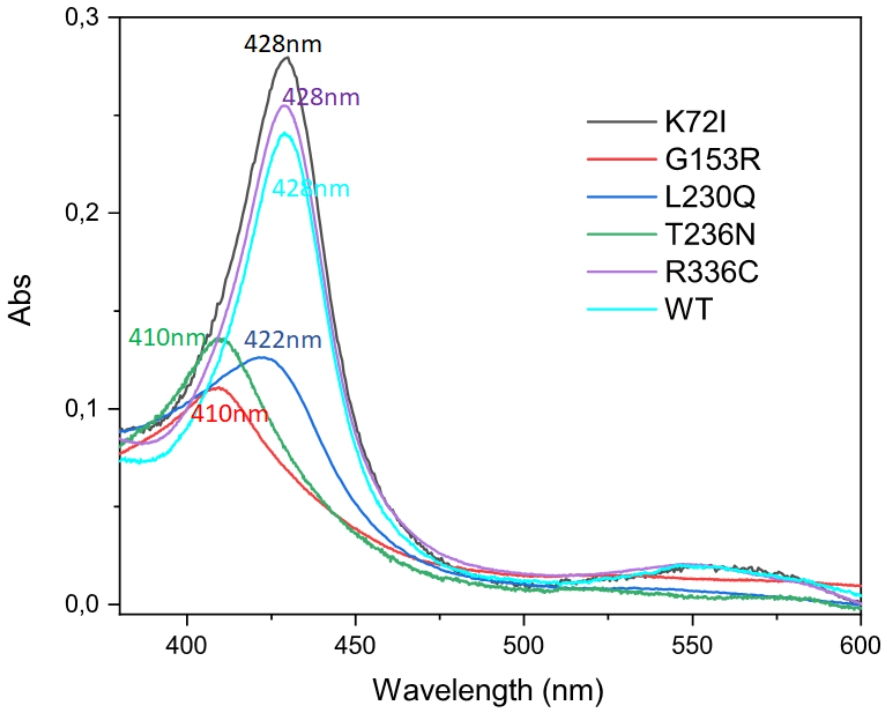

Figure 16. UV-Visible spectra depicting the absorbance profiles of the five CBS mutations, p.R336C, p.T236N, p.G153R, p.K72I, and p.L230Q, and were compared with the CBS^{WT} enzyme.

5.3 Characterization of the Qatari CBS^{R336C} Mutant Protein

Human CBS^{R336C} has been previously reported to be a B6 non-responsive mutation (Al-Dewik et al., 2019; Gupta et al., 2019). This study aimed to comprehensively analyze the Qatari CBS^{R336C} variant protein in order to gain a deeper understanding of the molecular mechanisms behind homocystinuria. Therefore, we aimed to assess the enzymatic activity of CBS^{R336C} mutant at different concentrations with the addition of pyridoxal and heme cofactors and directly compare it with the enzymatic activity of the CBS^{WT} protein. The activity was assessed by quantifying the fluorescence emission at a wavelength of 460 nm, with excitation at 368 nm. The results demonstrated a significant decrease in the activity of the CBS^{R336C} mutant, approximately 88% lower than that of the CBS^{WT}, as shown in **Figure 17**.

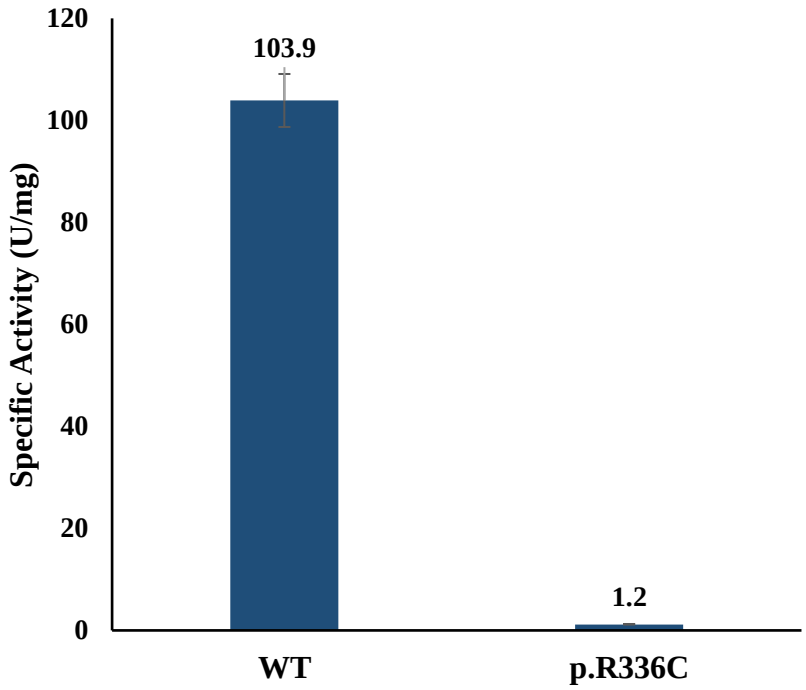

Figure 17. Specific Enzyme Activity between CBS^{WT} and CBS^{R336C} variant. Enzyme activity assays were conducted utilizing a CBS Activity Kit to evaluate and compare the specific activities of CBS^{WT} and the CBS^{R336C} variant. The data presented in this study demonstrate the discernible enzymatic activity profiles shown by the two protein variants. These findings provide valuable insights into the functional implications of the CBS^{R336C} mutation on the activity of cystathionine beta-synthase.

In this study, the utilization of HPLC was employed to qualitatively evaluate the enzymatic activity of CBS in two significant metabolic pathways. The assessment encompassed both the WT hCBS and the p.R336C mutation. The initial focus of the study involved a comprehensive investigation of the canonical reaction, which entails the condensation of L-Ser and L-Hcys to yield L-Cth along with the liberation of water (**Figure 18**). Additionally, the study examined the pathway responsible for generating H_2S, which involves the conversion of L-Cys and L-Hcys into L-Cth and H_2S (**Figure 19**). The HPLC analyses yielded similar findings regarding the impact of the p.R336C mutation on CBS enzymatic activity and its potential involvement in the abnormal metabolism of sulfur amino acids. These results enhance our overall comprehension of the pathophysiological implications associated with this mutation.

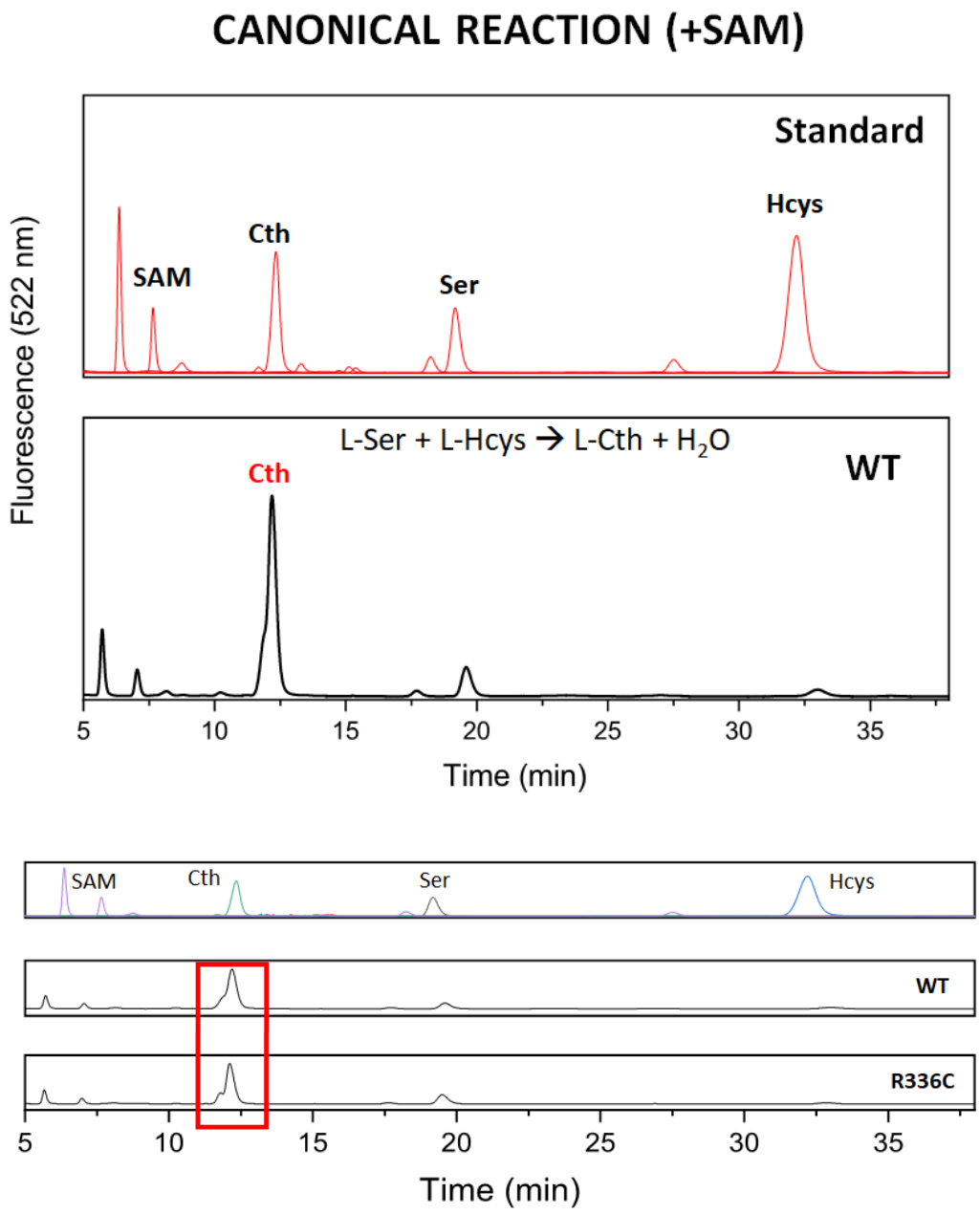

Figure 18. HPLC Analysis of CBS^{WT} and CBS^{R336C} Mutant Enzymatic Activity for canonical assay with the addition of SAM. Pure standard L-Ser, L-Hcys and L-Cth (top), and product obtained following 2 hours incubation of CBS single variants with 1 mM L-Ser and 0.8 mM L-Hcys.

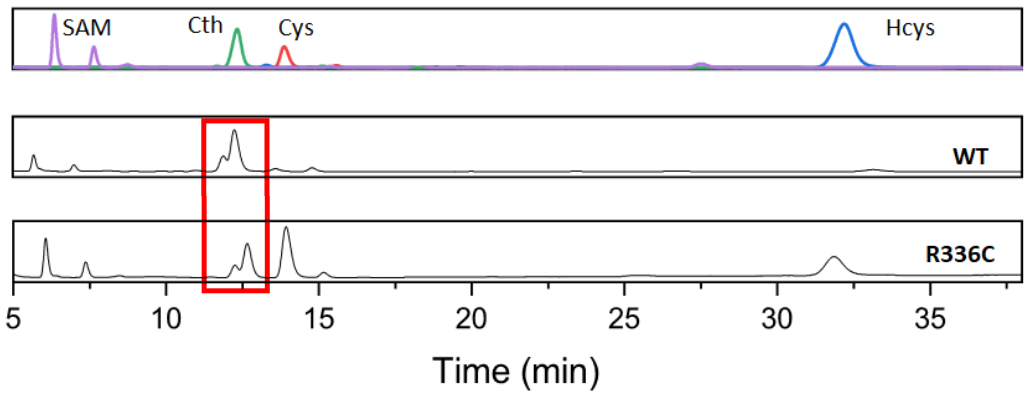

Figure 19. HPLC Analysis of CBS^{WT} and CBS^{R336C} Mutant Enzymatic Activity for H_2S production assay with the addition of SAM. Pure standard L-Cys, L-Hcys and L-Cth (top) and product obtained following 2 hours incubation of CBS single variants with 1 mM L-Cys and 0.8 mM L-Hcys.

The analysis of protein structure involved the utilization of PremPS (Predicting the Effects of Mutations on Protein Stability) to analyze the impact of the mutation on protein stability. According to the results, it was shown that CBS p.R336C is located at the interface between the catalytic core and the beginning alpha helix of the interdomain peptide linker. This linker connects the core to the Bateman module of the same subunit and is in close proximity to the core of a complementary subunit (Ereño-Orbea, Oyenarte, & Martínez-Cruz, 2013). It occupies a critical position at the interface of the catalytic and regulatory regions. The mutant structure was compared to the WT structure, revealing the absence of a significant charge-based (ionic) contact between R336 and D388. This connection is located within the second alpha helix of the interdomain linker and is disrupted due to the mutation at position 336 (**Figure 20**).

This lack of mutant interaction can potentially disrupt the overall structure of hCBS, leading to a ΔΔG value of 0.69 kCal/mol, and associated reduction in activity.

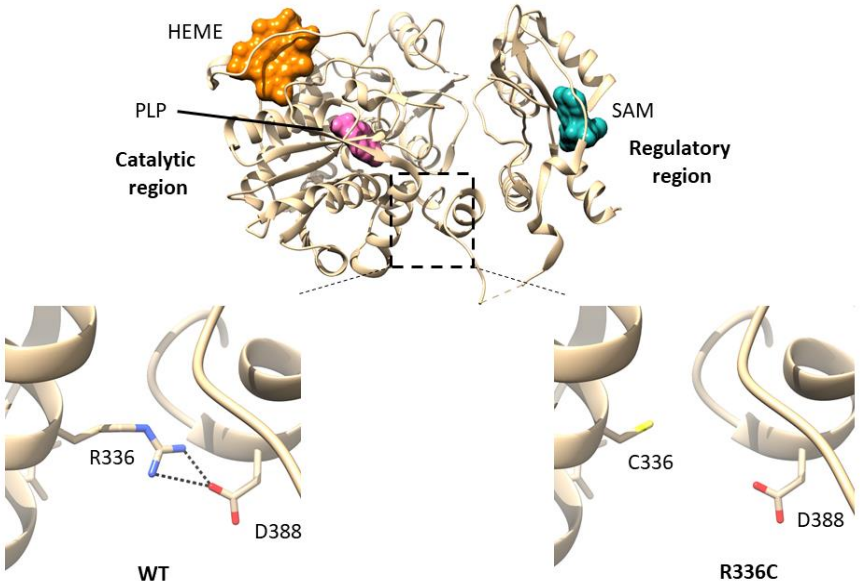

Figure 20. Structure-based protein stability analysis.

CD spectroscopy was utilized to investigate the secondary structure of the expressed recombinant CBS proteins. The obtained results indicated that there were no significant changes, implying that both the CBS^{WT} and CBS^{R336C} mutant proteins retained a similar overall structural conformation (**Figure 21**). Additional spectrum analysis was conducted to determine the α-helix and β-sheet content at a temperature of 25°C. The results showed that the α-helix content was 0.16 for the CBS^{WT} and 0.19 for the CBS^{R336C} mutant. Similarly, the β-sheet content was found to be 0.31 for the CBS^{WT} and 0.27 for the CBS^{R336C} mutant. The findings of this study indicate that there is a notable similarity in the secondary structure of the WT and mutant CBS proteins when subjected to the defined circumstances. This suggests that the p.R336C mutation does not cause significant changes in the secondary structural components of the enzyme.

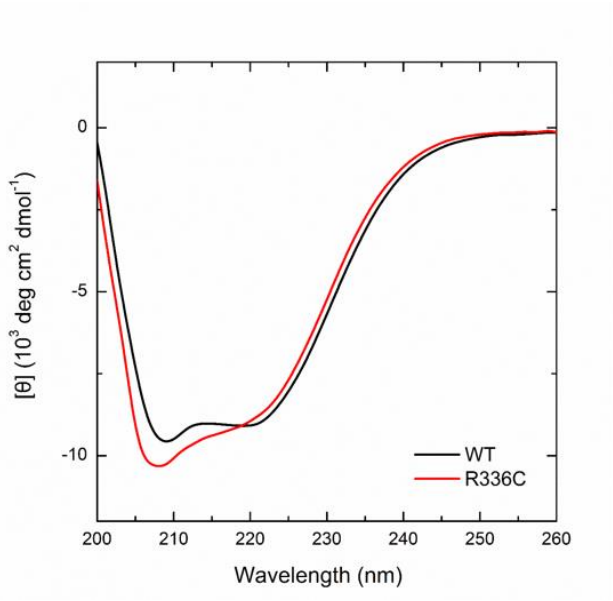

CBS WT Secondary structure estimate (20°C)

helix	β-strand	other
0.16	0.31	0.54

CBS p.R336C Secondary structure estimate (20°C)

helix	β-strand	other
0.19	0.27	0.54

Figure 21. Normalized far-UV CD spectra for WT (black) and R336C (red) CBS at 20°C.

In order to investigate the potential correlation between the significant decline in enzymatic activity observed in the CBS^{R336C} mutant and potential changes in the protein's thermostability, a series of comprehensive thermal unfolding experiments were performed. These experiments aimed to directly evaluate and compare the thermostabilities of both the CBS WT and mutant proteins. The analysis of far-UV circular dichroism (CD) spectra unveiled notable distinctions in both the thermal behavior and the final structural transformations of these protein variants. Both CBS forms exhibited two distinct and irreversible thermal transitions in the temperature range of 20 to 95°C (**Figures 22 and 23**). The initial transition, which exhibited a transition midpoint (Tm) of 41.2°C for the WT and 45.0°C for the mutant, was ascribed to the unfolding of the regulatory domain. The subsequent transition seen in this study,

characterized by Tm values of 71.5°C for the WT and 83.5°C for the mutant, can be attributed to alterations occurring inside the catalytic domain, as previously reported (Pey, Majtan, & Kraus, 2014; Pey et al., 2013).

While the first transition exhibited a degree of similarity between the two protein forms, as indicated by comparable Tm values and molar ellipticity changes, the catalytic domain of the CBS^{R336C} mutant demonstrated significantly enhanced thermal stability (ΔTm = 12°C) compared to the WT. In addition, it was observed that the WT protein exhibited a significant decrease in secondary structure (Δ[θ]222 nm = approximately 6000 $deg \cdot cm^2 \cdot dmol^{-1}$) during thermal unfolding. Conversely, the CBS^{R336C} mutant maintained a considerable amount of its secondary structure even at elevated temperatures of up to 95°C (Δ[θ]222 nm = approximately 2400 $deg \cdot cm^2 \cdot dmol^{-1}$). The aforementioned data suggest that there are different population distributions across oligomeric states and structural rearrangements in the CBS^{R336C} mutant. These rearrangements result in a more rigid and thermally stable architecture, similar to that of a molten globule state.

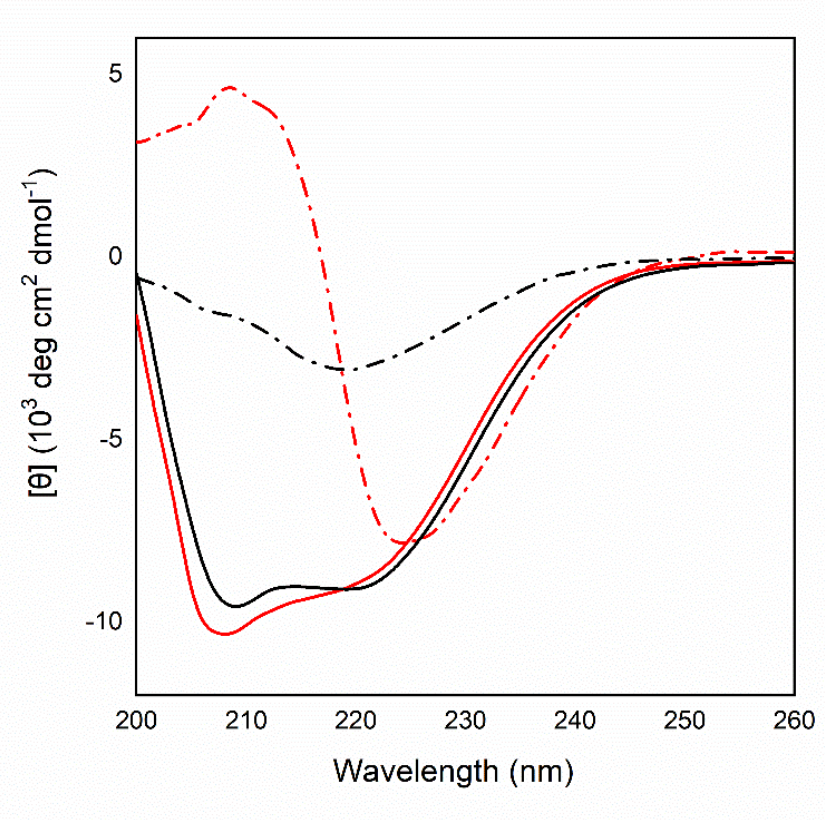

Figure 22. Normalized far-UV CD spectra for CBS^{WT} (black) and CBS^{R336C} (red) at 20°C (continuous line) and 95°C (dashed line).

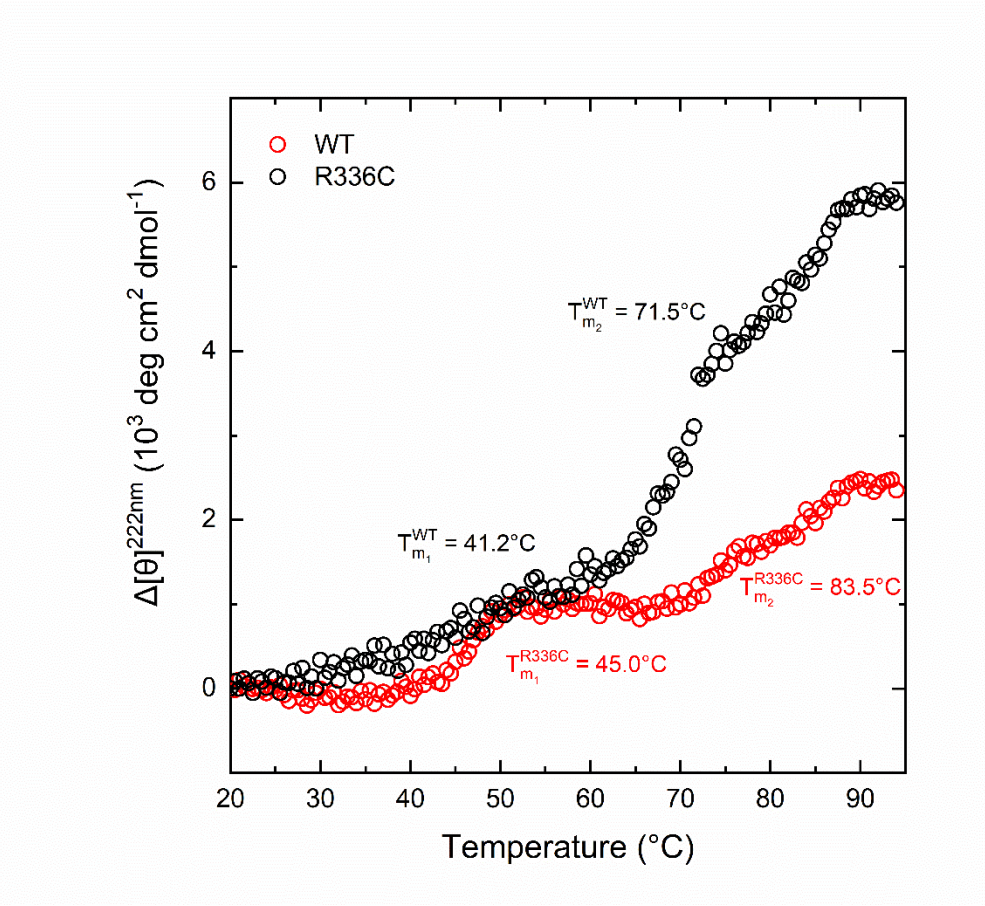

Figure 23. CD melting profile of CBS^{WT} (black) and CBS^{R336C} (red) monitored at 222 nm

Conformational stability assessments of the recombinant CBS proteins were conducted utilizing chemical denaturation assays. The analytical methodology employed in this study entailed the tracking of changes in protein spectra by the utilization of fluorescence emission spectroscopy. Guanidine hydrochloride (GuHCl) was utilized as a denaturant owing to its ability to disrupt noncovalent interactions, including salt bridges and hydrogen bonds. The outcomes unveiled a discernible distinction in the free energy change (ΔΔG_D-N) between the WT and mutant proteins, amounting to 0.72 kcal/mol (**Figure 24**). This observation strongly supports the notion that the CBS^{WT} protein exhibits greater thermodynamic stability in comparison to the CBS^{R336C} mutant. Therefore, our research results provide strong evidence for the

disruptive effect of the p.R336C mutation on the CBS protein.

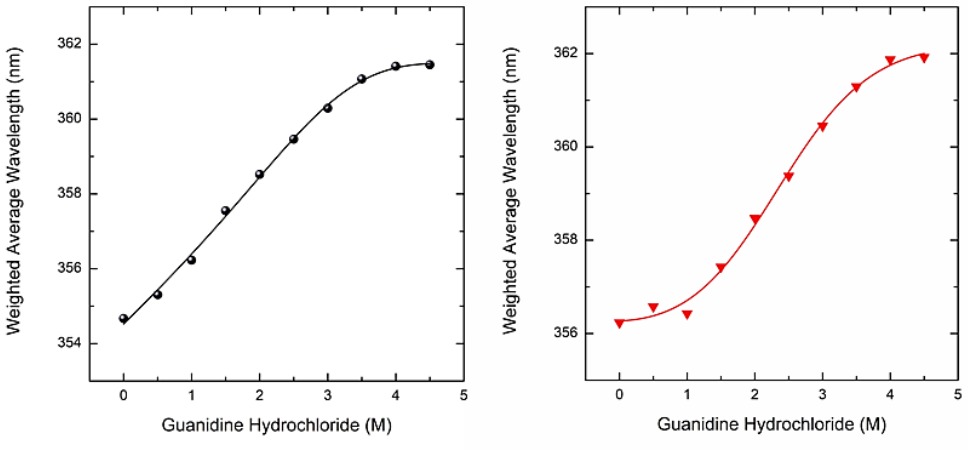

Protein Sample	$\Delta G_{N\text{-}D}^{H_2O}$ (kcal/mol)	m (kcal mol^{-1} M^{-1})	$[D]^{50\%}$ (M)
Wild type (WT)	2.41 ± 0.24	- 0.76 ± 0.07	3.17 ± 0.12
p.R336C Mutant	1.82 ± 0.07	-0.81 ± 0.03	2.25 ± 0.03

Figure 24. Chemical denaturation profiles of CBS^{WT} (black) and CBS^{R336C} (red), plotted as weighted average emission wavelength versus solution GuHCl concentration.

The study yielded numerous significant findings pertaining to this mutation. The utilization of biochemical assays demonstrated a discernible modification in the catalytic activity of the CBS^{R336C} in contrast to the CBS^{WT}, hence emphasizing its functional importance. In addition, the utilization of structural analysis methods such as spectroscopic techniques and molecular dynamics simulations has yielded significant findings on the conformational alterations caused by the p.R336C mutation. These findings have contributed valuable knowledge to our understanding of the mechanistic implications associated with this particular genetic variant.

5.4 Characterization of Novel CBS Variants Reported in Compound Heterozygous Homocystinuria Patient

5.4.1 Case presentation

CBS plays a crucial role in the metabolism of sulfur-containing amino acids. The *CBS* gene is located on chromosome 21q22.3 and consists of 18 exons (**Figure 25**). The transcription and translation of the CBS gene result in the production of a protein composed of 551 amino acids (Ensembl, 2023). The CBS enzyme functions as a tetramer, composed of four CBS protein subunits, and each subunit contributes to the overall enzymatic activity. Since the first mutation in the human *CBS* gene reported by Kozich and Kraus in 1992 (Kožich & Kraus, 1992), various *CBS* mutations have been reported in homocystinuria patients from multiple populations worldwide (D. W. Al-Sadeq & Nasrallah, 2020).

The present study studied novel compound heterozygous mutations, c.689T>A (L230Q) and 215A>T (K72I) in a Chinese patient with homocystinuria. Both K72I, located in exon 4, and L230Q, located in exon 8, were reported to be novel as they were not detected in 200 normal control samples. The patient was diagnosed with classical

homocystinuria at the age of 18 (Li et al., 2018). The major clinical features of the patient included skeletal abnormality, developmental delays, eye disorders, and vascular events. More specifically, the patient showed Marfanoid habitus with osteoporosis, severe scoliosis, and eye disorders, including ectopia lentis. Significantly increased plasma (268 μmol/L) and urinary (168 μmol/L) total homocysteine were observed. Blood methionine elevated to 258 μmol/L (normal range 10–50 μmol/L). Similar clinical features and elevated homocysteine were reported in a Han Chinese family with two novel CBS mutations (Gong et al., 2015). The patient was pyridoxine non-responsive, as no significant decrease in the plasma total homocysteine was reported after pyridoxine treatment (Li et al., 2018).

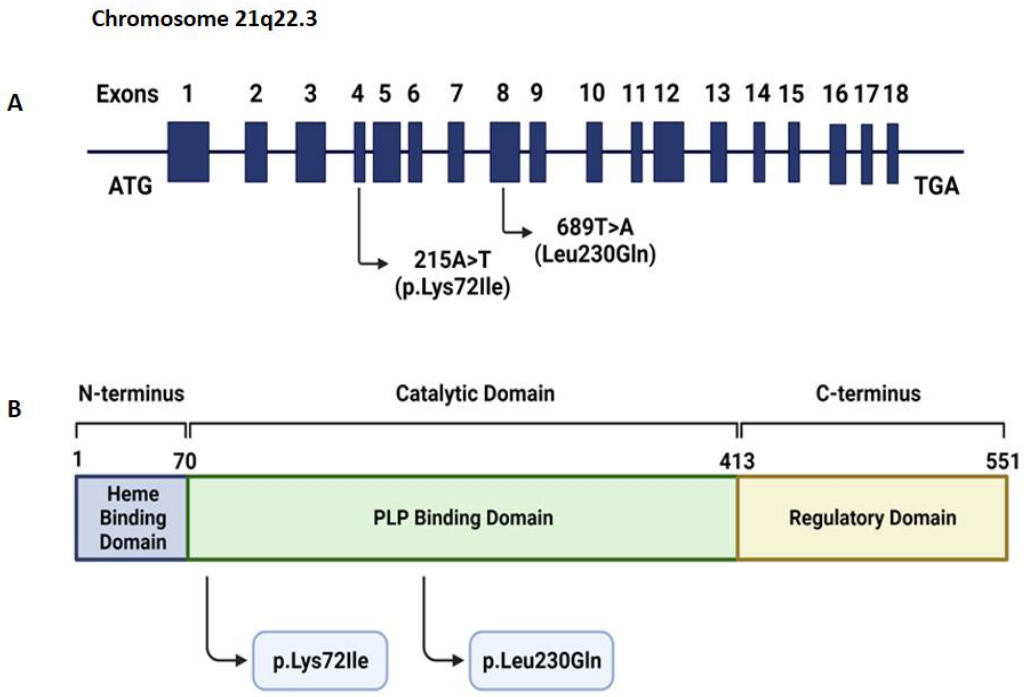

Figure 25. A) Schematic diagram showing human *CBS* gene, the genomic location of missense variants associated with classical homocystinuria. *CBS* gene is located in chromosome 21q22.3. Variant p.Lys72Ile (K72I) is located on exon 4, and variant p.Leu230Gln (L230Q) is on exon 8. B) Domain organization and structure of human CBS protein. Human CBS consists of three architectural regions. The N-terminal domain, encompassing residues 1-70, is responsible for binding the heme cofactor. Within the conserved catalytic core, spanning residues 70-386, lies the PLP cofactor, facilitating catalytic reactions. Finally, the C-terminal regulatory domain, spanning residues 386-551, consists of a flexible linker and a tandem of CBS domains (CBS1 and CBS2), which serve as binding sites for SAM.

5.4.2 Molecular modelling and structural comparison of the CBS models

The representative molecular modelling (MD) simulation models for CBS^{WT}, CBS^{K72I} and CBS^{L230Q} were used to explore the structural impact of these mutations at monomeric level. An overlay of these models is shown in **Figure 26**, and Supplementary Figures SM1 and SM2 from which it can be seen that all variants adopt the same overall folding, with small structural changes that are largely confined to the secondary structure level of the protein architecture. The CBS^{K72I} mutation results in to less extensive conformational changes compared to those of CBS^{L230Q} ($RMSD^{WT\text{-}K72I}$ = 5.0 Å and $RMSD^{WT\text{-}L230Q}$ = 6.1 Å respectively). These results are in excellent agreement with our circular dichroism (CD) experimental data (see below), where only small structural changes were detected and CBS^{L230Q} had the greater impact.

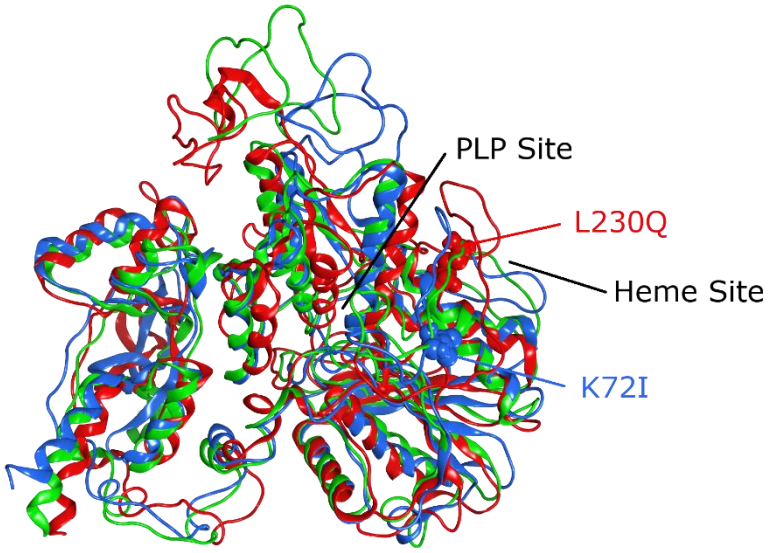

Figure 26. Overlayed MD structures for CBS^{WT} (green ribbons), CBS^{K72I} (blue ribbons) and CBS^{L230Q} (red ribbons).

The catalytic domain of CBS is known to contain a PLP binding site, where PLP as a cofactor is bound primarily by forming a Schiff bond with the ε-amino group of lysine at position 119. PLP is anchored in place by forming a network of hydrogen bonds with residues G256, T257, G258, G259 and T260, located between strands β8 and helix α8. **Figures 27A** and **27B** show an overlay of the PLP binding site for CBS^{WT} – CBS^{K72I} and CBS^{WT} – CBS^{L230Q}, respectively. The CBS^{K72I} PLP binding site has a similar arrangement to that of CBS^{WT} with most of the changes located on the 256-260 loop (the $RMSD^{WT\text{-}K72I}$ for the PLP catalytic site is 2.4 Å). On the other hand, the CBS^{L230Q} is much more distorted (the $RMSD^{WT\text{-}L230Q}$ for the PLP catalytic site is 4.7 Å) with key residues adopting a completely different orientation compared to that of CBS^{WT}. These large changes observed at the PLP binding site may result in sterical hindrances that may potentially affect the affinity of the CBS^{L230Q} mutant for the cofactor.

Another region of interest is the binding site for the heme cofactor, which is located in a hydrophobic pocket formed by residues 40 – 70 in the N-terminal domain of the protein. When bound, heme is axially coordinated by two amino acid residues, C52 and H65, while additional polar interactions with residues W54, R51, R224 and R266 are also observed. **Figure 28** shows the structure of the heme binding pocket in the CBS^{WT}, CBS^{K72I} and CBS^{L230Q} MD structure, while Table 3 summarizes the key properties of the heme binding cavity. CBS^{WT} and CBS^{K72I} form a cavity with similar surface area, although in the case CBS^{K72I} the pocket is wider, involves more protein residues and is shallower compared to that of CBS^{WT}. As a result, the volume of the CBS^{WT} cavity (270 $Å^3$) is 40% larger compared to that of CBS^{K72I} but both have the dimensions required to allow heme to enter the binding site. In contrast, the CBS^{L230Q} heme cavity is significantly shrunk, with a total volume of 101 $Å^3$ and only 18 residues involved in pocket formation. The CBS^{L230Q} heme pocket is narrow and does not have the depth

necessary to fully accommodate heme, which may reduce the mutant's affinity for the cofactor. This observation also agrees well with our UV-Visible measurements (see below), showing impaired CBS^{L230Q} – heme binding.

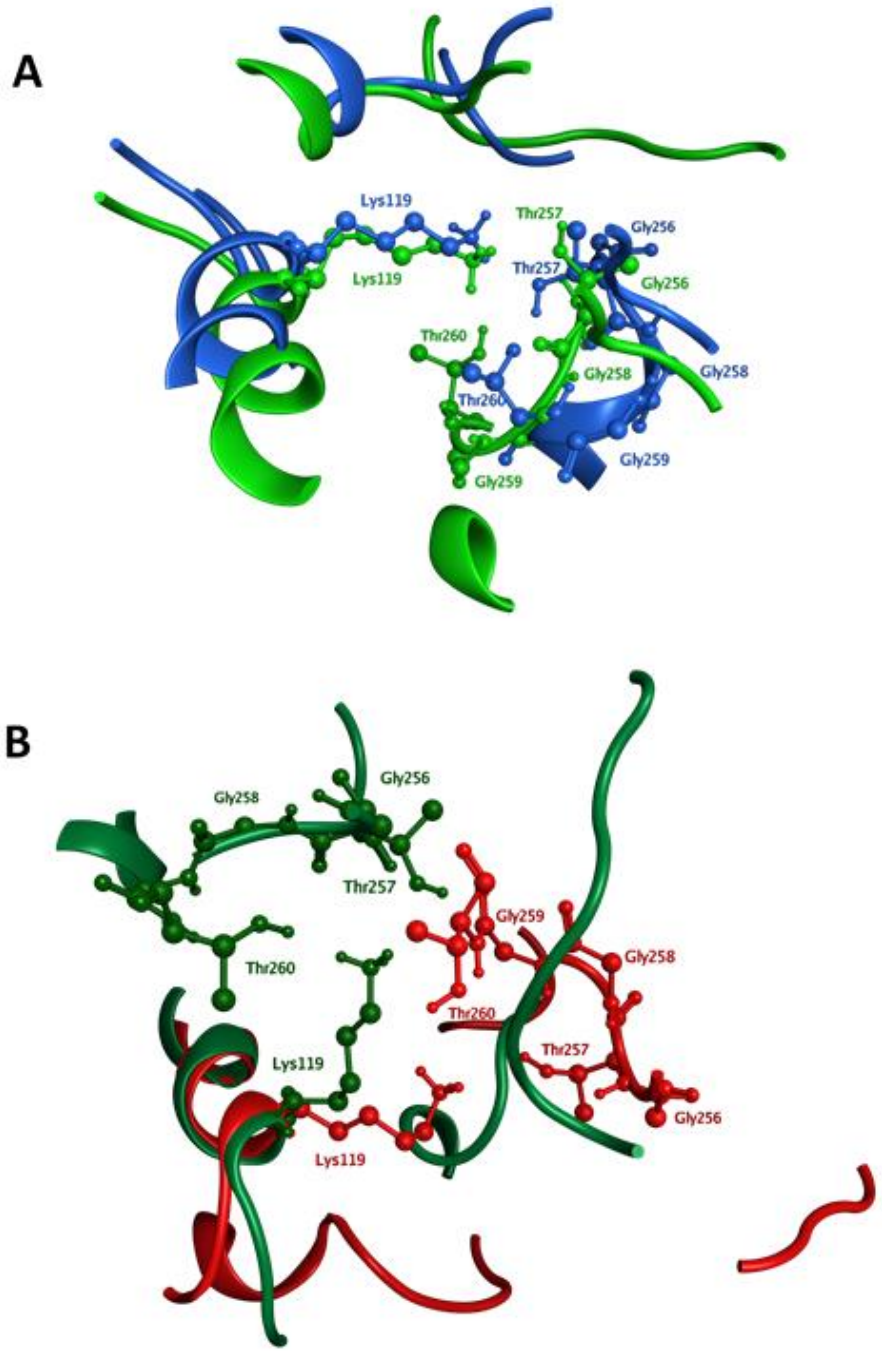

Figure 27. MD simulation of CBS^{WT} and mutants. A**)** Overlay of the CBS^{WT} (green) and CBS^{K72I} (blue) PLP binding site, based on the MD simulation structures of this study. B) Overlay of the CBS^{WT} (green) and CBS^{L230Q} (red) PLP binding site, based on the MD simulation structures of this study.

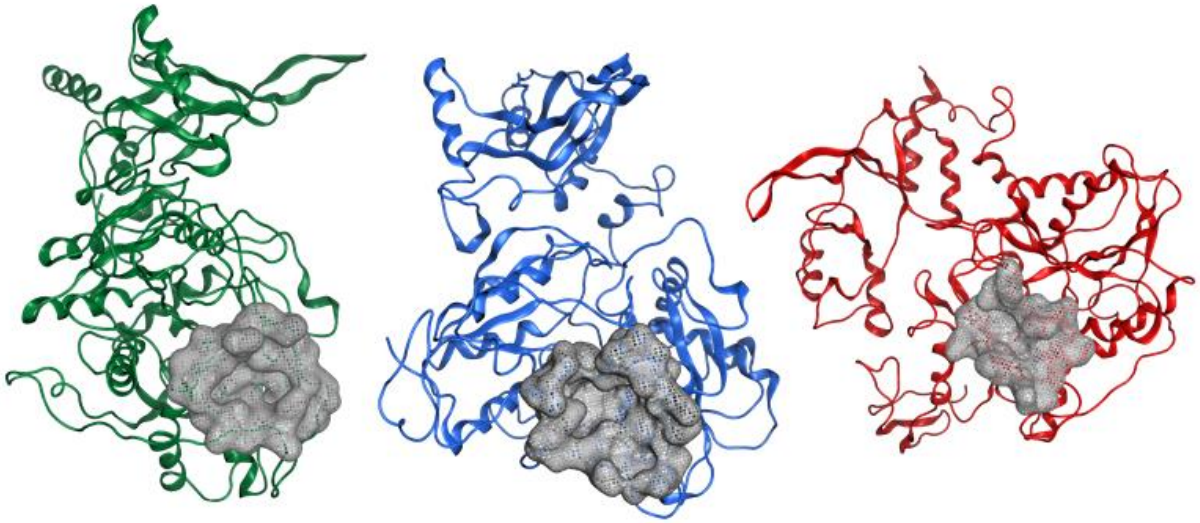

Figure 28. Surface model of the CBS^{WT} (green ribbons), CBS^{K72I} (blue ribbons), and CBS^{L230Q} (red ribbons) heme binding cavity (grey surface), based on the MD simulation structure of the protein. The basic characteristics of the cavity are summarized in Table 3.

Table 3. Properties of the CBS^{WT}, CBS^{K72I} and CBS^{L230Q} heme binding pockets, based on the MD simulation structures.

Protein	**CBS^{WT}**	**CBS^{K72I}**	**CBS^{L230Q}**
Surface Area ($Å^2$)	276	280	217
Cavity Volume ($Å^3$)	270	192	101
Residues	P46, D47, A48, P49, S50, R51, C52, W54, S61, E62, S63, P64, H65, D221, Q222, Y223, R224, N225, A226, S227, P229, L230, G258, T262, R266, P312, T313, V314, L315, D316, T318, V319	L28, E29, A48, P49, S50, R51, C52, T53, W54, Q55, P59, A60, S61, E62, S63, P64, D221, Q222, Y223, R224, N225, A226, S227, N228, P229, Y233, G258, G259, T260, T262, G263, R266, P312, T313, V314, L315, D316, V319	D47, A48, P49, S50, R51, C52, Q55, R58, R266, E289, I311, P312, T313, L315, D316, R317, T318, V319

5.4.3 GROMACS Simulations

To further explore the residual flexibility and stability of the mutated structures, the protein models were subjected to 50 ns MD simulations. The results are collectively shown in **Figure 29**. Analysis of the 50 ns trajectories revealed a very similar fluctuations pattern for all proteins, with RMSD values increasing rapidly until ~ 5 ns and stabilized around 1 nm after 10 ns of simulation time (**Figure 29A**).

The RMSF results of the CBS^{WT} and CBS^{K72I} protein models show nearly identical dynamic fluctuations for all residues, with higher RMSF values corresponding to loop regions or unstructured parts of the proteins as expected (mainly residues 1-50, 450-475 and 510-530). However, CBS^{L230Q} exhibits significantly increased fluctuations for residues 10-40, 381-447, 456-486, 503-508 and 532-551(**Figure 29B**), suggesting a less rigid, less stable protein structure for this mutant.

The structural compactness of CBS variants as a function of simulation time can be assessed using the radius of gyration (R_g) of the protein models (**Figure 29C**). Stable, well-folded conformations typically exhibit small R_g values with minimal fluctuations as the simulation progresses, while unfolded or unstable protein structures show significant fluctuations of R_g during the simulation. Our results show that CBS^{WT} and CBS^{K72I} have a stable R_g of ~ 2.5 nm after 10 ns, while CBS^{L230Q} has higher R_g values that fluctuate until ~ 30 ns of simulation time. At that point, CBS^{L230Q} adopts a conformation with a stable R_g which is slightly higher than that of CBS^{WT} and CBS^{K72I} . Similarly to the RMSF results, this can be attributed to a less rigid, less stable structure for CBS^{L230Q} . Finally, **Figure 29D** shows the change of the Solvent-Accessible Surface Area (SASA) over simulation time. No significant differences were observed for the CBS variants in this study, with all models stabilizing around SASA values of ~ 250 nm^2. This indicates minimal changes in the overall protein folding, without coordinated exposure to the solvent of the residues that were burried inside the structure at the beginning of the simulation. Overall, the MD simulation results suggest that CBS^{WT}

and CBS^{K72I} exhibit similar stability and dynamic behavior, while CBS^{L230Q} adopts a less stable conformation that is significantly more flexible than that of the other two variants.

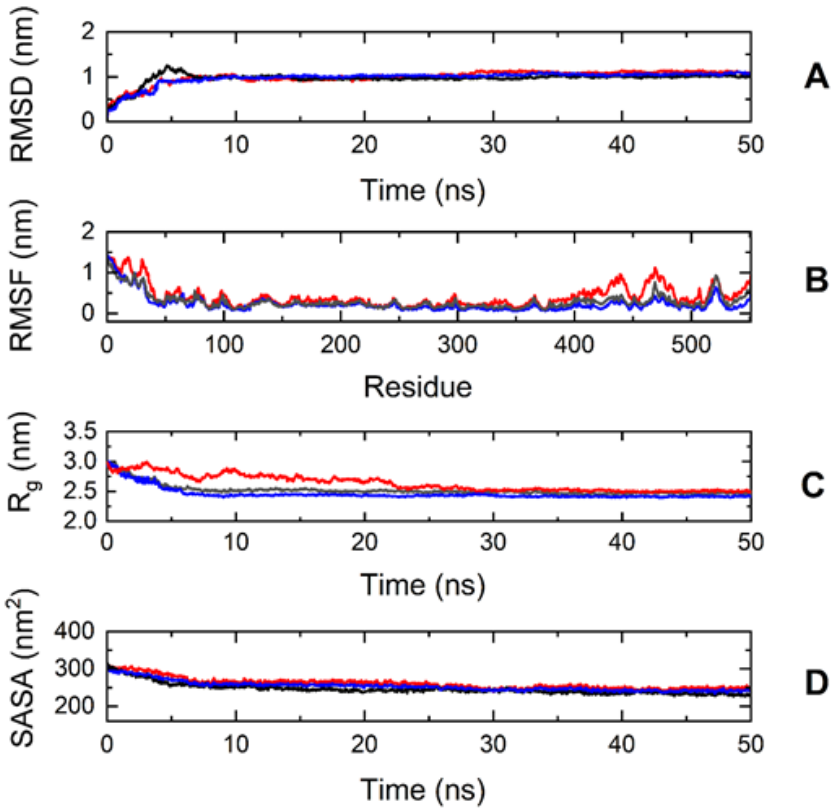

Figure 29. Trajectory analysis of CBS variants. CBS^{WT}, CBS^{K72I}, and CBS^{L230Q} traces are shown as black (—), blue (—), and red (—) lines respectively. A) RMSD of the protein's backbone atoms, when superimposing the simulated and initial structure as a function of MD simulation time. B) RMSF graph showing atomic fluctuations of protein residues during simulation. C) Total radius of gyration (R_g) of the protein's backbone atoms, as a function of MD simulation time. D) Protein's solvent accessible surface area (SASA) as a function of MD simulation time.

5.4.4 Spectroscopic features of CBS^{K72I} and CBS^{L230Q} variants

To define the structural and functional effects of the K72 and L230 substitutions, we expressed, purified and biochemically characterized the CBS^{K72I} and CBS^{L230Q} variants. Both mutant enzymes showed a single main band on the SDS-PAGE gel with molecular weight identical to CBS^{WT} (**Figure 30A**). The identity of the recombinant CBS proteins was also confirmed by western blot analysis using an anti-CBS antibody, as previously described (**Figure 30A**) (Ismail et al., 2019).

The recombinant CBS^{K72I} enzyme purified to homogeneity was red in color, while the CBS^{L230Q} variant was yellow. Absorption spectra in the UV-Visible region revealed that CBS^{K72I} binds heme similarly to CBS^{WT}, showing a sharp Soret band at 428 nm and a broad absorption envelope for the α/β region with maximal intensity at 553 nm (**Figure 30B**). On the other hand, by comparing the spectroscopic features of CBS^{WT} in the visible region with those of the CBS^{L230Q} variant, several lines of evidence indicate that the mutation alters the heme binding. First, in the CBS^{L230Q} mutant the absorbance maximum of the Soret peak shows a ∼10 nm blue shift accompanied by a 3.5-fold decrease in the maximum intensity as compared with the corresponding band of CBS^{WT} (**Figure 30B**). Second, no detectable bands can be observed in the α/β region in the CBS^{L230Q} spectrum. Thus, spectral data support the hypothesis that the Leu to Gln substitution in position 230 causes impaired heme binding. Far-UV CD spectra of the CBS^{K72I} and L203Q variants were very similar to those of the WT protein (**Figure 30C**), indicating in all cases a high content of α-helical structure, and that the mutations do not affect the secondary structure of the enzyme.

To acquire information on the effect of the mutations on the stability of the enzyme, the thermostability of the CBS^{K72I} and L203Q variants was measured by CD-monitored thermal unfolding and compared with that of the WT enzyme. These studies were performed by monitoring the decrease of the dichroic signal at 222 nm, which is

indicative of the loss of the protein secondary structure, in the temperature range of 15 ºC to 90 ºC (**Figure 30D**). All the CD-monitored heating scans reveal that, like the CBS^{WT}, the mutants are denatured in a single-step concerted process. Interestingly, the loss of the secondary structure of the CBS^{WT} and CBS^{K72I} occurs with melting temperatures (T_m) similar to each other (73.2 ± 0.2 °C for the WT and 70.0 ± 0.4 °C for the CBS^{K72I} mutant), while the unfolding of CBS^{L230Q} occurs at significantly lower temperature (T_m 56 ± 2 °C). Thus, the CBS^{L230Q} mutation appears to exert the most destabilizing effect on the protein (**Figure 30D**).

The thermodynamic stability of the proteins was investigated by chemical denaturation intrinsic fluorescence experiments. **Figure 31** shows the chemical denaturation profiles of CBS^{WT} and mutant proteins collected at 25 ºC. At high concentrations of guanidine hydrochloride, a well-known chaotrope, all variants undergo a reversible two-state unfolding transition with no apparent intermediate state involved. The fitting of a two-state denaturation model to the experimental data can be used to derive the thermodynamic stability parameters for all the proteins of this study. Table 4 summarizes these results and the corresponding standard deviations as determined by the fitting method. Based on the calculated free energy change for the chemically-induced unfolding process ($\Delta G_{N\text{-}D}^{H_2O}$), the thermodynamic stability of the CBS variants follows the order: $CBS^{L230Q} < CBS^{K72I} < CBS^{WT}$, as observed for the CD thermal denaturation (**Figure 31**).

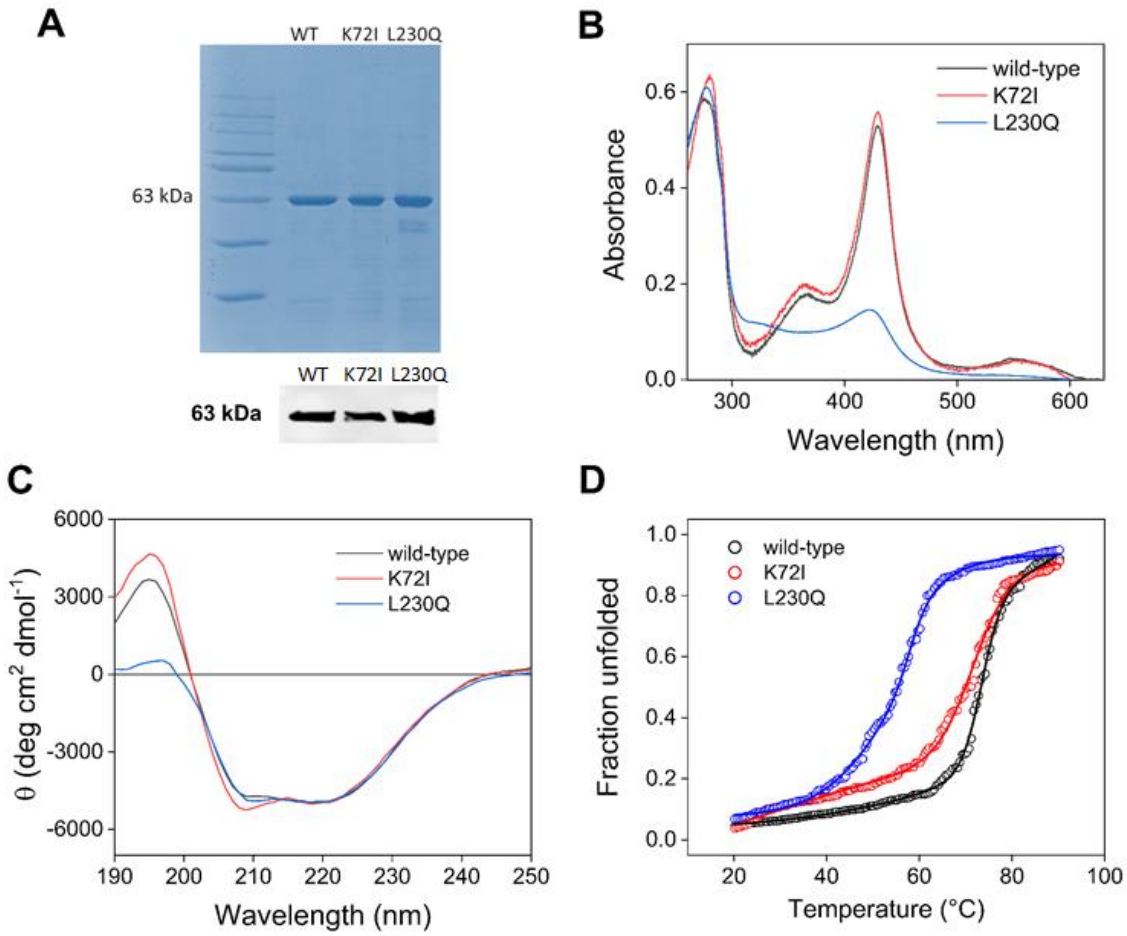

Figure 30. Spectroscopic properties of recombinant CBS variants. A) 10% SDS-PAGE analysis of purified recombinant CBS variants and western blotting with a polyclonal CBS antibody (1:1000 dilution)). The first lane from left is the molecular marker followed by the CBS WT, K72I, and L230Q samples B) UV-visible absorption spectra of 10 μM purified CBS variants in 20 mM sodium phosphate buffer pH 7.5. C) Far-UV CD spectra of 0.2 mg mL^{-1} CBS variants in 20 mM sodium phosphate buffer pH 7.5. D) Thermal denaturation of 0.2 mg mL^{-1} CBS variants recorded following ellipticity signal at 222 nm in sodium phosphate buffer pH 7.5.

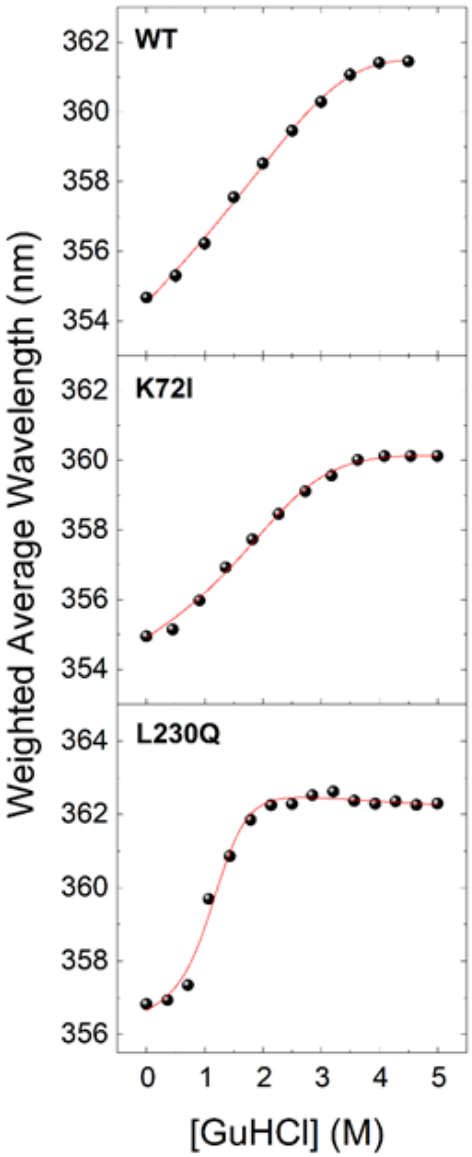

Figure 31. Chemical denaturation profiles of WT and mutant CBS proteins, as determined by steady-state fluorescence spectroscopy. Data are plotted as the weighted average wavelength of the protein fluorescence emission spectra at various guanidinium chloride concentrations ([GuHCl]), after excitation at 280 nm. Solid red lines represent the best fit to a simple two-state model of the form N↔□(D).

Table 4. Thermodynamic stability parameters for all CBS variants as derived by chemical denaturation experiments at 25ºC.

Protein	$\Delta G_{N-D}^{H_2O}$ (kcal/mol)	m (kcal mol^{-1} M^{-1})	$[D]^{50\%}$ (M)
WT	2.41 ± 0.24	- 0.76 ± 0.07	3.17 ± 0.12
K72I	2.16 ± 0.15	-0.92 ± 0.06	2.34 ± 0.05
L230Q	2.00 ± 0.17	-1.66 ± 0.13	1.21 ± 0.03

5.4.5 Effect of CBS^{K72I} and CBS^{L230Q} mutations on CBS catalytic activity

To explore the potential impact of the CBS^{K72I} and CBS^{L230Q} mutations on the catalytic properties of the CBS enzyme, we analyzed the ability of each variant to catalyze both canonical (L-Ser + L-Hcys) and H_2S-generating alternative (L-Cys + L-Hcys) reactions using reverse phase HPLC.While the HPLC profiles of the CBS^{K72I} mutant were superimposable to those of CBS^{WT}, the chromatograms for CBS^{L230Q} exhibited a decrease in the intensity of the L-Cth fluorescence peak. This suggests a lower extent of product formation, indicating that the CBS^{L230Q} variant is likely less efficient at generating L-Cth (**Figure 32**).

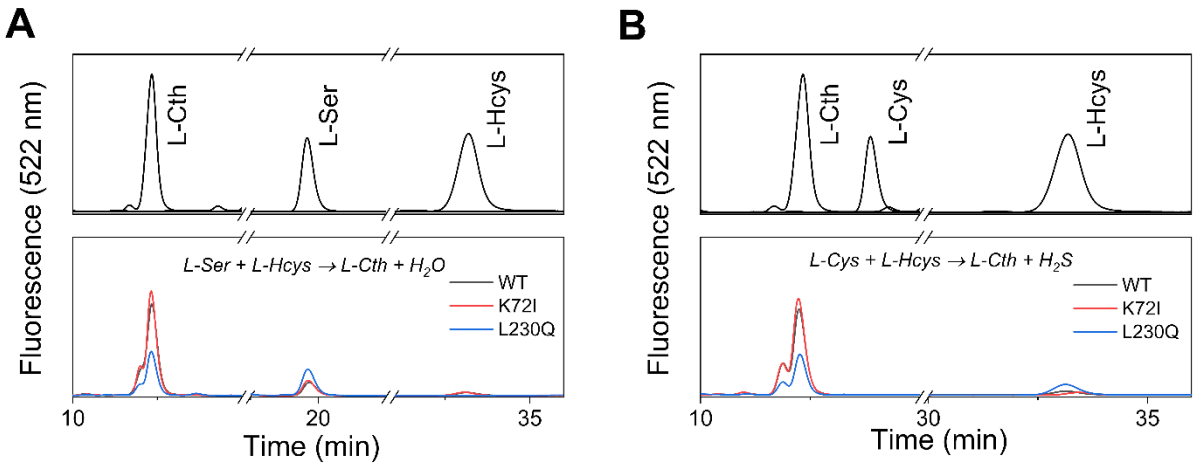

Figure 32. Analysis of L-Cth production for CBS variants using reverse phase HPLC. A) Pure standard L-Ser, L-Hcys and L-Cth (top), and product obtained following a 2 h incubation of CBS single variants with 1 mM L-Ser and 0.8 mM L-Hcys in the presence of 0.5 mM SAM. B) Pure standard L-Cys, L-Hcys and L-Cth (top) and product obtained following a 2 h incubation of CBS single variants with 1 mM L-Cys and 0.8 mM L-Hcys in the presence of 0.5 mM SAM.

To confirm the functional consequences of our HPLC observations, we determined steady-state enzyme kinetics for both CBS variants in the canonical and alternative H_2S-generating reactions. **Table 5** summarizes all the determined parameters, and **Figure 33** shows enzyme kinetic assays for CBS^{WT}, CBS^{K72I} and CBS^{L230Q} in the absence and presence of its allosteric activator SAM. The kinetic parameters of the canonical L-Ser + L-Hcys condensation reaction were measured by using a CBL-LDH coupled-coupled assay [19], while those for the L-Cys + L-Hcys condensation were determined using the lead acetate assay [20, 21]. Kinetic data obtained for CBS^{WT} were

in good agreement with those already reported by other groups [22, 23]. The K_m and k_{cat} values of CBS^{K72I} mutant did not exhibit substantial differences compared to those of CBS^{WT} for both canonical and alternative reactions, suggesting that the K72I mutation does not affect the kinetic properties of the enzyme. On the other hand, the L230Q mutation decreases the k_{cat} value for the canonical reaction by ~4-fold and 7-fold in the absence and presence of SAM, respectively, without affecting the K_m values for L-Ser. This results in an overall ~4-6-fold decrease in catalytic efficiency. Interestingly, the effect of the L230Q mutation on the enzyme's ability to catalyze the condensation of L-Cys and L-Hcys, yielding H_2S was even more pronounced. The L230Q mutation led to a small decrease in k_{cat} in the absence (~3-fold) and presence (~4-fold) of SAM. However, this was accompanied by a ~29-fold (without SAM) and 6-fold (with SAM) increase in K_m values for L-Cys. Thus, the net result was a dramatic decrease in the overall enzyme catalytic efficiency for H_2S synthesis both in the absence (~84-fold) and presence (~23-fold) of SAM compared to the CBS^{WT}.

Table 5. Steady-state enzyme kinetics of CBS variants for both the canonical and the alternative H_2S-generating reactions.

	Without SAM			With SAM		
	k_{cat} (s^{-1})	**K_m (mM)**	**k_{cat}/K_m ($mM^{-1}\ s^{-1}$)**	**k_{cat} (s^{-1})**	**K_m (mM)**	**k_{cat}/K_m ($mM^{-1}\ s^{-1}$)**
L-Ser + L-Hcys→L-Cth + H_2O						
WT	1.7 ± 0.1	7.0 ± 1.1	0.24 ± 0.05	4.7 ± 0.1	3.7 ± 0.3	1.3 ± 0.1
K72I	1.8 ± 0.1	7.2 ± 0.6	0.25 ± 0.03	5.3 ± 0.3	4.9 ± 0.8	1.1 ± 0.2
L230Q	0.44 ± 0.02	7.6 ± 0.7	0.06 ± 0.01	0.67 ± 0.04	3.0 ± 0.8	0.22 ±0.07
L-Cys + L-Hcys→L-Cth + H_2S						
WT	0.91 ± 0.03	0.9 ± 0.2	1.01 ± 0.25	3.3 ± 0.3	4.6 ± 1.4	0.7 ± 0.2
K72I	1.0 ± 0.1	1.6 ± 0.5	0.63 ± 0.25	2.9 ± 0.4	5.5 ± 2.2	0.5 ± 0.2
L230Q	0.32 ± 0.06	26 ± 8	0.012 ± 0.006	0.8 ± 0.1	26 ± 3	0.030 ± 0.007

Each result shown is the mean ± SE of three (n = 3) independent experiments.

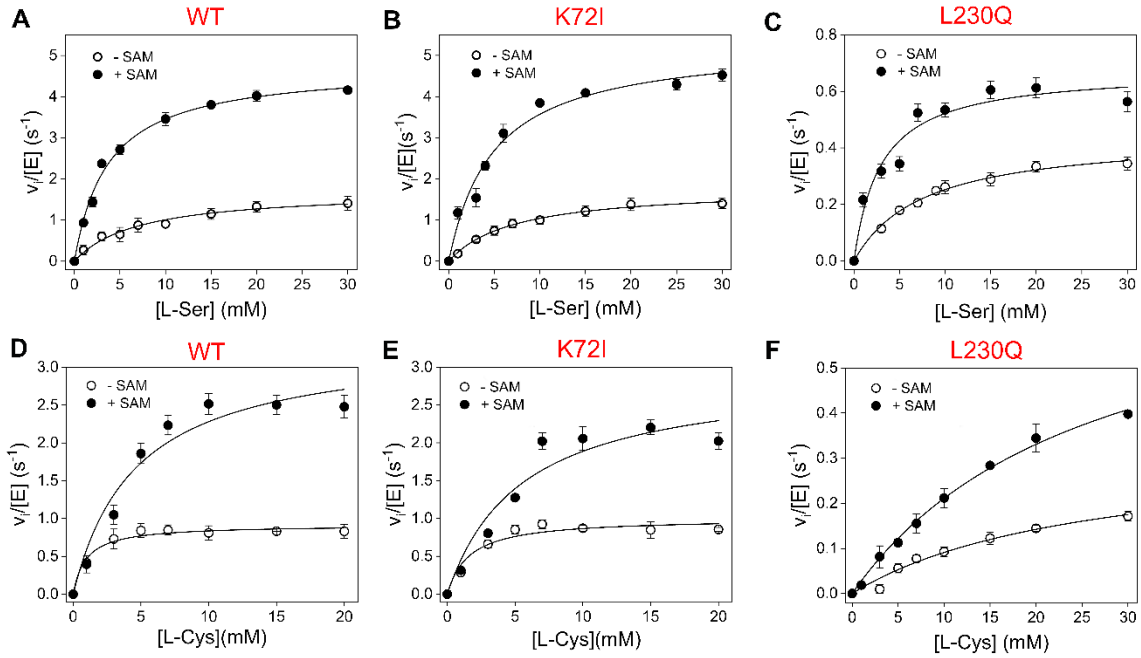

Figure 33. Enzyme kinetics. Steady-state enzyme kinetics was performed for CBS^{WT} (A,D), CBS^{K72I} (B,E) and CBS^{L230Q} (C,F) variants in the absence (open circle) and presence (solid circle) of 0.5 mM SAM. Enzyme kinetics for L-Ser + L-Hcys condensation (A-C) was executed using CBL-LDH coupled-coupled assay, while lead assay was used for determining kinetics parameters for the alternative L-Cys + L-Hcys condensation (D-F). Data were fitted using the Michaelis–Menten equation. These kinetic parameters are summarized in Table 5.

5.4 Characterization of Novel CBS Variants Reported in Homozygous Homocystinuria Patients

The present study investigated a novel homozygous mutation, c.707C>A (T236N) in a Chinese patient with homocystinuria. The mutation is located in exon 8 and was reported to be novel. The patient was diagnosed with classical homocystinuria at the age of 11 (Abraham et al., 2015). The major clinical features of the patient included skeletal abnormality, developmental delays, and eye disorders. More specifically, the patient showed osteoporosis and eye disorders, including ectopia lentis. Significantly increased plasma (222 μmol/L) and urinary (>500 μmol/L) total homocysteine were observed. Blood methionine elevated to 468 μmol/L (normal range 10–50 μmol/L). To confirm the identity of the recombinant CBS proteins, SDS-PAGE analysis followed by Coomassie Brilliant Blue and western blotting using an anti-CBS antibody was performed (**Figure 34**).

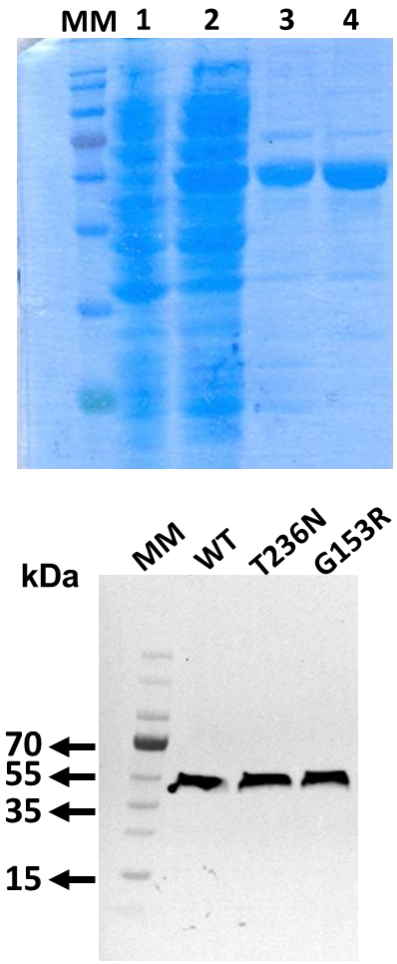

Figure 34. 10% SDS-PAGE analysis of purified recombinant CBS variants by coomassie brilliant blue (upped panel) and western blotting (lower panel) with a polyclonal CBS antibody (1:1000 dilution). Lane 1: T236N crude extract, Lane 2: G153R crude extract, Lane 3: T236N purified protein, and Lane 4: G153R purified protein.

Activity was determined by measuring fluorescence emission at 460 nm (excitation at 368 nm) (Abcam, 2021). Our enzymatic assays demonstrated a drastic reduction in CBS activity upon introduction of the p.T236N mutation, consistent with its classification as a pyridoxine non-responsive mutation (**Figure 35 and 36**). This severe impairment in enzymatic function was similar to previous reports of other CBS mutations in the catalytic domain (Kožich, Kruger, & Kraus, 2010; Kozich et al., 2010). However, our study is the first to characterize and assess the CBS^{T236N} mutation activity. The observed reduction in enzymatic activity highlights the importance of pyridoxal and heme cofactors in modulating CBS function, further emphasizing the potential therapeutic implications of cofactor supplementation in certain CBS deficiency cases (Roman, Mascarenhas, Ceric, Ballou, & Banerjee, 2023).

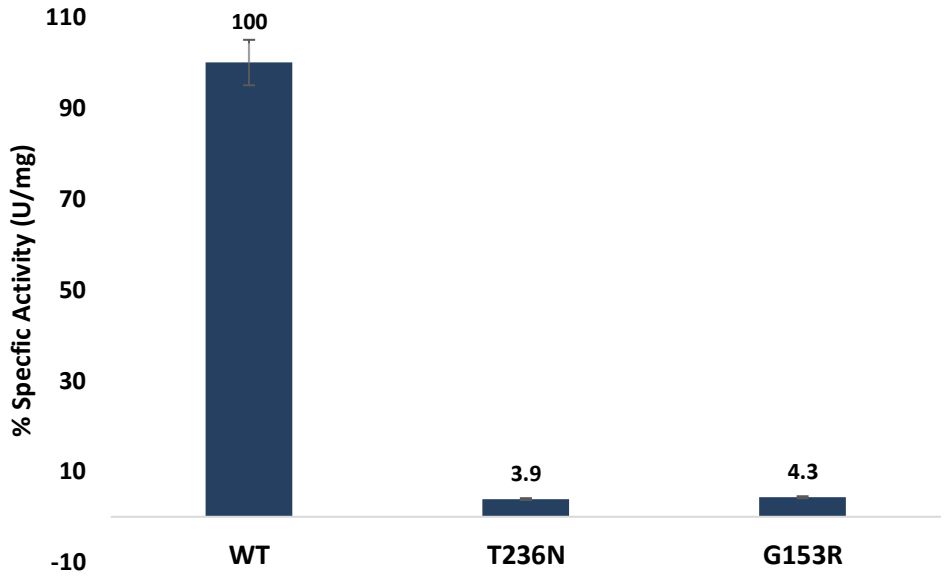

Figure 35. CBS^{WT}, CBS^{T236N}, and CBS^{G153R} enzymatic activity.

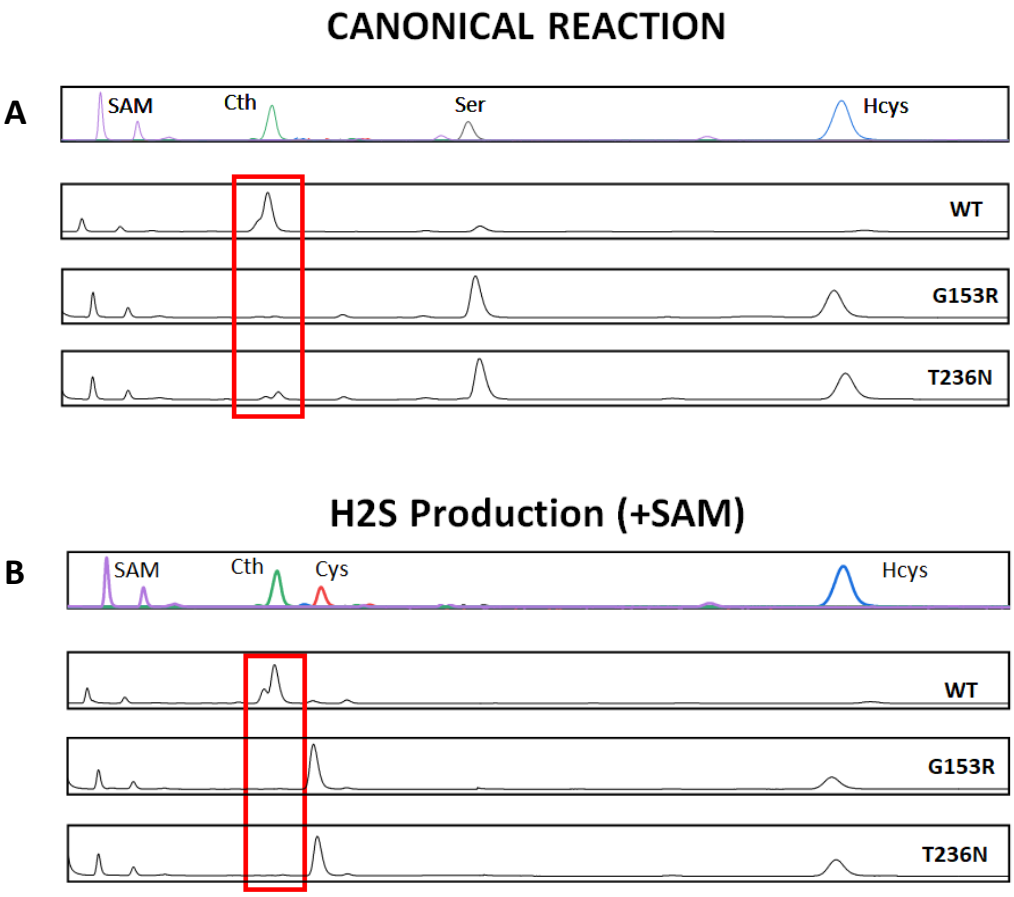

Figure 36. Analysis of L-Cth production for CBS variants using reverse phase HPLC. (A) Pure standard L-Ser, L-Hcys and L-Cth (top), and product obtained following 2 hours incubation of CBS single variants with 1 mM L-Ser and 0.8 mM L-Hcys. (B) Pure standard L-Cys, L-Hcys and L-Cth (top) and product obtained following 2 hours incubation of CBS single variants with 1 mM L-Cys and 0.8 mM L-Hcys.

The far-UV spectrum of CBS^{T236N} at 25°C revealed minor structural alterations while CBS^{G153R} was totally not stable at 25°C (**Figure 37 and 38**). Therefore, p.G153R mutation was not further characterized in this study. Analysis of the spectra using the BESTSEL online server (Micsonai et al., 2018) shows that the CBS^{T236N} mutant has a lower antiparallel (12.9%) and a higher parallel (14.3%) β-sheet content when compared to CBS^{WT} (19.9% and 6.1% respectively), indicating some differences in the overall protein architecture (Table 6). Heating CBS^{T236N} to 90°C only partially unfolds the structure, with the protein retaining a significant portion of its secondary structure elements. However, this thermal transition is irreversible since no further changes in the far-UV CD spectrum were observed when the sample was cooled to 25°C and visible protein aggregates formed in the cuvette as a direct result of the heating step.

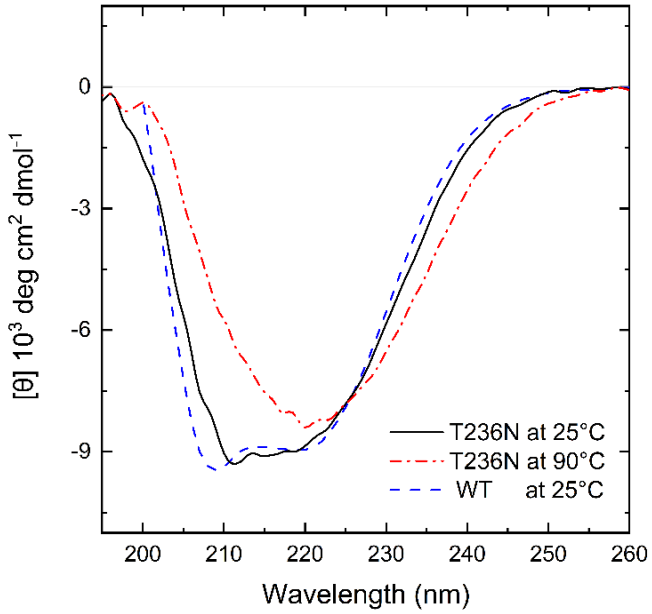

Figure 37. Far-UV CD spectra of 5 μM CBS^{WT} and CBS^{T236N}proteins in PBS buffer. The black solid line corresponds to CBS^{T236N}at 25°C, the red dash-dot line corresponds to CBS^{T236N}at 90°C, while the blue dash line corresponds to CBS^{WT} at 25°C for comparison purposes.

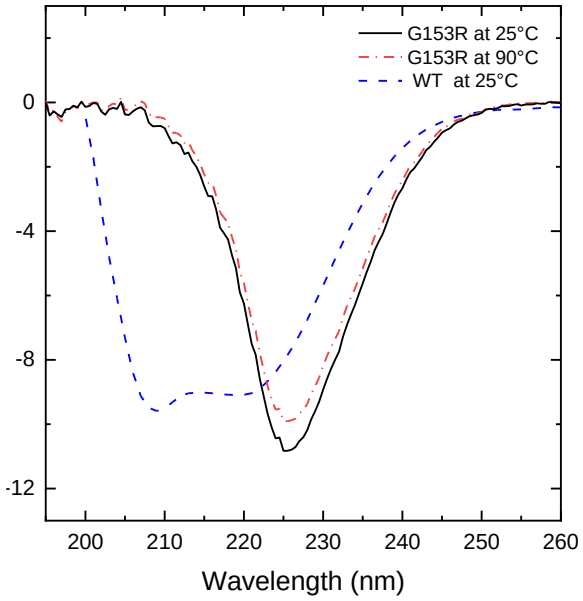

Figure 38. Far-UV CD spectra of 5 μM CBS^{WT} and CBS^{T236N}proteins in PBS buffer. The black solid line corresponds to CBS^{T236N}at 25°C, the red dash-dot line corresponds to CBS^{T236N}at 90°C, while the blue dash line corresponds to CBS^{WT} at 25°C for comparison purposes.

Table 6. Estimated secondary structure content (%) from experimental far-UV CD measurements calculated using the BESTSEL online server (Micsonai et al., 2018).

Protein	**Helix**	**Antiparallel**	**Parallel**	**Turn**	**Other**
CBS^{WT}	15.8	19.9	6.1	12.8	45.3
CBS^{T236N} (25°C)	15.4	12.9	14.3	14.0	43.4
CBS^{T236N} (90°C)	5.0	17.3	16.8	13.1	47.6

The thermal stability of CBS^{WT} and CBS^{T236N} was examined by heating the proteins at a steady rate from 25°C to 90°C and monitoring CD changes at 212 nm. The raw data were normalized as unfolded protein population for comparison purposes and the results are shown in **Figure 39**. Both the CBS^{WT} and CBS^{T236N} proteins unfold following a simple two-state transition, as shown by the characteristic sigmoidal melting curves. The CBS^{T236N} unfolding process exhibits lower comparativity compared to that of CBS^{WT}, as indicated by the temperature change required (ΔT) for a fully folded protein population to become unfolded ($\Delta T^{T236N} \sim 40$°C and $\Delta T^{WT} \sim 25$°C respectively). Interestingly, CBS^{T236N} appears to be significantly thermally destabilized, as the melting temperature of the transition (T_m, temperature at which only 50% of the protein population is folded) is almost 15°C lower than that of the CBS^{WT} ($T_m{}^{T236N}$ = 50.2°C and $T_m{}^{WT}$ = 64.8°C respectively). However, the non-reversibility of the transitions does not allow a more detailed thermodynamic analysis of these data. Threonine's hydroxyl group can participate in hydrogen bonding interactions, contributing to protein stability and folding (University, 2024). Asparagine's amide group can also engage in hydrogen bonding, albeit differently from the hydroxyl group.

The substitution may affect the network of hydrogen bonds within the protein, influencing its stability and function.

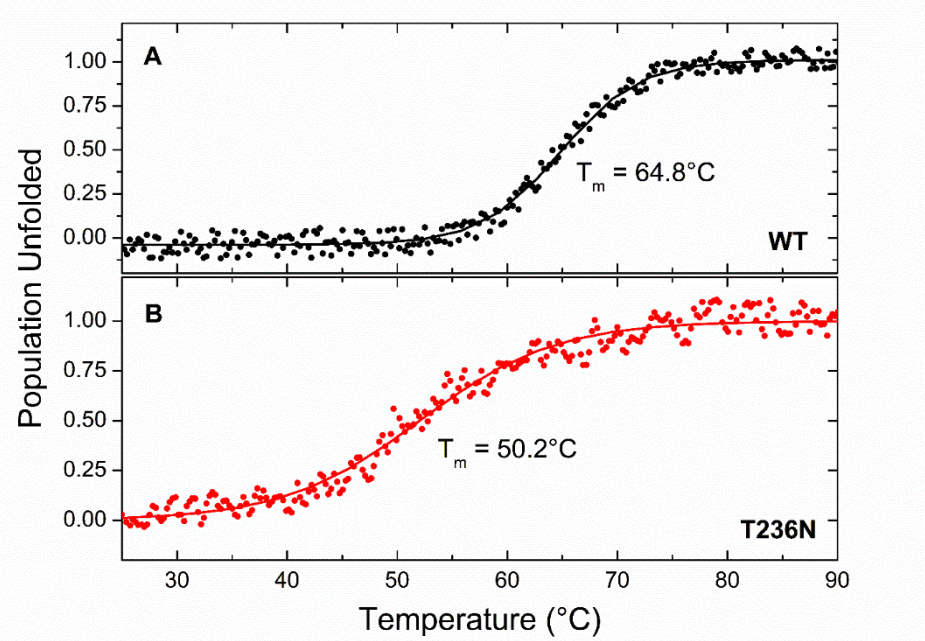

Figure 39. Thermal denaturation profiles of 5 μM CBS^{WT} (Panel A) and CBS^{T236N} (Panel B) CBS proteins in PBS buffer, monitored at 212 nm and normalized as the unfolded protein population. Circles represent experimental data and solid lines correspond to sigmoid fits as a guide to the eye.

To further investigate the impact of p.T236N on protein stability, we used chemical denaturation assays to compare recombinant CBS^{WT} and CBS^{T236N} proteins. This was achieved by monitoring changes in the fluorescence emission spectrum of the protein in the 300 – 450 nm range at different concentrations of a chemical denaturant. Guanidinium chloride (GuHCl) was used as a denaturant due to its ability to reversibly weaken or break noncovalent interactions, including salt bridges and hydrogen bonds (Group, 2022). The data of the chemical denaturation assays were processed as described in the Materials and Methods section and the final results are presented in **Figure 40** as plots of weighted average emission wavelength *versus* GuHCl concentration. Similar to the thermal transitions of CBS^{WT} and CBS^{T236N}, the chemical denaturation profiles show a two state unfolding process for both proteins, with the fluorescence emission spectra shifting towards higher wavelengths as the concentration of the denaturant increases. However, in this case, the reversibility of the process (dialysis of the samples back to original buffer conditions gives almost identical emission spectra) allows a more in-depth thermodynamic analysis. **Table 7** summarizes the thermodynamic stability parameters derived by nonlinear least-squares curve fitting of a simple two-state transition model to our experimental data (Figure 4, solid lines). The results showed that the free energy change difference ($\Delta\Delta G_{D-N}$) between CBS^{WT} and CBS^{T236N} was 1.26 kcal/mol, indicating that the CBS^{WT} protein is thermodynamically more stable than the CBS^{T236N} mutant. Taken together, CD and fluorescence data strongly suggest that CBS^{T236N} has a destabilizing effect on the CBS protein.

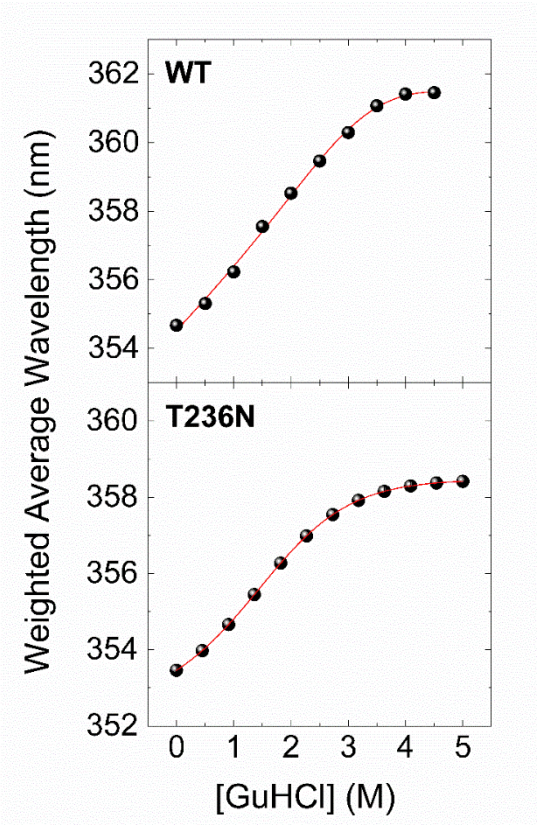

Figure 40. Chemical denaturation profiles of 0.05 mg/mL CBS^{WT} (upper panel) and CBS^{T236N} (lower panel) CBS proteins in PBS buffer at 25°C, plotted as weighted average emission wavelengths at various denaturant concentrations. Solid lines correspond to nonlinear least squares fits of a simple two-state thermodynamic model to the experimental data.

Table 7. Thermodynamic stability parameters for CBS^{WT} and CBS^{T236N}as derived by chemical denaturation experiments at 25ºC.

Protein	**ΔG_{N-D} (kcal/mol)**	**m (kcal mol^{-1} M^{-1})**	**$[D]^{50\%}$ (M)**
CBS^{WT}	2.41 ± 0.24	- 0.76 ± 0.07	3.17 ± 0.12
CBS^{T236N}	1.15 ± 0.04	-0.74 ± 0.06	1.55 ± 0.05

To gain better insight into the effect of the mutation on protein structure and dynamics, we performed a series of molecular dynamics simulations for both CBS^{WT} and CBS^{T236N} proteins. An overlay of the representative structural models for CBS^{WT} and CBS^{T236N} is shown in **Figure 41**. The MD results suggest that both proteins adopt a similar conformation, however, small changes in secondary structure elements and in their relative position are evident throughout the protein structure, consistent with our far-UV CD data (root-mean-square deviation (RMSD) = 4.4 Å). Analysis of the local interactions for T236 in WT and N236 in p.T236N (**Figure 42**) shows that the network of stabilizing bonds is significantly less extensive in the case of the mutant, which may justify the reduced stability (both thermal and thermodynamic) observed during our CD and fluorescence experiments. Further analysis of the simulation trajectories revealed almost identical behavior for both proteins in terms of RMSD, root-mean-square-fluctuations (RMSF), radius of gyration (R_g) and solvent-accessible surface area (SASA) over the simulation time, suggesting a minimal impact of the mutation on the protein dynamics and general folding (**Figure 43**).

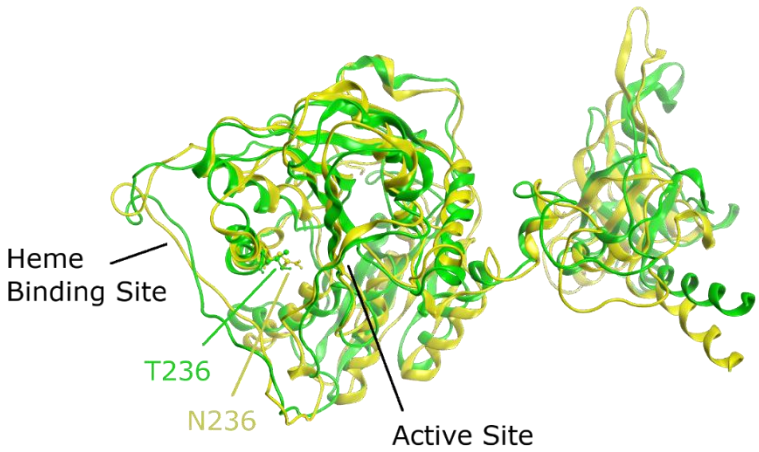

Figure 41. Overlayed representative MD structures for CBS^{WT} (green ribbons) and CBS^{T236N} (yellow ribbons). Residues at position 236 are shown as ball-stick models, while the black lines show the location of the cofactor binding sites.

Figure 42. Local interactions at position 236 for CBS^{WT} (panel A) and CBS^{T236N} (panel B) based on the representative structures of the MD simulations. In the case of

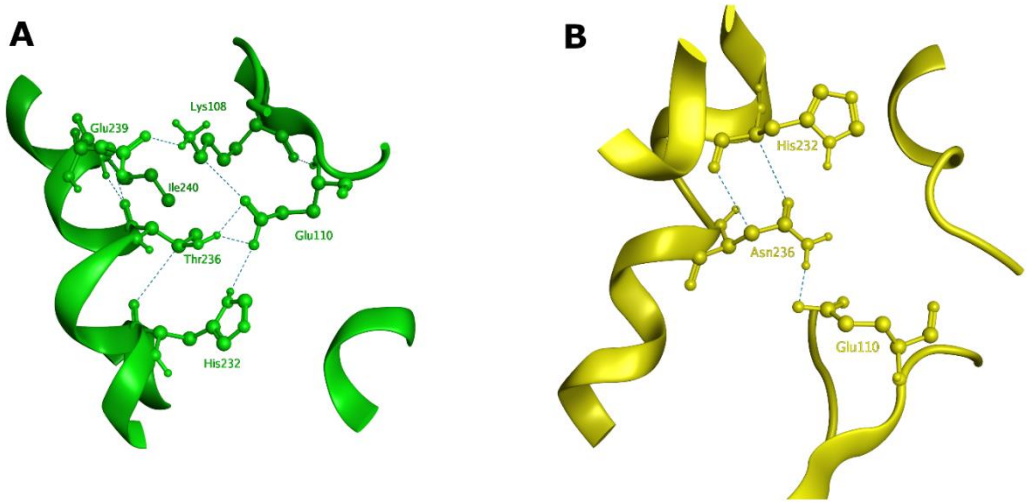

CBS^{T236N}, only the His232 and Glu110 interactions are preserved from the original network of stabilizing bonds.

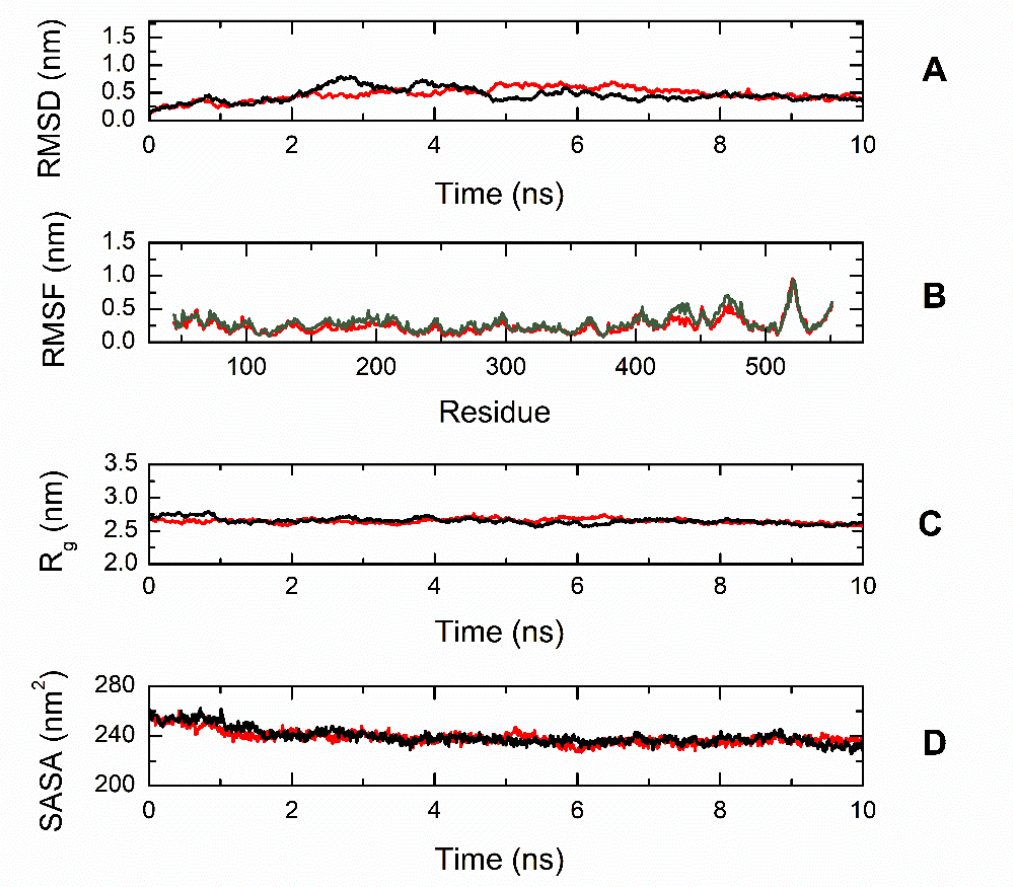

Figure 43. Trajectory analysis of CBS^{WT} (black, —) and CBS^{T236N} (—) proteins. A) Root mean square deviation (RMSD) of the protein backbone atoms as a function of MD simulation time. B) root-mean-square-fluctuations (RMSF) of individual residues for the duration of the simulation. C) Total radius of gyration (R_g) of the protein backbone atoms as a function of MD simulation time. D) Solvent accessible surface area (SASA) of the protein as a function of MD simulation time. All parameters indicate a similar dynamic behavior for WT and mutant CBS.

5.6 Chemical Chaperones Treatment in CRSIPR-Cas HEK293T Cells

In this pivotal phase of our research, we have accomplished the successful transfection of HEK293T cells with the pcDNA3.1-EGFP plasmid employing the Lipofectamine transfection method. This achievement marks a crucial step in our experimental framework, as it lays the foundation for our subsequent investigations aimed at rescuing the impaired CBS activity in these cells through treatment with various chemical chaperones. The main objective of this transfection experiment was to construct a reliable and genetically modified cellular model that would allow us to investigate the impact of chemical chaperone treatments on the CBS activity. The utilization of the plasmid to express the enhanced green fluorescent protein (EGFP) serves as a convenient marker to visually verify the efficacy of gene delivery and the efficiency of transfection.

Upon examination using a fluorescent microscope, substantial population of transfected cells exhibiting intense EGFP fluorescence were observed (**Figure 44**). The evident and lively signal not only validated the efficiency of our transfection methodology but also demonstrated the capability to transiently modify the genetic composition of HEK293T cells. This accomplishment is a significant milestone in the research, as it provides us with the opportunity to go deeper into the examination of the impact of chemical chaperones on CBS activity within this particular cellular model.

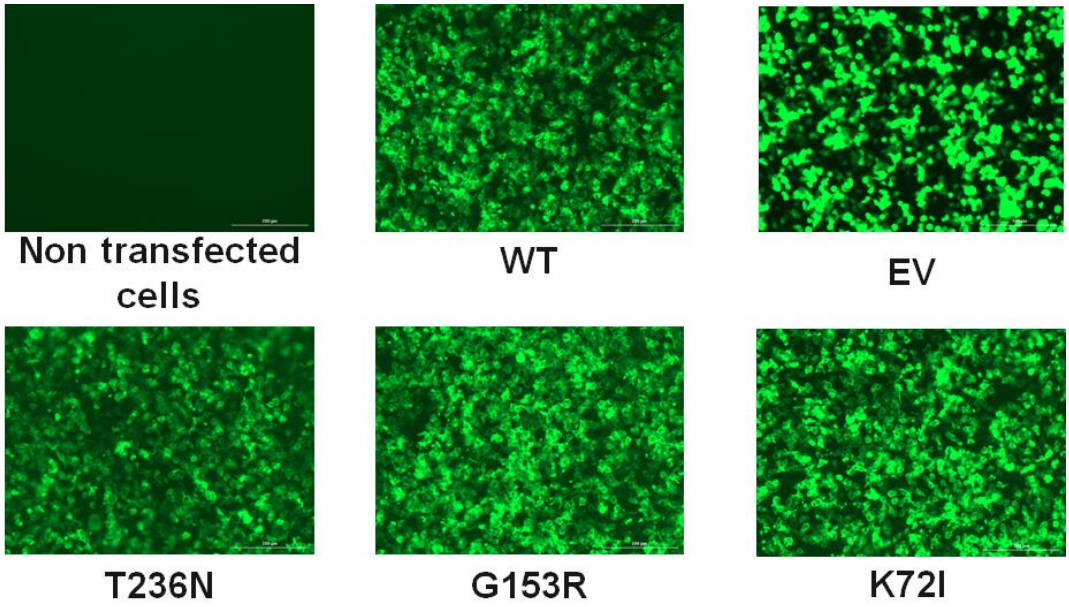

Figure 44. Transfection of HEK293T Cells with Plasmid Constructs. This figure demonstrated the successful transfection of HEK293T cells with plasmids encoding for different CBS variants, including the CBS^{WT} and mutants. Fluorescence microscopy was employed to visualize the expression of enhanced green fluorescent protein (EGFP), which is co-expressed with CBS in the transfected cells as a marker.

The successful transfection of these cells is a critical step in our experimental design, enabling subsequent investigations into the impact of these CBS variants on cellular function and the potential for genetic or pharmacological interventions. Our initial assessment focused on gene expression levels through the observation of EGFP fluorescence, which is encoded by the delivered plasmid constructs. Remarkably, the results yielded no statistically significant differences in EGFP fluorescence intensity across the CBS plasmids (**Figure 45**). This finding implies that the CBS mutations did

not have a significant impact on the level of gene expression in the conditions that were examined.

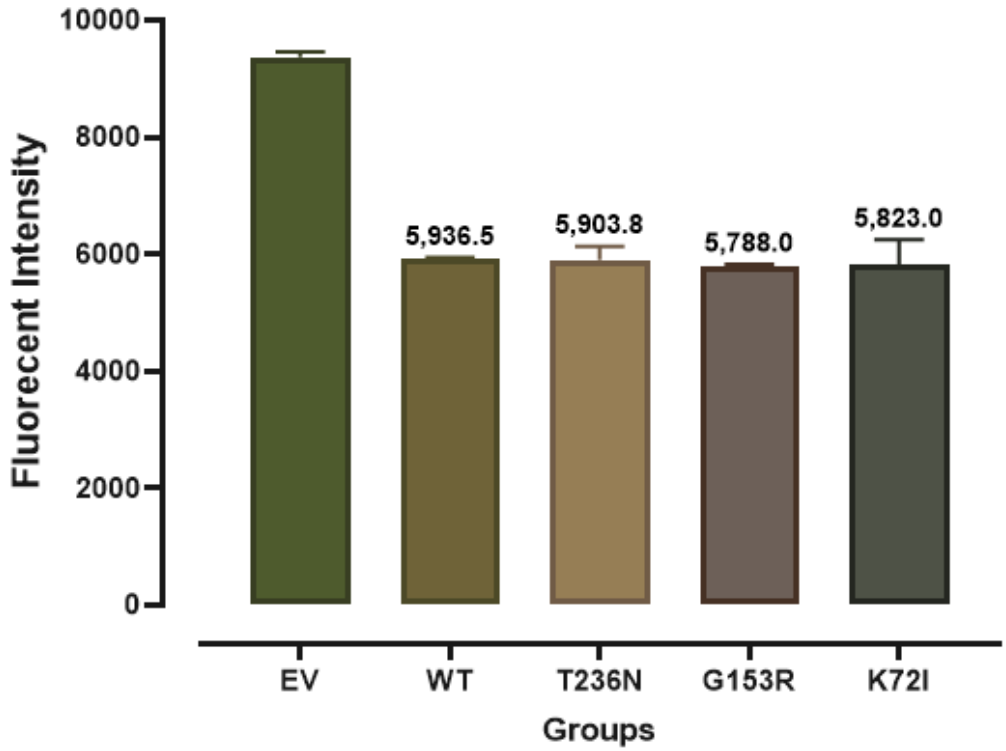

Figure 45. Fluorescent Intensity Analysis of Transfected Cells. Fluorescent intensity data for HEK293T cells transfected with various CBS plasmid constructs, including empty vector (EV), wild-type (WT) and mutant variants (CBS^{T236N}, CBS^{G153R}, and CBS^{K72I}), were analyzed. The data revealed no statistically significant differences in EGFP fluorescence intensity among the different CBS plasmids, indicating that the examined CBS mutations did not significantly affect gene expression levels in the transfected cells.

Given these results, we proceeded to investigate protein expression levels using Western blot analysis to gain deeper insights into the impact of these mutations at the protein level. This subsequent analysis will provide critical information regarding whether the observed lack of differences at the gene expression level extends to protein expression and whether any post-transcriptional regulatory mechanisms are at play. Western blot analysis was performed to determine if the observed similarities in gene expression translated to corresponding protein expression levels. The findings revealed interesting observations, particularly highlighting a significant disparity in protein expression between the CBS^{T236N} and CBS^{G153R} mutants in comparison to the CBS^{WT} (**Figure 46** and **47**). These two mutants exhibited significantly different protein expression levels, suggesting that these specific mutations impacted post-transcriptional processes influencing protein production. In contrast, the CBS^{K72I} variant exhibited a protein expression profile that was nearly indistinguishable from the WT, suggesting that this mutation had minimal impact on the expression of CBS protein. These findings mark a pivotal turning point in our exploration of CBS mutations, emphasizing the importance of post-transcriptional regulatory mechanisms in determining protein expression outcomes.

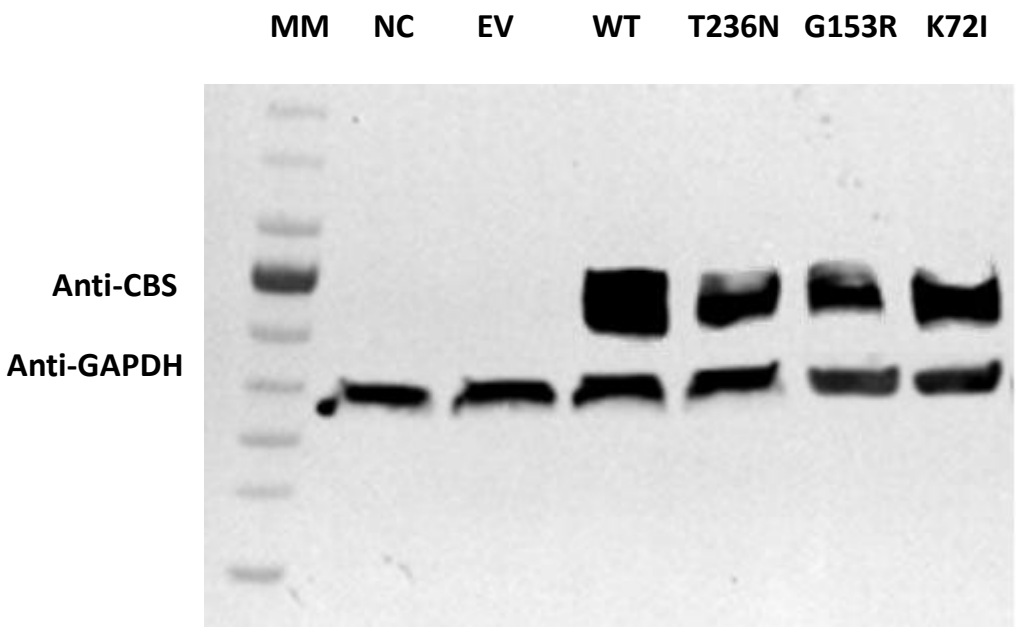

Figure 46. Western blot for transfected HEK293T cells. Cells were divided into six groups: Non-transfected cells (NC), transfected with empty vector (EV), transfected with CBS^{WT} plasmid (WT), transfected with a plasmid carrying T236N mutation, G153R mutation, and K72I mutation.

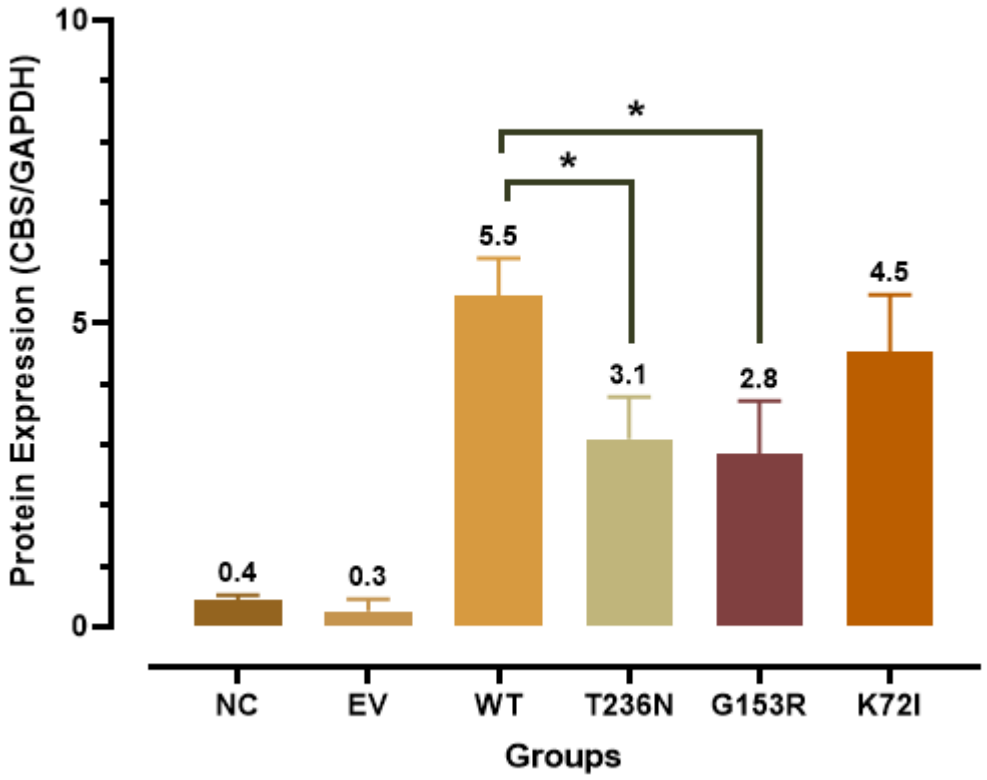

Figure 47. Western blot analysis of CBS protein expression in HEK293T cells transfected with various CBS plasmid constructs. The results reveal distinct protein expression patterns among the mutants and the CBS^{WT}. Notably, CBS^{T236N} and CBS^{G153R} mutants exhibit significantly different protein expression levels compared to WT, indicating the influence of these mutations on post-transcriptional regulation. In contrast, CBS^{K72I} exhibits protein expression levels similar to WT, highlighting the distinct effects of different CBS mutations on protein expression.

In an effort to rescue the impaired CBS protein function resulting from the various mutations (p.T236N, p.G153R, p.K72I) identified in our study, we conducted a series of experiments involving the treatment of transfected HEK293T cells with different chemical chaperones, including betaine, taurine, trimethylamine N-oxide (TMAO), 3% ethanol, and bortezomib. The primary objective was to examine the capability of these chaperones in restoring the stability and functionality of the mutant CBS proteins. To assess the effectiveness of these chaperones in reducing the destabilizing impacts of the mutations, we utilized Native gel electrophoresis. Unfortunately, our findings indicate that none of the chemical chaperones demonstrated a discernible impact on the stability of the mutant CBS proteins (**Figure 48 and 49**). Despite the considerable potential exhibited by these chaperones in addressing protein misfolding and instability in various contexts, the finidings suggested hat they may not be efficacious in ameliorating the specific structural alterations caused by the mutations in the CBS protein investigated in this study. Further studies are warranted investigate alternate therapeutic approaches for mitigating the functional impairments linked to these mutations in individuals with homocystinuria.

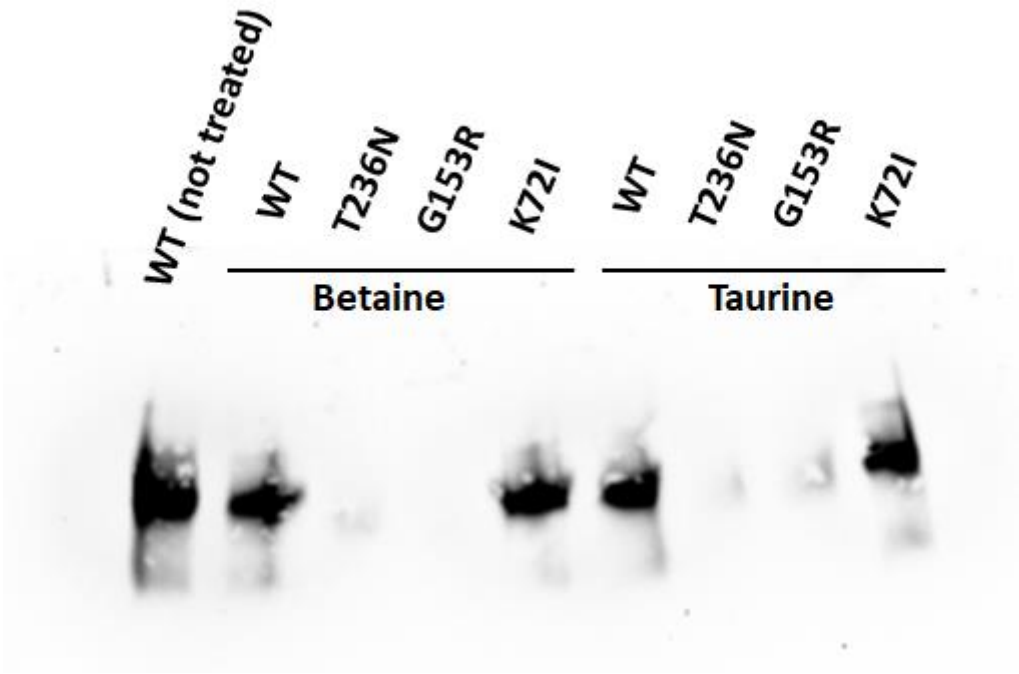

Figure 48. Representative native blot analysis of CBS^{WT}, CBS^{T236N}, CBS^{G153R}, and CBS^{K72I} proteins in transfected HEK293T cells and treated with betaine and taurine.

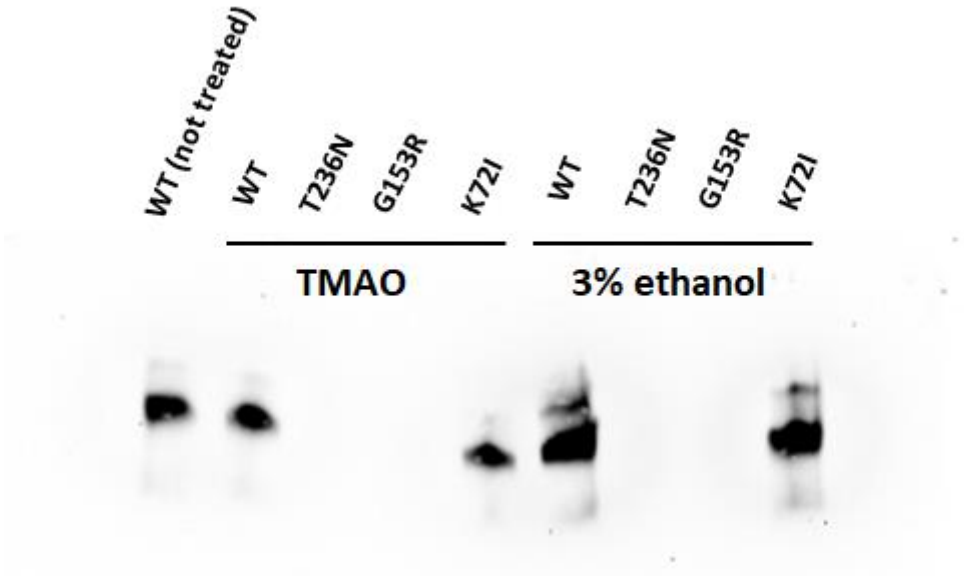

Figure 49. Representative native blot analysis of CBS^{WT}, CBS^{T236N}, CBS^{G153R}, and CBS^{K72I} proteins in transfected HEK293T cells and treated with TMAO and 3% ethanol.

Furthermore, the achievement of efficient transfection in HEK293T cells serves as the fundamental basis for our ongoing research endeavors. The provision of a genetically engineered cell line offers us a foundational platform upon which we can conduct our further experimental investigations. The purpose of these research is to investigate the regulation of CBS activity and the ability of chemical chaperones to restore its functionality within the specific cell line under study. The significance of this transfection approach is highlighted by its robustness, as it plays a crucial role in our research efforts. It provides us with a valuable platform to investigate new possibilities in our pursuit to understand and solve the decreased CBS activity, as well as its implications in the pathogenesis of homocystinuria. Finally, crystallization trials were initiated using the CBS^{R336C} mutated protein, identifying potential crystals that require further screening and optimization of the experimental conditions (**Figure 50**).

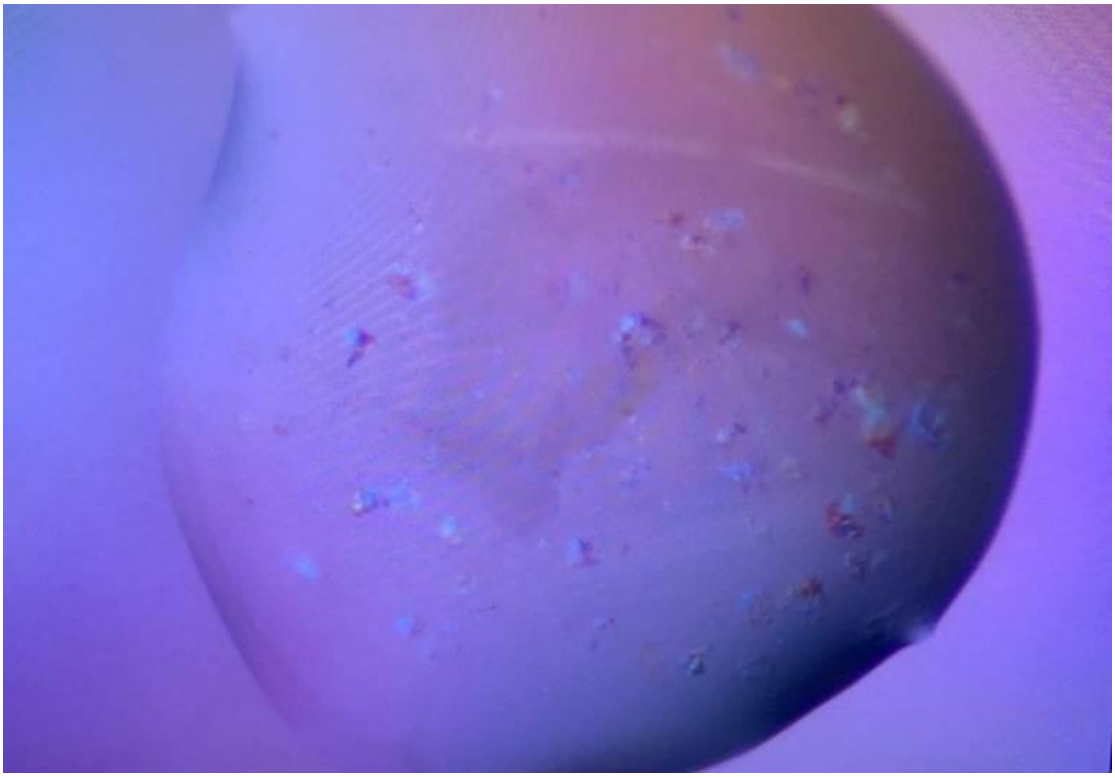

Figure 50. Closeup of a hanging drop of CBS where 1:1 (protein:well solution) was put on the drop with the well solution consisting of 10 mg of CBS^{R336C}.

Chapter 5: Discussion

Understanding genetic disorders, especially new mutations, is crucial for improving diagnosis and treatment. Investigation of the molecular bases could be a starting point towards better understanding of complex CBS mutations. They have been implicated in a range of disorders, most notably homocystinuria, highlighting the importance of understanding their impact on molecular function and stability. Molecular techniques allow us to pinpoint the exact location and nature of these mutations, providing a roadmap for subsequent analyses. Biochemical approaches then enable us to assess the functional consequences of these mutations, revealing how they alter enzymatic activity, substrate affinity, and reaction kinetics. Lastly, biophysical methods offer insights into the structural ramifications of these mutations, shedding light on changes in protein conformation, stability, and interactions with other biomolecules. By integrating these three approaches, we aim to provide a comprehensive characterization of CBS novel mutations, thereby contributing to our understanding of their role in disease pathogenesis and potentially informing therapeutic strategies.

Embedded within the genetic landscape of Qatar lies the CBS p.R336C mutation, with profound implications for health and disease. This mutation, serving as a founder mutation within the Qatari population, presents a unique opportunity to unravel the intricate interplay between genetic variation and disease susceptibility. The successful bacterial expression and purification of the CBS^{R336C} mutant allowed for a detailed examination of its molecular characteristics in comparison to the CBS^{WT} recombinant protein. Enzymatic assays conducted unveiled a substantial decrease of around 98% in CBS enzymatic activity following the introduction of the p.R336C mutation, highlighting the severe impairment of protein function caused by this mutation. This significant reduction in enzymatic activity emphasizes the critical role

of residue 336 in maintaining the functional integrity of CBS and underscores the detrimental impact of the p.R336C mutation on protein function (Al-Sadeq et al., 2022; Al-Dewik et al., 2019). Our study corroborates previous findings regarding the enzymatic activity of the CBS^{R336C} mutant, aligning with reports indicating a residual activity ranging from approximately 6% of the WT (S.-J. Lee et al., 2005) or a complete loss of activity (Roser Urreizti et al., 2006).

A similar enzymatic pattern was observed with other CBS mutations in a previous study that characterized 14 mutations found in the hCBS gene trying to investigate potential pathogenic nature. Eleven of these mutations exhibited an activity lower than 4% of the wild-type protein, supporting the pathogenicity of these variants (Roser Urreizti et al., 2006). The R>C substitution likely exerts its effects by disrupting hydrogen-bonding interactions crucial for protein stability (Kozich et al., 2010). This modification likely perturbs CBS properties such as stability and activity, contributing to the observed enzymatic dysfunction. These insights contribute to our understanding of the structural and functional consequences of the CBS^{R336C} mutation, shedding light on its role in CBS-related mutations and informing potential therapeutic interventions.

CD experiments have provided valuable insights into the impact of the p.R336C mutation on the structural and stability profiles of the CBS protein. The findings revealed that the p.R336C mutation did not induce significant alterations in the secondary structure of the CBS protein, indicating minimal impact on the overall protein conformation. Yet, analysis of CD spectra unveiled notable differences in the thermal unfolding mechanisms between CBS^{WT} and CBS^{R336C} mutant proteins, suggesting altered protein stability associated with the mutation. These results underscore the intricate interplay between structural changes and stability dynamics induced by the p.R336C mutation. A study conducted by Janosik et al. initially demonstrated that CBS deficiency could be classified as a protein misfolding disorder

(Janošík et al., 2001). Through experiments involving patient fibroblast lines, they assessed CBS using electrophoresis in native-PAGE followed by Western blot analysis. They observed that CBS mutants failed to assemble into active tetramers, instead forming inactive aggregates. Importantly, these aggregated forms of CBS lacked heme, leading to the proposition that heme might be crucial for proper folding and the formation of active CBS tetramers (T. Majtan et al., 2010).

Similarly, the results from chemical denaturation experiments further support the notion that the p.R336C mutation exerts a destabilizing effect on the CBS protein. The comparison between the CBS^{WT} and the CBS^{R336C} mutant revealed that the WT protein displayed greater thermodynamic stability, underscoring the destabilizing impact of the p.R336C mutation on protein structure and function. These findings contribute to a deeper understanding of the pathogenicity associated with the p.R336C mutation, elucidating its role in the development of a severe homocystinuria phenotype. By unraveling the mechanistic insights into how this mutation influences protein stability, our study provides valuable knowledge that can inform future research endeavors aimed at developing targeted therapeutic strategies for individuals affected by CBS-related mutations.

Characterization of compound heterozygous L230Q and K72I mutations

In this study, the kinetic and biochemical properties of two novel CBS missense mutations, L230Q and K72I, have been examined. The SNP in exon 4, c.215A>T, results in the replacement of lysine at residue 72 (K72) with isoleucine (I72), and the SNP in exon 8 leads to leucine-glutamine replacement at residue 230. These mutations have been identified in a Chinese patient, who was diagnosed at the age of 18 with classical homocystinuria, characterized by skeletal abnormalities, developmental delays, eye disorders, and vascular events as the major clinical features. Interestingly,

the patient with the two pathogenic mutations was unresponsive to vitamin B_6 (a PLP precursor) supplementation as stated by the clinical data. This pathogenic association prompted us to evaluate the biochemical phenotypes associated with the two variants by characterizing the mutant enzymes, obtained as recombinant forms.

The purified CBS^{K72I} mutant exhibited no discernible differences compared to the CBS^{WT} enzyme. UV-visible spectroscopic analysis showed the presence of heme in CBS^{K72I} and steady-state kinetic analysis further confirmed that this variant closely resembles the CBS^{WT} in terms of kinetic parameters. This similarity extends to both its primary CBS activity, involving L-Cth synthesis, and its ability to generate H_2S from L-Hcys and L-Cys as an alternative reaction. Furthermore, the CBS^{K72I} variant exhibited stimulation levels by SAM similar to those of the CBS^{WT}. The minimal impact caused by the K72I mutation on the enzyme's activity and overall stability can be readily explained through its three-dimensional structure. The residue K72 is positioned in an external region of the protein, at the termination point of the heme-binding domain, yet it remains distant from the cofactor. Significantly, its side chain extends towards the solvent and does not engage in any intra- or intermolecular interaction network with other residues that might compromise the functional integrity upon substitution. Therefore, the alternative placement of an isoleucine at this site merely introduces a more localized hydrophobic characteristic, which has no discernible effect on the enzyme's general solubility or its mode of oligomerization.

Unlike the CBS^{K72I} mutant, the CBS^{L230Q} mutant displays significant deviations from the CBS^{WT} enzyme. Specifically, CBS^{L230Q} exhibits compromised heme binding, reduced stability and enzymatic activity when compared to the native enzyme. The canonical B-type heme found in CBS^{WT}, which is bound axially to the thiolate group of C52 and the imidazole moiety of residue H65, is recognized as a redox sensor able to bind exogenous ligands (CO and NO) and to modulate CBS activity, provide

structural stability, and enhance protein folding [25]. The interaction between the heme and the PLP active site is thought to result from molecular interactions occurring at both ends of α-helix containing amino acid residues 258-272 (formerly named as either helix- α8 [26] or helix-α9 [27] in different articles). Specifically, at the heme end of this helix, residue R266 forms electrostatic interactions with the C52 thiolate, while at the opposite end, T257 and T260 participate in a hydrogen bond network with the PLP phosphate moiety. Functional and spectroscopic investigations on the clinically relevant variants of R266, T257 and T260 have validated the involvement of these residues in conveying information about the heme's redox state and ligand binding to the PLP site [26].

We found that the pathogenic mutant in which the hydrophobic side chain of L230 is substituted for a larger, polar side chain of glutamine residue exhibited a substantial loss of heme content and a significant decrease in overall protein stability and enzyme activity. The L230 residue is situated within 4 Å of the axial ligand. This proximity indicates that the nonpolar amino acid leucine, together with other nearby residues like H67, A226, P229, Y233 or V314, plays a role in maintaining a favorable hydrophobic environment for the heme group. Thus, although the volume of amino acid at that position is one of the factors that affects the heme cavity, we propose a contribution of the hydrophobicity at the 230-position to the control mechanism of the heme binding process. Additionally, similar to the behavior observed for the R266 residue, the reduction in both canonical and alternative activities observed in the L230Q mutant suggests that even subtle structural changes in the heme pocket can be conveyed to the PLP site. Remarkably, the CBS^{L230Q} variant exhibits a more pronounced impairment in alternative H_2S production compared to canonical activity involving the condensation of L-Ser and L-Hcys, a phenomenon previously observed with other mutations [28, 29]. In the canonical reaction, we observed no significant differences in

the K_m value for L-Ser between the CBS^{L230Q} variant and the CBS^{WT}, but the k_{cat} was approximately 4-fold lower, resulting in a 4-fold decrease in the mutant's catalytic efficiency. Conversely, in the alternative reaction, substantial differences in K_m for L-Cys were noted, with an approximately 29-fold increase in the mutant compared to the CBS^{WT} protein, leading to an overall 84-fold decrease in the catalytic efficiency. As suggested for other mutations [28], the distinct impacts of the mutation on two comparable β-elimination reactions may indicate the residue's influence on the leaving group of H_2S versus H_2O, respectively. In addition to the compromised protein stability and heme loss observed in the mutant, the reduced clearance of homocysteine via H_2S synthesis, rather than the conventional reaction, likely plays a role in the accumulation of homocysteine in individuals carrying the L230Q mutation.

The differential effects of the L230Q mutation on the canonical and H_2S synthesis reactions were also observed in the presence of SAM. When compared to CBS^{WT}, the CBS^{L230Q} variant exhibits a roughly 6-fold reduction in catalytic efficiency for the canonical reaction and a substantial ~23-fold reduction for the H_2S synthesis. Interestingly, in the L-Ser+L-Hcys canonical condensation, the decrease in catalytic efficiency is primarily driven by the reduction in the k_{cat} value, as the K_m value for L-Ser remains the same to that of the CBS^{WT}. Conversely, in the H_2S alternative reaction, the overall decrease in catalytic efficiency is influenced by both a significant increase in K_m values for L-Cys and a decrease in k_{cat}.

The finding that the purified CBS^{L230Q} variant cannot achieve the maximum activity level observed in SAM-activated CBS^{WT} supports the importance of retaining heme and its communication with PLP for optimal SAM-responsive activity. This finding offers a possible explanation for the observed impairment in homocysteine metabolism in the patient and underscores the functional significance of SAM regulation of CBS *in vivo*.

Notably, while the expression levels and the yield of the soluble CBS^{L230Q} variant are comparable to those of the WT, and no notable structural changes are evident in terms of secondary structure, (both CBS^{WT} and CBS^{L230Q} proteins exhibit high α-helix content), CD measurements have unveiled a substantial decrease in the thermal stability of the CBS protein due to the L230Q mutation, with a reduction of 15 °C. Thus, the mutation of L230 to a polar residue such as a glutamine dramatically affected the overall stability of the protein.

It worth mentioning that the appearance of a pathogenic profile in heterozygous individuals might be due to the combination of recessive mutations that might result in dominant phenotypes, that are not detected in individuals carrying each single mutation. Establishing whether this is the actual case of the patient described in this manuscript would require further studies. Recent studies demonstrate the enzyme's capacity to form long linear polymeric chains of variable length, composed of dimers, which can adopt two different conformations, basal or activated, in the absence or presence of S-adenosylmethionine, respectively. In heterozygous individuals the composition of these chains becomes complicated, as they could potentially include assemblies such as K72I and K72I, K72I and L230Q, or L230Q and L230Q. It is currently unknown whether the intracellular formation of CBS enzyme polymers induces a pathogenic state or if, on the contrary, they represent the natural "healthy" and active state of the enzyme. The resulting oligomers and polymers from the combination of these dimeric species could include different percentages of each dimer, depending on the particular conditions and background of each individual. In the absence of further knowledge, it is very difficult to predict, for example, if the different combination of various types of dimers carrying a different mutation in each subunit is the underlying reason for a pathological phenotype, or if any of the combinations of these dimeric species contributes a dominant effect.

Turning our attention to the mutations scrutinized in our manuscript, it is worth noting that the K72I variant, initially presumed to be a polymorphism accompanying the L230Q variant in a Chinese patient, was deemed pathological just on the basis of its location in a highly conserved region of the protein at the sequence level. However, when we have analyzed the three-dimensional structure of the enzyme, it became evident that the presence of an isoleucine instead of a lysine in such a conserved area (in terms of aminoacid sequence) does not impact neither the overall enzyme fold, nor its activity or its allosteric regulation by S-adenosylmethione. As mentioned in our manuscript, residue at position 72 points outwards the enzyme, directly to the surrounding solvent, without affecting any intra- or inter-molecular interactions. In line with our prior findings, we have conducted an *in silico* analysis to assess the combined effect of both mutations in complementary polypeptide chains within a dimeric species of hCBS. This analysis encompassed the enzyme's overall folding, the arrangement of critical residues in the catalytic site, and in the heme-binding site. As anticipated, the K72I mutation exhibited no significant differences in all these protein regions compared to the enzyme carrying solely the L230Q mutation. Conversely, the L230Q mutation causes a steric hindrance between the mutated residue and the heme molecule, explaining why this CBS variant does not bind heme and exhibits significantly lower catalytic activity. By extension, these findings strongly suggest that the pathological effect found in the K72I+L230Q heterozygous patient primarily stems from the L230Q variant.

In summary, our comprehensive approach, encompassing computational, spectroscopic, and kinetic analyses, has provided valuable insights into the structural, functional, and kinetic consequences of the K72I and L230Q mutations in CBS. These findings significantly contribute to the expanding knowledge on CBS mutations and their implications in metabolic disorders.

Characterization of homozygous T236N mutation

Despite the extensive research conducted over the past three decades, it remains a scarcity of comprehensive molecular and biochemical characterization for CBS missense mutations. More than 200 CBS patient mutations have been documented to date, distributed across all three domains of this modular protein (Database, 2019). Our study represents the first comprehensive characterization of the novel CBS p.T236N mutation. By employing a range of biochemical and biophysical techniques, including enzymatic assays, CD analysis, and thermal stability studies, we provide novel insights into the impact of the p.T236N mutation on CBS protein function and stability.

The mutation was reported in a Chinese patients suffering from significantly increased plasma (222 μmol/L) and urinary (>500 μmol/L) total homocysteine. Blood methionine elevated to 468 μmol/L (normal range 10–50 μmol/L). Similar clinical features and elevated homocysteine were reported in a Han Chinese family with two novel CBS mutations (Gong et al., 2015). Interestingly, the patient was unresponsive to vitamin B6 (a PLP precursor) supplementation as reported in the clinical data (Li et al., 2018). This pathogenic association prompted us to evaluate the biochemical phenotypes associated with the variant.

The CBS^{T236N} mutant displays significant deviations from the CBS^{WT} enzyme. Specifically, CBS^{T236N} exhibits reduced stability and enzymatic activity when compared to the native enzyme. The canonical B-type heme present in CBS^{WT}, bound axially to the thiolate group of C52 and the imidazole part of residue H65, serves as a redox detector capable of interacting with external ligands such as CO and NO (Zhong, Lisi, Collins, Dawson, & Pletneva, 2014). This interaction plays a role in regulating CBS activity, ensuring structural integrity, and promoting proper protein folding (Oliveriusová, Kery, Maclean, & Kraus, 2002). The interaction between heme and the

PLP active site is believed to occur through molecular interactions involving amino acid residues 258-272 situated at both ends of an α-helix. This helix has been referred to as either helix-α8 or helix-α9 (Ereño-Orbea, Oyenarte, et al., 2013; Smith et al., 2012). Specifically, at one end of this helix, residue R266 forms electrostatic interactions with the C52 thiolate, while at the opposite end, T257 and T260 engage in a hydrogen bond network with the PLP phosphate group. Functional and spectroscopic studies on clinically relevant variants of R266, T257, and T260 have confirmed the role of these residues in transmitting information regarding the heme's redox state and ligand binding to the PLP site (Smith et al., 2012). We found that the pathogenic mutant in which the side chain of T236 is substituted for a larger side chain of aspargine residue exhibited a significant decrease in overall protein stability and enzyme activity. In addition, since asparagine has a larger side chain compared to threonine due to its amide group, this potentially leads to steric hindrance or altered interactions within the protein structure (Porras-Dominguez, Lothier, Limami, & Tcherkez).

The functional diversity of CBS mutations located within the catalytic domain has been studied, revealing that different mutations target various residues with distinct consequences. For instance, mutations affecting residues involved in pyridoxal-5'-phosphate (PLP) binding or catalytic activity may result in a broader spectrum of biochemical phenotypes, including variable responsiveness to pyridoxine supplementation (Kozich et al., 2010; Miles & Kraus, 2004). In contrast, the CBS^{T236N} mutation specifically affects residue 236 within the CBS protein's catalytic domain and exhibits a consistent pyridoxine non-responsive phenotype, suggesting a unique mechanism of pathogenicity. Biophysical characterization studies have demonstrated distinct structural and stability profiles among CBS mutations in the catalytic domain, with some variants exhibiting severe protein destabilization or misfolding (Tomas Majtan, Pey, & Kraus, 2016). Future comparative studies exploring the functional

consequences and structural alterations associated with different CBS mutations within the catalytic domain are warranted to elucidate their diverse pathogenic mechanisms and improve personalized treatment strategies.

Chmeical Chaperones Treatment

The transfection of HEK293T cells with plasmids containing various CBS mutations, followed by treatment with different chemical chaperones, was undertaken in this study to explore the potential of these chaperones to rescue the altered protein structure and stability associated with these mutations. The aim was to gain insights into potential therapeutic strategies for CBS deficiency, specifically homocystinuria, a severe genetic disorder linked to CBS mutations. The findings of our study indicate that, despite the administration of various chemical chaperones, none of the interventions were successful in fully restoring the stability of the mutant CBS proteins. This finding highlights the complex nature of the structural alterations induced by these mutations. It implies that these alterations extend beyond ordinary protein misfolding and likely encompass significant modifications in the conformation and stability of the protein.

The lack of success in restoring protein stability with chemical chaperones may be attributed to several factors. The CBS protein is a multifaceted enzyme consisting of multiple domains, characterized by intricate interactions. Mutations in this protein can lead to structural alterations that cannot be easily rectified by small molecules. Furthermore, the effectiveness of chemical chaperones may vary depending on the type and location of the mutation within the protein. Some mutations have the potential to disrupt essential interactions affect the overall protein structure in ways that are challenging to reverse.

The findings of this study emphasize the significance of employing a comprehensive strategy to tackle the difficulties presented by CBS mutations in individuals with homocystinuria. Although chemical chaperones show potential as a therapeutic approach, our research indicates that their effectiveness in restoring protein stability may be constrained, particularly for the specific mutations investigated in this study. Future research should explore alternative strategies, such as gene therapy or enzyme replacement therapy, which may offer more comprehensive solutions to this debilitating genetic disorder.

The cell culture experiments performed in this study are characterized by a several of limitations that that merit consideration. It is important to acknowledge that cell culture models offer significant contributions to our understanding of biological mechanisms. However, it is crucial to recognize that these models naturally present a simplified representation of *in vivo* systems. The process of simplification employed in this study implies that the outcomes may not entirely reproduce the intricate interplays and microenvironment inherent in a real creature. Furthermore, the utilization of a solitary cell line, HEK293T, although commonly employed in research, may not account for the diversity of responses that different cell types might exhibit. Moreover, using CRISPR-Cas cells, although designed to investigate the impact of specific mutations, they exhibited increased sensitivity to certain treatments, rendering them less robust than their unmodified counterparts. This heightened sensitivity was particularly evident when applying extended treatment durations, as the modified cells could not tolerate the experimental conditions for more than 24 hours. As a result, this constraint required the adoption of shorter treatment durations, which may hinder the thorough evaluation of prolonged cellular reactions or chronic conditions.

Crystallization trials were initiated using the CBS^{R336C} mutated protein, identifying potential crystals that require further screening and optimization of the

experimental conditions. These preliminary findings suggest promising avenues for elucidating the structural alterations induced by the mutation and may offer insights into potential therapeutic strategies. Further refinement of the crystalization setup is underway to facilitate detailed structural analysis and inform future drug discovery efforts.

Limitations

While our study contributes valuable insights into the functional consequences of the CBS mutations and its implications for CBS-related disorders, it had some limitations. Firstly, our investigation primarily focuses on *in vitro* biochemical and biophysical analyses, which may not fully recapitulate the complex physiological and cellular contexts in which CBS operates. Therefore, the extrapolation of our findings to *in vivo* settings should be approached with caution. Additionally, although bacterial expression systems, like *E. coli*, are frequently chosen for their simplicity, cost-effectiveness in generating human proteins, and rapid growth, they have certain drawbacks, particularly concerning the study of human proteins such as CBS. The absence of PTMs, which are crucial for the correct functionality, stability, and activity of many eukaryotic proteins, is considered a significant limitation. Since bacterial system lack the machinery to perform these modifications, this could cause the production of misfolded or inactive proteins. Collectively, these factors cumulatively restrict the capacity to investigate the authentic functional characteristics of human proteins when they are expressed in bacterial systems.

Furthermore, our study is restricted to the characterization of CBS mutations, and thus, the generalizability of our results to other CBS mutations or broader patient populations may be limited. Moreover, while our future plans include the generation of CRISPR-Cas-edited cellular models, these experiments are yet to be conducted, and their success and utility remain to be determined. Lastly, the identification of chemical and molecular chaperones as potential therapeutic candidates is preliminary, and further validation studies are required to assess their efficacy, safety, and clinical relevance. Despite these limitations, our study lays the groundwork for future investigations aimed at deepening our understanding of CBS-related disorders and advancing therapeutic strategies for affected individuals.

Future plan

The future direction of this project encompasses a multifaceted approach aimed at further elucidating the molecular mechanisms underlying CBS mutations and advancing therapeutic strategies for homocystinuria. Firstly, efforts will be directed towards protein crystallization studies of the studied mutations to obtain high-resolution structural insights into the CBS protein and its interactions with cofactors and ligands. By determining the three-dimensional structure of CBS variants, particularly the CBS^{R336C} mutation, we aim to elucidate the structural basis of enzymatic dysfunction and identify potential targets for rational drug design.

In parallel, we plan to leverage CRISPR-Cas technology to generate HEK293T cell lines harboring specific CBS mutations, including the CBSR336C variant. These cellular models will serve as invaluable tools for investigating the functional consequences of CBS mutations in a physiologically relevant context. By employing a combination of biochemical, cellular, and omics approaches, we aim to dissect the molecular pathways affected by CBS mutations and identify novel therapeutic targets for intervention. Moreover, mouse model harboring p.R336C Qatari mutation was generated for further studying the mutation and rescuing the defective protein function and activity. This model will provide valuable insights into the pathophysiological mechanisms underlying homocystinuria associated with this specific mutation.

Furthermore, our future endeavors will focus on screening for additional chemical and molecular chaperones capable of modulating CBS protein stability and activity. Building upon our initial screening efforts, we will employ high-throughput screening assays and structure-based drug design strategies to identify small molecules and chaperone candidates with the potential to rescue CBS function. These efforts will be complemented by in vitro and in vivo validation studies to assess the efficacy and

safety of candidate compounds in restoring CBS activity and ameliorating disease phenotypes.

In summary, the future trajectory of this project is aimed at leveraging multidisciplinary approaches to deepen our understanding of CBS-related mutations and develop innovative therapeutic interventions. By advancing our knowledge of CBS biology and pathophysiology, we aim to pave the way for precision medicine approaches tailored to the individual needs of patients affected by CBS deficiency and related conditions.

Chapter 6: Conclusion

Although CBS protein has been extensively studied, the precise molecular mechanism by which the CBS^{R336C}, CBS^{K72I}, CBS^{L230Q}, and CBS^{T236N} mutants results in severe phenotypes remains unclear. This is primarily due to the lack of a comprehensive understanding of the impact of these mutation on the molecular properties of this protein. Therefore, this study investigated the effects of novel CBS missense mutations on biochemical and biophysical properties. As a result, we showed that these mutations, except CBS^{K72I}, significantly alter the stability of the human CBS protein, leading to a dramatic decrease in specific enzyme activity, which explains the severe phenotype of the respective patients. Other potential mechanisms may also be involved, such as disruption of other important protein-protein or protein-cofactor interactions.

Through this concerted effort, we aimed not only to deepen our understanding on disease pathogenesis, but also pave the way for more personalized therapeutic interventions tailored to the specific molecular signatures of individual patients. By elucidating the molecular basis of pyridoxine non-responsiveness in CBS deficiency, our research seeks to shed light on a critical aspect of this complex disorder and provide hope for improved clinical management and outcomes for affected individuals. Shedding light on the molecular consequences of this genetic variant within the CBS protein could establish new foundations for developing drugs that can correct and/or regulate the activity and activation of the CBS enzyme in a personalized manner.

References

Abcam. (2021). Cystathionine beta Synthase Assay Kit. Retrieved from https://www.abcam.com/cystathionine-beta-synthase-assay-kit-ab241043.html

Abe, K., & Kimura, H. (1996). The possible role of hydrogen sulfide as an endogenous neuromodulator. *Journal of Neuroscience, 16*(3), 1066-1071.

Abraham, M. J., Murtola, T., Schulz, R., Páll, S., Smith, J. C., Hess, B., & Lindahl, E. (2015). GROMACS: High performance molecular simulations through multi-level parallelism from laptops to supercomputers. *SoftwareX*, *1*, 19-25.

Adams, C. J., Kopp, M. C., Larburu, N., Nowak, P. R., & Ali, M. M. (2019). Structure and molecular mechanism of ER stress signaling by the unfolded protein response signal activator IRE1. *Frontiers in Molecular Biosciences, 6*.

Addgene. (2024). Plasmid pET28a. Retrieved from https://www.addgene.org/vector-database/2565/

Aitken, S. M., & Kirsch, J. F. (2003). Kinetics of the yeast cystathionine beta-synthase forward and reverse reactions: continuous assays and the equilibrium constant for the reaction. *Biochemistry, 42*(2), 571-578. doi:10.1021/bi026681n

Al-Sadeq, Thanassoulas, A., Islam, Z., Kolatkar, P., Al-Dewik, N., Safieh-Garabedian, B., . . . Nomikos, M. (2022). Pyridoxine non-responsive p. R336C mutation alters the molecular properties of cystathionine beta-synthase leading to severe homocystinuria phenotype. *Biochimica et Biophysica Acta (BBA)-General Subjects*, *1866*(7), 130148.

Al-Sadeq, D. W., & Nasrallah, G. K. (2020). The Spectrum of Mutations of Homocystinuria in the MENA Region. *Genes, 11*(3), 330.

Al-Dewik, N., Ali, A., Mahmoud, Y., Shahbeck, N., Ali, R., Mahmoud, L., . . . El-Akouri, K. (2019). Natural history, with clinical, biochemical, and molecular characterization of classical homocystinuria in the Qatari population. *Journal of inherited metabolic disease*.

Applegarth, D. A., & Toone, J. R. (2000). Incidence of inborn errors of metabolism in British Columbia, 1969–1996. *Pediatrics, 105*(1), e10-e10.

Bank, D. (2020). Bortezomib. Retrieved from https://www.drugbank.ca/drugs/DB00188

Barber, G., & Spaeth, G. (1967). Pyridoxine therapy in homocystinuria. *Lancet, 1*.

Berendsen, H. J., Postma, J. v., Van Gunsteren, W. F., DiNola, A., & Haak, J. R. (1984). Molecular dynamics with coupling to an external bath. *The Journal of chemical physics, 81*(8), 3684-3690.

Berendsen, H. J., van der Spoel, D., & van Drunen, R. (1995). GROMACS: A message-passing parallel molecular dynamics implementation. *Computer physics communications, 91*(1-3), 43-56.

Betaine. Monogragh. (2003). *Alternative Medicine Review, 8*(2), 193-196.

Bhopatkar, A. A., Uversky, V. N., & Rangachari, V. (2020). Disorder and cysteines in proteins: A design for orchestration of conformational see-saw and modulatory functions. *Prog Mol Biol Transl Sci, 174*, 331-373. doi:10.1016/bs.pmbts.2020.06.001

Blau, N., Van Spronsen, F. J., & Levy, H. L. (2010). Phenylketonuria. *The Lancet, 376*(9750), 1417-1427.

Böhm, G., Muhr, R., & Jaenicke, R. (1992). Quantitative analysis of protein far UV circular dichroism spectra by neural networks. *Protein Engineering, Design and Selection, 5*(3), 191-195.

Bravo, R., Parra, V., Gatica, D., Rodriguez, A. E., Torrealba, N., Paredes, F., . . . Jaimovich, E. (2013). Endoplasmic reticulum and the unfolded protein response: dynamics and metabolic integration. In *International review of cell and molecular biology* (Vol. 301, pp. 215-290): Elsevier.

Brittanica. (2022). Disorders of amino acid metabolism. Retrieved from https://www.britannica.com/science/metabolic-disease/Disorders-of-carbohydrate-metabolism

Bussi, G., Donadio, D., & Parrinello, M. (2007). Canonical sampling through velocity rescaling. *The Journal of chemical physics, 126*(1).

Carson, N., & Carre, I. (1969). Treatment of homocystinuria with pyridoxine. A preliminary study. *Archives of disease in childhood, 44*(235), 387.

Carson, N. A., & Neill, D. (1962). Metabolic abnormalities detected in a survey of mentally backward individuals in Northern Ireland. *Archives of disease in childhood, 37*(195), 505.

Ciechanover, A., & Kwon, Y. T. (2017). Protein quality control by molecular chaperones in neurodegeneration. *Frontiers in neuroscience, 11*, 185.

Clayton, P. T. (2006). B 6-responsive disorders: a model of vitamin dependency. *Journal of inherited metabolic disease, 29*(2-3), 317-326.

Conter, C., Favretto, F., Dominici, P., Martinez-Cruz, L. A., & Astegno, A. (2023). Key substrate recognition residues in the active site of cystathionine beta-synthase

from Toxoplasma gondii. *Proteins*. doi:10.1002/prot.26507

Conter, C., Fruncillo, S., Favretto, F., Fernández-Rodríguez, C., Dominici, P., Martínez-Cruz, L. A., & Astegno, A. (2022). Insights into Domain Organization and Regulatory Mechanism of Cystathionine Beta-Synthase from Toxoplasma gondii. *Int J Mol Sci, 23*(15). doi:10.3390/ijms23158169

Conter, C., Fruncillo, S., Fernández-Rodríguez, C., Martínez-Cruz, L. A., Dominici, P., & Astegno, A. (2020). Cystathionine β-synthase is involved in cysteine biosynthesis and H2S generation in Toxoplasma gondii. *Scientific reports, 10*(1), 14657.

Conter, C., Fruncillo, S., Fernández-Rodríguez, C., Martínez-Cruz, L. A., Dominici, P., & Astegno, A. (2020). Cystathionine β-synthase is involved in cysteine biosynthesis and H(2)S generation in Toxoplasma gondii. *Sci Rep, 10*(1), 14657. doi:10.1038/s41598-020-71469-x

Craig, S. A. (2004). Betaine in human nutrition. *The American journal of clinical nutrition, 80*(3), 539-549.

Cusworth, D., & Dent, C. (1969). Homocystinuria. *Biochemical Journal, 111*(3), 1P.

Dalmas, B., Hunter, G. J., & Bannister, W. H. (1994). Prediction of protein secondary structure from circular dichroism spectra using artificial neural network techniques. *Biochemistry and molecular biology international, 34*(1), 17-26.

Damba, T., Zhang, M., Buist-Homan, M., van Goor, H., Faber, K. N., & Moshage, H. (2019). Hydrogen sulfide stimulates activation of hepatic stellate cells through increased cellular bio-energetics. *Nitric Oxide, 92*, 26-33.

Database, T. H. G. M. (2019). cystathionine-beta-synthase. Retrieved from

http://www.hgmd.cf.ac.uk/ac/gene.php?gene=CBS

de Franchis, R., Kraus, E., Kozich, V., Sebastio, G., & Kraus, J. P. (1999). Four novel mutations in the cystathionine beta-synthase gene: effect of a second linked mutation on the severity of the homocystinuric phenotype. *Hum Mutat, 13*(6), 453-457. doi:10.1002/(sici)1098-1004(1999)13:6<453::Aid-humu4>3.0.Co;2-k

de Franchis, R., Kraus, E., Kozich, V., Sebastio, G., & Kraus, J. P. (1999). Four novel mutations in the cystathionine β-synthase gene: Effect of a second linked mutation on the severity of the homocystinuric phenotype. *Human mutation, 13*(6), 453-457.

Dicker-Brown, A., Fonseca, V. A., Fink, L. M., & Kern, P. A. (2001). The effect of glucose and insulin on the activity of methylene tetrahydrofolate reductase and cystathionine-β-synthase: studies in hepatocytes. *Atherosclerosis, 158*(2), 297-301.

DT, C. (2001). Maple syrup urine disease (branched-chain ketoaciduria). *The metabolic and molecular bases of inherited disease*, 1971-2005.

El-Said, M. F., Badii, R., Bessisso, M., Shahbek, N., El-Ali, M. G., El-Marikhie, M., . . . Hoffmann, G. F. (2006). A common mutation in the CBS gene explains a high incidence of homocystinuria in the Qatari population. *Human mutation, 27*(7), 719-719.

El Bashir, H., Dekair, L., Mahmoud, Y., & Ben-Omran, T. (2014). Neurodevelopmental and cognitive outcomes of classical homocystinuria: experience from Qatar. In *JIMD Reports, Volume 21* (pp. 89-95): Springer.

Elsaid, M. F., Bener, A., Lindner, M., Alzyoud, M., Shahbek, N., Abdelrahman, M. O., . . . Hoffmann, G. F. (2007). Are heterocygotes for classical homocystinuria at risk of vitamin B12 and folic acid deficiency? *Molecular genetics and metabolism, 92*(1-2), 100-103.

Ensembl. (2023). Gene: CBS ENSG00000160200. Retrieved from https://www.ensembl.org/Homo_sapiens/Gene/Summary?g=ENSG00000160200;r=21:43053191-43076943

Ereño-Orbea, J., Majtan, T., Oyenarte, I., Kraus, J. P., & Martínez-Cruz, L. A. (2013). Structural basis of regulation and oligomerization of human cystathionine β-synthase, the central enzyme of transsulfuration. *Proceedings of the National Academy of Sciences, 110*(40), E3790-E3799.

Ereño-Orbea, J., Oyenarte, I., & Martínez-Cruz, L. A. (2013). CBS domains: Ligand binding sites and conformational variability. *Archives of biochemistry and biophysics, 540*(1-2), 70-81.

Evande, R., Blom, H., Boers, G. H., & Banerjee, R. (2002). Alleviation of intrasteric inhibition by the pathogenic activation domain mutation, D444N, in human cystathionine β-synthase. *Biochemistry, 41*(39), 11832-11837.

Evande, R., Ojha, S., & Banerjee, R. (2004). Visualization of PLP-bound intermediates in hemeless variants of human cystathionine β-synthase: evidence that lysine 119 is a general base. *Archives of biochemistry and biophysics, 427*(2), 188-196.

Fernández-Rodríguez, C., Conter, C., Oyenarte, I., Favretto, F., Quintana, I., Martinez-Chantar, M. L., . . . Martínez-Cruz, L. A. (2023). Structural basis of the inhibition of cystathionine γ-lyase from Toxoplasma gondii by

propargylglycine and cysteine. *Protein Sci, 32*(4), e4619. doi:10.1002/pro.4619

Ficicioglu, C. (2017). Disorders of Amino Acid Metabolism. In *Metabolic Diseases* (pp. 47-116): IOS Press.

Field-Smith, A., Morgan, G. J., & Davies, F. E. (2006). Bortezomib (Velcade™) in the treatment of multiple myeloma. *Therapeutics and clinical risk management, 2*(3), 271.

Gallagher, P. M., Ward, P., Tan, S., Naughten, E., Kraus, J. P., Sellar, G. C., . . . Whitehead, A. S. (1995). High frequency (71%) of cystathionine β-synthase mutation G307S in Irish homocystinuria patients. *Human mutation, 6*(2), 177-180.

Gallego-Villar, L., Hannibal, L., Häberle, J., Thöny, B., Ben-Omran, T., Nasrallah, G., . . . Blom, H. (2017). Cysteamine revisited: repair of arginine to cysteine mutations. *Journal of inherited metabolic disease, 40*(4), 555-567.

Gámez, A., Yuste-Checa, P., Brasil, S., Briso-Montiano, Á., Desviat, L. R., Ugarte, M., . . . Pérez, B. (2018). Protein misfolding diseases: prospects of pharmacological treatment. *Clinical genetics, 93*(3), 450-458.

Gan-Schreier, H., Kebbewar, M., Fang-Hoffmann, J., Wilrich, J., Abdoh, G., Ben-Omran, T., . . . Al Khal, A. L. (2010). Newborn population screening for classic homocystinuria by determination of total homocysteine from Guthrie cards. *The Journal of pediatrics, 156*(3), 427-432.

Gaustadnes, M., Wilcken, B., Oliveriusova, J., McGill, J., Fletcher, J., Kraus, J. P., & Wilcken, D. E. (2002). The molecular basis of cystathionine beta-synthase deficiency in Australian patients: genotype-phenotype correlations and

response to treatment. *Hum Mutat, 20*(2), 117-126. doi:10.1002/humu.10104

Gong, B., Liu, L., Li, Z., Ye, Z., Xiao, Y., Zeng, G., . . . Yang, Z. (2015). Novel Compound Heterozygous CBS Mutations Cause Homocystinuria in a Han Chinese Family. *Sci Rep, 5*, 17947. doi:10.1038/srep17947

Gorenberg, E. L., & Chandra, S. S. (2017). The role of co-chaperones in synaptic proteostasis and neurodegenerative disease. *Frontiers in neuroscience, 11*, 248.

Gramer, G., Abdoh, G., Ben-Omran, T., Shahbeck, N., Ali, R., Mahmoud, L., . . . Okun, J. G. (2017). Newborn screening for remethylation disorders and vitamin B 12 deficiency-evaluation of new strategies in cohorts from Qatar and Germany. *World Journal of Pediatrics, 13*(2), 136-143.

Group, Q. C. (2022). Action of Guanidine Hydrochloride on Proteins. Retrieved from https://www.qinmuchem.com/news/action-of-guanidine-hydrochloride-on-proteins.html

Guex, N., & Peitsch, M. C. (1997). SWISS-MODEL and the Swiss-Pdb Viewer: an environment for comparative protein modeling. *electrophoresis, 18*(15), 2714-2723.

Gupta, S., Gallego-Villar, L., Wang, L., Lee, H. O., Nasrallah, G., Al-Dewik, N., . . . Ben-Omran, T. (2019). Analysis of the Qatari R336C Cystathionine β-Synthase Protein in Mice. *Journal of inherited metabolic disease*.

Gupta, S., Kelow, S., Wang, L., Andrake, M. D., Dunbrack, R. L., & Kruger, W. D. (2018). Mouse modeling and structural analysis of the p. G307S mutation in human cystathionine β-synthase (CBS) reveal effects on CBS activity but not stability. *Journal of Biological Chemistry, 293*(36), 13921-13931.

Gupta, S., & Kruger, W. D. (2011). Cystathionine beta-synthase deficiency causes fat loss in mice. *PloS one, 6*(11), e27598.

Gupta, S., Wang, L., & Kruger, W. D. (2017). The c. 797 G> A (p. R266K) cystathionine β-synthase mutation causes homocystinuria by affecting protein stability. *Human mutation, 38*(7), 863-869.

Huemer, M., Diodato, D., Schwahn, B., Schiff, M., Bandeira, A., Benoist, J.-F., . . . Garcia-Cazorla, A. (2017). Guidelines for diagnosis and management of the cobalamin-related remethylation disorders cblC, cblD, cblE, cblF, cblG, cblJ and MTHFR deficiency. *Journal of inherited metabolic disease, 40*, 21-48.

Huemer, M., Kožich, V., Rinaldo, P., Baumgartner, M. R., Merinero, B., Pasquini, E., . . . Blom, H. J. (2015). Newborn screening for homocystinurias and methylation disorders: systematic review and proposed guidelines. *Journal of inherited metabolic disease, 38*(6), 1007-1019.

Ignoul, S., & Eggermont, J. (2005). CBS domains: structure, function, and pathology in human proteins. *American Journal of Physiology-Cell Physiology, 289*(6), C1369-C1378.

Ismail, H. M., Krishnamoorthy, N., Al-Dewik, N., Zayed, H., Mohamed, N. A., Giacomo, V. D., . . . Blom, H. J. (2019). In silico and in vivo models for Qatari-specific classical homocystinuria as basis for development of novel therapies. *Human mutation, 40*(2), 230-240.

Janošík, M., Oliveriusová, J., Janošíková, B., Sokolová, J., Kraus, E., Kraus, J. P., & Kožich, V. (2001). Impaired heme binding and aggregation of mutant cystathionine β-synthase subunits in homocystinuria. *The American Journal of Human Genetics, 68*(6), 1506-1513.

Jhee, K.-H., McPhie, P., & Miles, E. W. (2000). Domain architecture of the heme-independent yeast cystathionine β-synthase provides insights into mechanisms of catalysis and regulation. *Biochemistry, 39*(34), 10548-10556.

Jumper, J., Evans, R., Pritzel, A., Green, T., Figurnov, M., Ronneberger, O., . . . Hassabis, D. (2021). Highly accurate protein structure prediction with AlphaFold. *Nature, 596*(7873), 583-589. doi:10.1038/s41586-021-03819-2

Kabil, O., Zhou, Y., & Banerjee, R. (2006). Human Cystathionine β-Synthase Is a Target for Sumoylation. *Biochemistry, 45*(45), 13528-13536. doi:10.1021/bi0615644

Keller, R., Chrastina, P., Pavlíková, M., Gouveia, S., Ribes, A., Kölker, S., . . . Dionisi-Vici, C. (2019). Newborn screening for homocystinurias: recent recommendations versus current practice. *Journal of inherited metabolic disease, 42*(1), 128-139.

Kelly, P., Furie, K., Kistler, J., Barron, M., Picard, E., Mandell, R., & Shih, V. (2003). Stroke in young patients with hyperhomocysteinemia due to cystathionine beta-synthase deficiency. *Neurology, 60*(2), 275-279.

Kery, V., Poneleit, L., & Kraus, J. P. (1998). Trypsin cleavage of human cystathionine β-synthase into an evolutionarily conserved active core: structural and functional consequences. *Archives of biochemistry and biophysics, 355*(2), 222-232.

Kopecka, J., Krijt, J., Rakova, K., & Kozich, V. (2011). Restoring assembly and activity of cystathionine beta-synthase mutants by ligands and chemical chaperones. *J Inherit Metab Dis, 34*(1), 39-48. doi:10.1007/s10545-010-9087-5

Kopecká, J., Krijt, J., Raková, K., & Kožich, V. (2011). Restoring assembly and activity of cystathionine β-synthase mutants by ligands and chemical chaperones. *J Inherit Metab Dis, 34*(1), 39-48. doi:10.1007/s10545-010-9087-5

Kožich, V., & Kraus, J. P. (1992). Screening for mutations by expressing patient cDNA segments in E. coli: Homocystinuria due to cystathionine β-synthase deficiency. *Human mutation, 1*(2), 113-123.

Kožich, V., Kruger, W. D., & Kraus, J. P. (2010). Cystathionine β-synthase (CBS) Deficiency: Genetics. In *Encyclopedia of Life Sciences*.

Kozich, V., Sokolová, J., Klatovská, V., Krijt, J., Janosík, M., Jelínek, K., & Kraus, J. P. (2010). Cystathionine beta-synthase mutations: effect of mutation topology on folding and activity. *Hum Mutat, 31*(7), 809-819. doi:10.1002/humu.21273

Kraus, J. P., Janosik, M., Kozich, V., Mandell, R., Shih, V., Sperandeo, M. P., . . . Gaustadnes, M. (1999). Cystathionine beta-synthase mutations in homocystinuria. *Hum Mutat, 13*(5), 362-375. doi:10.1002/(sici)1098-1004(1999)13:5<362::Aid-humu4>3.0.Co;2-k

Kruger, W., Wang, L., Jhee, K., Singh, R., & Elsas, L. (2003). Cystathionine β-synthase deficiency in Georgia (USA): Correlation of clinical and biochemical phenotype with genotype. *Human mutation, 22*(6), 434-441.

Kruger, W. D., & Cox, D. R. (1995). A yeast assay for functional detection of mutations in the human cystathionine β-synthase gene. *Human molecular genetics, 4*(7), 1155-1161.

Lai, W. K. C., & Kan, M. Y. (2015). Homocysteine-induced endothelial dysfunction. *Annals of Nutrition and Metabolism, 67*(1), 1-12.

Lee, N., & Kim, D. (2022). Toxic Metabolites and Inborn Errors of Amino Acid Metabolism: What One Informs about the Other. *Metabolites*, *12*(6). doi:10.3390/metabo12060527

Lee, S.-J., Lee, D. H., Yoo, H.-W., Koo, S. K., Park, E.-S., Park, J.-W., . . . Jung, S.-C. (2005). Identification and functional analysis of cystathionine beta-synthase gene mutations in patients with homocystinuria. *Journal of human genetics, 50*(12), 648.

Lee, S. J., Lee, D. H., Yoo, H. W., Koo, S. K., Park, E. S., Park, J. W., . . . Jung, S. C. (2005). Identification and functional analysis of cystathionine beta-synthase gene mutations in patients with homocystinuria. *J Hum Genet, 50*(12), 648-654. doi:10.1007/s10038-005-0312-2

Li, D.-X., Li, X.-Y., Dong, H., Liu, Y.-P., Ding, Y., Song, J.-Q., . . . Yang, Y.-L. (2018). Eight novel mutations of CBS gene in nine Chinese patients with classical homocystinuria. *World Journal of Pediatrics, 14*(2), 197-203.

Lindner, M., Abdoh, G., Fang-Hoffmann, J., Shabeck, N., Al Sayrafi, M., Al Janahi, M., . . . Bener, A. (2007). Implementation of extended neonatal screening and a metabolic unit in the State of Qatar: developing and optimizing strategies in cooperation with the Neonatal Screening Center in Heidelberg. *Journal of Inherited Metabolic Disease: Official Journal of the Society for the Study of Inborn Errors of Metabolism, 30*(4), 522-529.

Longhi, R. C., Fleisher, L. D., Tallan, H. H., & Gaull, G. E. (1977). Cystathionine β-synthase deficiency: A qualitative abnormality of the deficient enzyme modified by vitamin B 6 therapy. *Pediatric research, 11*(2), 100.

Longo, N. (2014). Inherited Disorders of Amino Acid Metabolism in Adults. In D.

Kasper, A. Fauci, S. Hauser, D. Longo, J. L. Jameson, & J. Loscalzo (Eds.), *Harrison's Principles of Internal Medicine, 19e*. New York, NY: McGraw-Hill Education.

Lu, S. C. (2013). Glutathione synthesis. *Biochimica et Biophysica Acta (BBA)-General Subjects, 1830*(5), 3143-3153.

Maclean, K. N., Sikora, J., Kožich, V., Jiang, H., Greiner, L. S., Kraus, E., . . . Brodsky, G. L. (2010). A novel transgenic mouse model of CBS-deficient homocystinuria does not incur hepatic steatosis or fibrosis and exhibits a hypercoagulative phenotype that is ameliorated by betaine treatment. *Molecular genetics and metabolism, 101*(2-3), 153-162.

Majtan, T., Liu, L., Carpenter, J. F., & Kraus, J. P. (2010). Rescue of cystathionine beta-synthase (CBS) mutants with chemical chaperones: purification and characterization of eight CBS mutant enzymes. *J Biol Chem, 285*(21), 15866-15873. doi:10.1074/jbc.M110.107722

Majtan, T., Pey, A. L., Gimenez-Mascarell, P., Martínez-Cruz, L. A., Szabo, C., Kožich, V., & Kraus, J. P. (2017). Potential pharmacological chaperones for cystathionine beta-synthase-deficient homocystinuria. In *Targeting Trafficking in Drug Development* (pp. 345-383): Springer.

Majtan, T., Pey, A. L., & Kraus, J. P. (2016). Kinetic stability of cystathionine beta-synthase can be modulated by structural analogs of S-adenosylmethionine: potential approach to pharmacological chaperone therapy for homocystinuria. *Biochimie, 126*, 6-13.

Majumder, A., Singh, M., George, A. K., Behera, J., Tyagi, N., & Tyagi, S. C. (2018). Hydrogen sulfide improves postischemic neoangiogenesis in the hind limb of

cystathionine-β-synthase mutant mice via PPAR-γ/VEGF axis. *Physiol Rep, 6*(17), e13858. doi:10.14814/phy2.13858

Matern, D., Tortorelli, S., Oglesbee, D., Gavrilov, D., & Rinaldo, P. (2007). Reduction of the false-positive rate in newborn screening by implementation of MS/MS-based second-tier tests: the Mayo Clinic experience (2004–2007). *Journal of inherited metabolic disease, 30*(4), 585-592.

Maurisse, R., De Semir, D., Emamekhoo, H., Bedayat, B., Abdolmohammadi, A., Parsi, H., & Gruenert, D. C. (2010). Comparative transfection of DNA into primary and transformed mammalian cells from different lineages. *BMC Biotechnology, 10*(1), 9. doi:10.1186/1472-6750-10-9

MedlinePlus. (2020). Betaine. Retrieved from https://medlineplus.gov/druginfo/meds/a608012.html

Medscape. (2016). Pyridoxine Deficiency. Retrieved from https://emedicine.medscape.com/article/124947-overview

Meier, M., Oliveriusova, J., Kraus, J. P., & Burkhard, P. (2003). Structural insights into mutations of cystathionine β-synthase. *Biochimica et Biophysica Acta (BBA)-Proteins and Proteomics, 1647*(1-2), 206-213.

Melenovská, P., Kopecká, J., Krijt, J., Hnízda, A., Raková, K., Janošík, M., . . . Kožich, V. (2015). Chaperone therapy for homocystinuria: the rescue of CBS mutations by heme arginate. *Journal of inherited metabolic disease, 38*(2), 287-294.

Micsonai, A., Wien, F., Bulyáki, É., Kun, J., Moussong, É., Lee, Y. H., . . . Kardos, J. (2018). BeStSel: a web server for accurate protein secondary structure prediction and fold recognition from the circular dichroism spectra. *Nucleic*

Acids Res, 46(W1), W315-w322. doi:10.1093/nar/gky497

Miles, E. W., & Kraus, J. P. (2004). Cystathionine β-synthase: structure, function, regulation, and location of homocystinuria-causing mutations. *Journal of Biological Chemistry, 279*(29), 29871-29874.

Morris, A. A., Kožich, V., Santra, S., Andria, G., Ben-Omran, T. I., Chakrapani, A. B., . . . Huemer, M. (2017a). Guidelines for the diagnosis and management of cystathionine beta-synthase deficiency. *Journal of inherited metabolic disease, 40*, 49-74.

Morris, A. A., Kožich, V., Santra, S., Andria, G., Ben-Omran, T. I., Chakrapani, A. B., . . . Huemer, M. (2017b). Guidelines for the diagnosis and management of cystathionine beta-synthase deficiency. *Journal of inherited metabolic disease, 40*(1), 49-74.

Mudd, S., Levy, H., & Kraus, J. (2001). The Online Metabolic and Molecular Bases of Inherited Disease. *Scriver, CR*, 2007-2056.

Mudd, S. H., Edwards, W. A., Loeb, P. M., Brown, M. S., & Laster, L. (1970). Homocystinuria due to cystathionine synthase deficiency: the effect of pyridoxine. *J Clin Invest, 49*(9), 1762-1773.

Mudd, S. H., Finkelstein, J. D., Irreverre, F., & Laster, L. (1964). Homocystinuria: an enzymatic defect. *LIVER, 1*(1), 1.

Mustafa, A. K., Gadalla, M. M., & Snyder, S. H. (2009). Signaling by gasotransmitters. *Science signaling, 2*(68), re2-re2.

Nature. (2020). Protein quality control. Retrieved from https://www.nature.com/subjects/protein-quality-control

Niu, W.-N., Yadav, P. K., Adamec, J., & Banerjee, R. (2015). S-glutathionylation enhances human cystathionine β-synthase activity under oxidative stress conditions. *Antioxidants & redox signaling*, *22*(5), 350-361.

Okun, J. G., Gan-Schreier, H., Ben-Omran, T., Schmidt, K. V., Fang-Hoffmann, J., Gramer, G., . . . Al Khal, A. L. (2016). Newborn Screening for Vitamin B 6 Non-responsive Classical Homocystinuria: Systematical Evaluation of a Two-Tier Strategy. In *JIMD Reports, Volume 32* (pp. 87-94): Springer.

Oliveriusová, J., Kery, V. r., Maclean, K. N., & Kraus, J. P. (2002). Deletion Mutagenesis of Human Cystathionine β-Synthase: Impact on activity, oligomeric status, ands-adenosylmethionine regulation. *Journal of Biological Chemistry*, *277*(50), 48386-48394.

Oyenarte, I., Majtan, T., Ereno, J., Corral-Rodríguez, M. A., Kraus, J. P., & Martínez-Cruz, L. A. (2012). Purification, crystallization and preliminary crystallographic analysis of human cystathionine β-synthase. *Acta Crystallographica Section F: Structural Biology and Crystallization Communications*, *68*(11), 1318-1322.

Panagaki, T., Lozano-Montes, L., Janickova, L., Zuhra, K., Szabo, M. P., Majtan, T., . . . Szabo, C. (2022). Overproduction of hydrogen sulfide, generated by cystathionine β-synthase, disrupts brain wave patterns and contributes to neurobehavioral dysfunction in a rat model of down syndrome. *Redox Biol, 51*, 102233. doi:10.1016/j.redox.2022.102233

Pey, A. L., Majtan, T., & Kraus, J. P. (2014). The role of surface electrostatics on the stability, function and regulation of human cystathionine β-synthase, a complex multidomain and oligomeric protein. *Biochimica et Biophysica Acta (BBA)-*

Proteins and Proteomics, 1844(9), 1453-1462.

Pey, A. L., Majtan, T., Sanchez-Ruiz, J. M., & Kraus, J. P. (2013). Human cystathionine β-synthase (CBS) contains two classes of binding sites for S-adenosylmethionine (SAM): Complex regulation of CBS activity and stability by SAM. *Biochemical Journal, 449*(1), 109-121.

Pey, A. L., Ying, M., Cremades, N., Velazquez-Campoy, A., Scherer, T., Thöny, B., . . . Martinez, A. (2008). Identification of pharmacological chaperones as potential therapeutic agents to treat phenylketonuria. *J Clin Invest, 118*(8), 2858-2867.

Poloni, S., Hoss, G. W., Sperb-Ludwig, F., Borsatto, T., Doriqui, M. J. R., Leão, E. K., . . . de Souza, C. F. (2018). Diagnosis and Management of Classical Homocystinuria in Brazil: A Summary of 72 Late-Diagnosed Patients. *Journal of Inborn Errors of Metabolism and Screening, 6*, 2326409818788900.

Porras-Dominguez, J., Lothier, J., Limami, A. M., & Tcherkez, G. d-amino acids metabolism reflects the evolutionary origin of higher plants and their adaptation to the environment. *Plant, Cell & Environment, n/a*(n/a). doi:https://doi.org/10.1111/pce.14826

Roman, J. V., Mascarenhas, R., Ceric, K., Ballou, D. P., & Banerjee, R. (2023). Disease-causing cystathionine β-synthase linker mutations impair allosteric regulation. *Journal of Biological Chemistry, 299*(12).

Schiff, M., & Blom, H. J. (2012). Treatment of inherited homocystinurias. *Neuropediatrics, 43*(06), 295-304.

Scott, J. W., Hawley, S. A., Green, K. A., Anis, M., Stewart, G., Scullion, G. A., . . .

Hardie, D. G. (2004). CBS domains form energy-sensing modules whose binding of adenosine ligands is disrupted by disease mutations. *J Clin Invest, 113*(2), 274-284.

Scriver, C. R. (2001). *The metabolic & molecular bases of inherited disease* (Vol. 4): New York; Montreal: McGraw-Hill.

Selley, M., Close, D., & Stern, S. (2002). The effect of increased concentrations of homocysteine on the concentration of (E)-4-hydroxy-2-nonenal in the plasma and cerebrospinal fluid of patients with Alzheimer's disease. *Neurobiology of aging, 23*(3), 383-388.

Singh, L. R., Chen, X., Kožich, V., & Kruger, W. D. (2007). Chemical chaperone rescue of mutant human cystathionine β-synthase. *Molecular genetics and metabolism, 91*(4), 335-342.

Singh, L. R., Gupta, S., Honig, N. H., Kraus, J. P., & Kruger, W. D. (2010). Activation of mutant enzyme function in vivo by proteasome inhibitors and treatments that induce Hsp70. *PLoS Genet, 6*(1).

Singh, L. R., & Kruger, W. D. (2009). Functional rescue of mutant human cystathionine β-synthase by manipulation of Hsp26 and Hsp70 levels in Saccharomyces cerevisiae. *Journal of Biological Chemistry, 284*(7), 4238-4245.

Singh, S., Padovani, D., Leslie, R. A., Chiku, T., & Banerjee, R. (2009). Relative contributions of cystathionine β-synthase and γ-cystathionase to H2S biogenesis via alternative trans-sulfuration reactions. *Journal of Biological Chemistry, 284*(33), 22457-22466.

Smith, A. T., Su, Y., Stevens, D. J., Majtan, T., Kraus, J. P., & Burstyn, J. N. (2012).

Effect of the disease-causing R266K mutation on the heme and PLP environments of human cystathionine β-synthase. *Biochemistry*, *51*(32), 6360-6370.

Stabler, S. P., Korson, M., Jethva, R., Allen, R. H., Kraus, J. P., Spector, E. B., . . . Mudd, S. H. (2013). Metabolic profiling of total homocysteine and related compounds in hyperhomocysteinemia: utility and limitations in diagnosing the cause of puzzling thrombophilia in a family. In *JIMD Reports-Volume 11* (pp. 149-163): Springer.

Stipanuk, M. H. (2004). Sulfur amino acid metabolism: pathways for production and removal of homocysteine and cysteine. *Annu. Rev. Nutr., 24*, 539-577.

Tamizhselvi, R., Moore, P. K., & Bhatia, M. (2007). Hydrogen sulfide acts as a mediator of inflammation inacute pancreatitis: in vitro studies using isolated mouse pancreatic acinar cells. *Journal of cellular and molecular medicine, 11*(2), 315-326.

Tawfik, A., Markand, S., Al-Shabrawey, M., Mayo, J. N., Reynolds, J., Bearden, S. E., . . . Smith, S. B. (2014). Alterations of Retinal Vasculature in Cystathionine–β-Synthase Heterozygous Mice: A Model of Mild to Moderate Hyperhomocysteinemia. *The American journal of pathology, 184*(9), 2573-2585.

The Human Gene Database. (2022). Cystathionine Beta-Synthase. Retrieved from https://www.genecards.org/cgi-bin/carddisp.pl?gene=CBS

Tortorelli, S., Turgeon, C. T., Lim, J. S., Baumgart, S., Day-Salvatore, D.-L., Abdenur, J., . . . Oglesbee, D. (2010). Two-tier approach to the newborn screening of methylenetetrahydrofolate reductase deficiency and other remethylation

disorders with tandem mass spectrometry. *The Journal of pediatrics, 157*(2), 271-275.

Townsend, D. M., Tew, K. D., & Tapiero, H. (2004). Sulfur containing amino acids and human disease. *Biomed Pharmacother, 58*(1), 47-55. doi:10.1016/j.biopha.2003.11.005

Turgeon, C. T., Magera, M. J., Cuthbert, C. D., Loken, P. R., Gavrilov, D. K., Tortorelli, S., . . . Matern, D. (2010). Determination of total homocysteine, methylmalonic acid, and 2-methylcitric acid in dried blood spots by tandem mass spectrometry. *Clinical chemistry, 56*(11), 1686-1695.

Uhlén, M., Fagerberg, L., Hallström, B. M., Lindskog, C., Oksvold, P., Mardinoglu, A., . . . Asplund, A. (2015). Proteomics. Tissue-based map of the human proteome. *Science (New York, NY), 347*(6220), 1260419-1260419.

University, W. O. (2024). Protein Structure. Retrieved from https://wou.edu/chemistry/courses/online-chemistry-textbooks/ch450-and-ch451-biochemistry-defining-life-at-the-molecular-level/chapter-2-protein-structure/

Uppala, J. K., Gani, A. R., & Ramaiah, K. V. (2017). Chemical chaperone, TUDCA unlike PBA, mitigates protein aggregation efficiently and resists ER and non-ER stress induced HepG2 cell death. *Scientific reports, 7*(1), 3831.

Urreizti, R., Asteggiano, C., Cozar, M., Frank, N., Vilaseca, M. A., Grinberg, D., & Balcells, S. (2006). Functional assays testing pathogenicity of 14 cystathionine-beta synthase mutations. *Human mutation, 27*(2), 211-211.

Urreizti, R., Balcells, S., Rodes, M., Vilarinho, L., Baldellou, A., Couce, M. L., . . .

Grinberg, D. (2003). Spectrum of CBS mutations in 16 homocystinuric patients from the Iberian Peninsula: high prevalence of T191M and absence of I278T or G307S. *Hum Mutat, 22*(1), 103. doi:10.1002/humu.9153

Valayannopoulos, V., Schiff, M., Guffon, N., Nadjar, Y., García-Cazorla, A., Casanova, M. M.-P., . . . Peña-Quintana, L. (2019). Betaine anhydrous in homocystinuria: results from the RoCH registry. *Orphanet journal of rare diseases, 14*(1), 66.

van Gunsteren, W. F., Billeter, S., Eising, A., Hünenberger, P., Krüger, P., Mark, A., . . . Tironi, I. (1996). Biomolecular simulation: the GROMOS96 manual and user guide. *Vdf Hochschulverlag AG an der ETH Zürich, Zürich, 86*, 1-1044.

Vang, S., Longley, K., Steer, C. J., & Low, W. C. (2014). The unexpected uses of urso- and tauroursodeoxycholic acid in the treatment of non-liver diseases. *Global advances in health and medicine, 3*(3), 58-69.

Walter, J. H., Jahnke, N., & Remmington, T. (2011). Newborn screening for homocystinuria. *Cochrane Database of Systematic Reviews*(8).

Weber Hoss, G. R., Sperb-Ludwig, F., Schwartz, I. V. D., & Blom, H. J. (2020). Classical homocystinuria: A common inborn error of metabolism? An epidemiological study based on genetic databases. *Mol Genet Genomic Med, 8*(6), e1214. doi:10.1002/mgg3.1214

Wilcken, B. (2017). Therapeutic targets in homocystinuria due to cystathionine β-synthase deficiency: new European guidelines. In: Taylor & Francis.

Wilcken, D. E., Dudman, N. P., & Tyrrell, P. A. (1985). Homocystinuria due to cystathionine β-synthase deficiency—the effects of betaine treatment in

pyridoxine-responsive patients. *Metabolism, 34*(12), 1115-1121.

Wiley, V., Webster, D., & Loeber, G. (2019). Screening Pathways through China, the Asia Pacific Region, the World. In: Multidisciplinary Digital Publishing Institute.

Yamanishi, M., Kabil, O., Sen, S., & Banerjee, R. (2006). Structural insights into pathogenic mutations in heme-dependent cystathionine-β-synthase. *Journal of inorganic biochemistry, 100*(12), 1988-1995.

Yap, S. (2012). Classical homocystinuria: newborn screening with early treatment effectively prevents complications. *Hamdan Medical Journal, 212*(1202), 1-12.

Yap, S., Boers, G. H., Wilcken, B., Wilcken, D. E., Brenton, D. P., Lee, P. J., . . . Naughten, E. R. (2001). Vascular outcome in patients with homocystinuria due to cystathionine β-synthase deficiency treated chronically: a multicenter observational study. *Arteriosclerosis, thrombosis, and vascular biology, 21*(12), 2080-2085.

Yuan, X., Zhang, J., Xie, F., Tan, W., Wang, S., Huang, L., . . . Yuan, Q. (2017). Loss of the protein cystathionine β-synthase during kidney injury promotes renal tubulointerstitial fibrosis. *Kidney and Blood Pressure Research, 42*(3), 428-443.

Zhong, F., Lisi, G. P., Collins, D. P., Dawson, J. H., & Pletneva, E. V. (2014). Redox-dependent stability, protonation, and reactivity of cysteine-bound heme proteins. *Proc Natl Acad Sci U S A, 111*(3), E306-315. doi:10.1073/pnas.1317173111

Zschocke, J., Kebbewar, M., Gan-Schreier, H., Fischer, C., Fang-Hoffmann, J., Wilrich, J., . . . Lindner, M. (2009). Molecular neonatal screening for

homocystinuria in the Qatari population. *Human mutation, 30*(6), 1021-1022.

Zuhra, K., Augsburger, F., Majtan, T., & Szabo, C. (2020). Cystathionine-β-synthase: Molecular Regulation and Pharmacological Inhibition. *Biomolecules, 10*(5), 697.

Zuhra, K., Augsburger, F., Majtan, T., & Szabo, C. (2020). Cystathionine-β-Synthase: Molecular Regulation and Pharmacological Inhibition. *Biomolecules, 10*(5). doi:10.3390/biom10050697

Appendix:

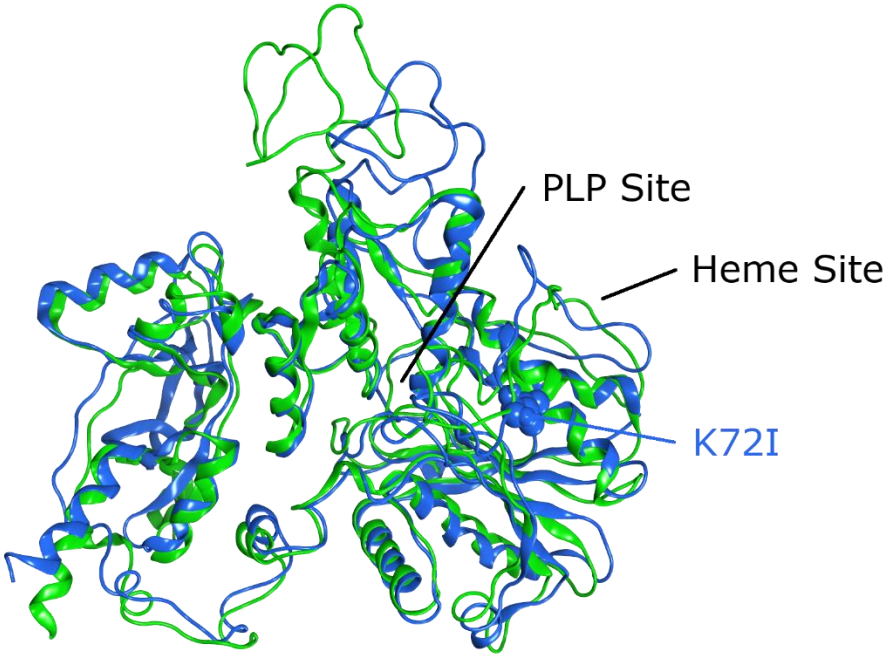

Figure SM1. Superimposed MD structures for CBS^{WT} (green ribbons) and CBS^{K72I} (blue ribbons). The K72I mutation is depicted as a space-filling models for reasons of emphasis (blue), while the black lines show the location of the cofactor binding sites. Based on the MD results, all variants adopt a similar folding, with small structural changes that are largely confined to the secondary structure level of the protein architecture.

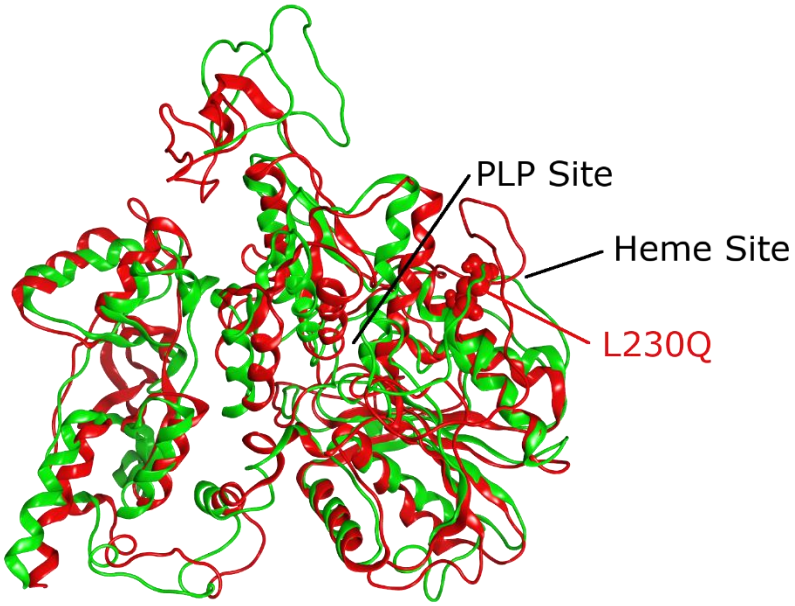

Figure SM2. Superimposed MD structures for CBS^{WT} (green ribbons) and CBS^{L230Q} (red ribbons). The L230Q mutation is depicted as a space-filling models for reasons of emphasis (red), while the black lines show the location of the cofactor binding sites. Based on the MD results, the heme binding site shows significant structural changes due to the CBS^{L230Q} mutation.